



**A Content-Based Brain Tumor Images System  
for Classification, Retrieval and Diagnosis**

**نظام مُعتمِد على مُحتوى صور ورم الدِّماغ لأغراض التصنيف  
والأسترجاع والتَّشخيص**

**By**

**Muhannad Hamad Hussein**

**(401220039)**

**Supervisor**

**Dr. Sadeq AlHamouz**

**Master Thesis**

Submitted in Partial Fulfillment of the Requirements for

the Master Degree in Computer Science

Faculty of Information Technology

Department of Computer Science

Middle East University

Amman – Jordan

January 2016

بِسْمِ اللَّهِ الرَّحْمَنِ الرَّحِيمِ

وَاقْرَأْ كِتَابَ التَّوْرَةِ

صدق الله العظيم

سورة الذاريات اية ( ٢١ )

## Authorization statement

I am **Muhannad Hamad Hussein** the Middle East University to supply a copy my  
Thesis to libraries, establishment or individuals.

**Signature:**

A handwritten signature in blue ink, consisting of a large, stylized loop followed by a horizontal line and a small mark.

**Date: 10/1/2016**

## اقرار تفويض

انا مهند حمد حسين أفوض جامعه الشرق الاوسط بتزويد نسخ من رسالتي للمكتبات  
اوالمؤسسات او الهيئات او الافراد عنده طلبها.



التوقيع:

التاريخ: 2016/1/10

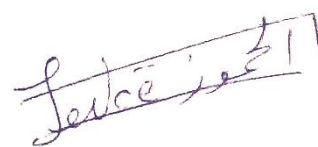
Middle East University  
Examination Committee Decision

This is to certify that the thesis entitled "**A Content-Based Brain Tumor Images System for Classification, Retrieval and Diagnosis**" was successfully defended and approved in 2016.

**Examination Committee Members**

**Signature**

**Dr. Sadeq AlHamouz (Supervisor & Member)**  
Associate Professor, Department of Computer Science  
Head Department of Computer Information Systems  
Middle East University (MEU)



**Dr. Mohammed Abbas Al-Husainy (Chairman)**  
Associate Professor, Department of Computer Science  
Middle East University (MEU)



**Dr. Emad Mahmoud Al-Shawakfa (External Member)**  
Associate Professor.  
Head Department of Computer Information Systems  
AL Yarmouk University



## Acknowledgements

I would like to thank my mother, my family, my teachers and my friends for their continuous support during my study. I also would like to thank my great supervisor **Dr. Sadeq Al-Hamouz** for his support, encouragement, proofreading of thesis drafts, and for helping me throughout my studies, putting me in the right step of scientific research.

I would like to thank **Dr. Mohammed Abbas Al-Husainy & Dr. Emad Mahmoud Al-Shawakfa**.

In addition, I would like to thank the Information Technology Faculty members at the Middle East University (MEU).

## **Dedication**

This thesis is dedicated to all the people who never stopped believing in me.

To my great father may god have mercy on him and light his grave. To my mother that made me the man I am. To my brother and sisters who never stopped supporting me during the journey of my life.

## Table of Contents

الاية الكريمة .....	<b>II</b>
<b>AUTHORIZATION FORM</b> .....	<b>III</b>
اقرار التفويض .....	<b>IV</b>
<b>COMMITTEE DECISION</b> .....	<b>V</b>
<b>ACKNOWLEDGMENT</b> .....	<b>VI</b>
<b>DEDICATION</b> .....	<b>VII</b>
<b>Table of Contents</b> .....	<b>VIII</b>
<b>List of Tables</b> .....	<b>XI</b>
<b>List of Figures</b> .....	<b>XIII</b>
<b>List of Abbreviations</b> .....	<b>XVI</b>
<b>ABSTRACT</b> .....	<b>XVIII</b>
الملخص.....	<b>XX</b>
<b>Chapter 1: Introduction (Background of the study and its Importance)</b> .....	<b>1</b>
1.1.Introduction .....	1
1.2.Research Motivation .....	2
1.3.Contribution .....	3
1.4.Problem Statement .....	4
1.5.Methodology .....	4
1.6.Thesis Outline .....	5
<b>Chapter 2: Theoretical Background and Literature Review</b> .....	<b>6</b>
2.1. Introduction .....	6
2.2. Text Based Image Retrieval (TBIR) .....	7
2.3.Sketch Based Image Retrieval (SBIR).....	7
2.4. Content Based Image Retrieval (CBIR) .....	8
2.5. The Semantic Gap (SG) .....	10
2.6. K Nearest Neighbours (KNN)) .....	10
2.7. Literature Review .....	13
2.7.1 Non-Medical Content-Based Image Retrieval .....	13
2.7.2 Medical Content-Based Image Retrieval .....	14

<b>Chapter 3: Proposed CBBIR System Algorithm: Implementation and Methodology</b>	<b>20</b>
3.1.Introduction	20
3.2.The Proposed CBBIR System Framework	21
3.3.PHASE (1): Brain MRI Dataset Pre-Processing	23
3.3.1 Brain MRI Dataset Collection	23
3.3.2 Brain MRI Dataset Noise Removal	24
3.3.3 Why Magnetic Resonance Imaging (MRI)	25
3.3.3.1 What is Image Contrast?	26
3.3.4 What is the Difference between MRI scans: T1, T1c, T2 and FLAR?	27
3.3.5 Magnetic Resonance Images Viewing and Overlaying	30
3.4.Features Extraction and Dimensions Reduction	36
3.4.1 Colour Features Extraction	36
3.4.1.1 Colour Sets	37
3.4.1.2 Colour Histogram	38
3.4.1.3 Normalized HSV Colour Histogram	43
3.4.1.4 HSV Histogram Normalization	46
3.4.1.5 Colour Moments	48
3.4.1.6 Colour Correlograms	49
3.4.2 Shape Features Extraction	51
3.4.2.1 Wavelet Moments	53
3.4.3 Texture Features Extraction	59
3.4.3.1 Gabor Filter	60
3.4.3.2 Log-Gabor Filter	66
3.4.3.3 Feature Extraction based on Log-Gabor Filter	67
3.5.Classification and Retrieval Phase	68
3.5.1 K Nearest Neighbour (KNN) Classification Engine	68
3.5.2 Similarity Metrics	71
<b>Chapter 4: Experimental Results</b>	<b>75</b>
4.1. Introduction	75
4.2. Retrieval Parameters	75
4.3. The Graphical User Interface of Our Proposed CBBIR System	76
4.4. CBBIR System: Experimental Results and Performance Analysis	80

4.4.1 CBBIR System Performance Analysis: Precision .....	81
4.4.2 CBBIR System Performance Analysis: Recall .....	96
4.5. Comparison of Similarity Measures for Different Number of Retrieved Images .....	107
4.6. Comparison of CBBIR System Performance to other Retrieval Systems Based on BRATS Dataset .....	119
4.7. Comparison of CBBIR System Performance to other Retrieval Systems Based on Different Brain MR Datasets .....	121
<b>Chapter 5 : Conclusions, Recommendations and Future Work .....</b>	<b>124</b>
<b>References .....</b>	<b>126</b>

## List of Tables

Table (3.1): The range of numbers and the corresponding disease category .....	24
Table (4.1): Precision of CBBIR System (BT =53), Similarity Measure: L1 .....	83
Table (4.2): Precision of CBBIR System (BT =53), Similarity Measure: L2 .....	84
Table (4.3): Precision of CBBIR System (BT =53), Similarity Measure: Standardized L2 .....	85
Table (4.4): Precision of CBBIR System (BT =53), Similarity Measure: Cityblock ....	86
Table (4.5): Precision of CBBIR System (BT =53), Similarity Measure: Minkowski .	87
Table (4.6): Precision of CBBIR System (BT =53), Similarity Measure: Chebychev ..	88
Table (4.7): Precision of CBBIR System (BT =53), Similarity Measure: Cosine .....	89
Table (4.8): Precision of CBBIR System (BT =53), Similarity Measure: Correlation .	90
Table (4.9): Precision of CBBIR System (BT =53), Similarity Measure: Spearman ....	91
Table (4.10): Precision of CBBIR System (BT =53), Similarity Measure: Normalized L2 .....	92
Table (4.11): Recall of CBBIR System (BT =20), Similarity Measure: L1 .....	96
Table (4.12): Recall of CBBIR System (BT =20), Similarity Measure: L2 .....	97
Table (4.13): Recall of CBBIR System (BT =20), Similarity Measure: Chebyshev .....	98
Table (4.14): Recall of CBBIR System (BT =20), Similarity Measure: CityBlock .....	99
Table (4.15): Recall of CBBIR System (BT =20), Similarity Measure: Correlation ..	100
Table (4.16): Recall of CBBIR System (BT =20), Similarity Measure: Cosine .....	101
Table (4.17): Recall of CBBIR System (BT =20), Similarity Measure: Minkowski .	102
Table (4.18): Recall of CBBIR System (BT =20), Similarity Measure: Normalized L1	103
Table (4.19): Recall of CBBIR System (BT =20), Similarity Measure: Spearman ....	104
Table (4.20): Recall of CBBIR System (BT =20), Similarity Measure: Standardized L2 .....	105
Table (4.21): Precision of CBBIR System (BT =53), Similarity Measure: L1 .....	108
Table (4.22): Precision of CBBIR System (BT =53), Similarity Measure: L2 .....	109
Table (4.23): Precision of CBBIR System (BT =53), Similarity Measure: Standardized L2 .....	110
Table (4.24): Precision of CBBIR System (BT =53), Similarity Measure: Chebychev .....	111

Table (4.25): Precision of CBBIR System (BT =53), Similarity Measure: Cityblock	112
Table (4.26): Precision of CBBIR System (BT =53), Similarity Measure: Correlation .....	113
Table (4.27): Precision of CBBIR System (BT =53), Similarity Measure: Cosine .....	114
Table (4.28): Precision of CBBIR System (BT =53), Similarity Measure: Spearman	115
Table (4.29): Precision of CBBIR System (BT =53), Similarity Measure: Minkowski .....	116
Table (4.30): Precision of CBBIR System (BT =53), Similarity Measure: Normalized L2 .....	117

## List of Figures

Figure (2.1): Image Retrieval Systems Classification .....	6
Figure (2.2): General structure of all content-based image retrieval systems .....	9
Figure (3.1): Framework of the proposed CBBIR system .....	21
Figure (3.2): Framework of Proposed Retrieval Engine .....	22
Figure (3.3): The effect of contrast increasing .....	26
Figure (3.4): The effect of contrast decreasing .....	26
Figure (3.5): Steps of Attenuated Inversion-Recovery MRI mechanism .....	28
Figure (3.6): One axial slice of an MR image of a high-grade glioma patient .....	29
Figure (3.7): Axial, Coronal and Sagittal Displays of the Brain MR Image .....	31
Figure (3.8): (a) Coronal (b) Sagittal (c) Axial Displays.....	31
Figure (3.9): The final view of an overlay Brain tumor MRI image .....	32
Figure (3.10): (a) $T_1$ weighted MRI image layer (b) $T_{1c}$ weighted MRI image layer (c) $T_2$ weighted layer (d) $T_{2FLAIR}$ MRI image layer (final overlay image)	33
Figure (3.11): The slices of a brain tumor MR volume image .....	34
Figure (3.12): The .bmp format of final brain MRI image .....	34
Figure (3.13): Brain Tumor Zones Segmentation in three levels .....	35
Figure (3.14): Colour Spaces .....	39
Figure (3.15): (a) RGB colour space (b) HSV colour space.....	42
Figure (3.16): RGB and HSV colour distribution of Brain Tumor MR Image .....	44
Figure (3.17): RGB and HSV colour distribution of Brain Disease MR Image .....	45
Figure (3.18): The Tumor regions in Brain MR Images (a) small region (b) wide region .....	46
Figure (3.19): Two Bins Normalized Histograms ( $h_0, h_1$ ) with ( $r = 1$ ) .....	47
Figure (3.20): Wavelet Decomposition of an image .....	54
Figure (3.21): 2D Discrete Wavelet Transform of brain MR image .....	54
Figure (3.22): Discrete Wavelet Transform (Level 2) of a brain MR image .....	55
Figure (3.23): Discrete Wavelet Transform (Level 4) of a brain MR image .....	56
Figure (3.24): Daubechies wavelets family .....	56
Figure (3.25): Coiflet wavelets family .....	57

Figure (3.26): A Brain MR image decomposed by Coiflet wavelet at level 4 .....	58
Figure (3.27): Frequency response of the Gabor filter bank. The contours represent the half-peak magnitude of the filter responses in the Gabor filter family. The filter parameters used here are: $K=4$ , $N = 4$ , and $F_0 = 0.4$ .....	63
Figure (3.28): Real parts of 2x2 Gabor Filter .....	64
Figure (3.29): Magnitudes of 2x2 Gabor Filter .....	65
Figure (3.30): K Nearest Neighbor Classification .....	69
Figure (3.31): L2 Distance Between Two Points .....	72
Figure (4.1): The Graphical User (GUI) Interface of Our Proposed CBBIR System ...	76
Figure (4.2): The Features Extraction Engine of the proposed CBBIR GUI .....	77
Figure (4.3): The CBBIR Retrieval Engine of the proposed CBBIR GUI .....	78
Figure (4.4): The Top ( $N =20$ ) Retrieved Brain MR images .....	79
Figure (4.5): Sample Retrieval CBBIR System Using Similarity Measure: L2 .....	84
Figure (4.6): Sample Retrieval CBBIR System Using Similarity Measure: Standardized L2 .....	85
Figure (4.7): Sample Retrieval CBBIR System Using Similarity Measure: Cityblock	86
Figure (4.8): Sample Retrieval CBBIR System Using Similarity Measure: Minkowski .....	87
Figure (4.9): Sample Retrieval CBBIR System Using Similarity Measure: Chebychev .....	88
Figure (4.10): Sample Retrieval CBBIR System Using Similarity Measure: Cosine ..	89
Figure (4.11): Sample Retrieval CBBIR System Using Similarity Measure: Correlation .....	90
Figure (4.12): Sample Retrieval CBBIR System Using Similarity Measure: Spearman .....	91
Figure (4.13): Sample Retrieval CBBIR System Using Similarity Measure: Normalized L2 .....	92
Figure (4.14): Precision Comparison between the Similarity Measures of CBBIR System (BT=53).....	93
Figure (4.15): Sample Retrieval CBBIR System Using Similarity Measure: L2 .....	97
Figure (4.16): Sample Retrieval CBBIR System Using Similarity Measure: Chebyshev .....	98
Figure (4.17): Sample Retrieval CBBIR System Using Similarity Measure: Cityblock .....	99

Figure (4.18): Sample Retrieval CBBIR System Using Similarity Measure: Correlation .....	100
Figure (4.19): Sample Retrieval CBBIR System Using Similarity Measure: Cosine .....	101
Figure (4.20): Sample Retrieval CBBIR System Using Similarity Measure: Minkowski .....	102
Figure (4.21): Sample Retrieval CBBIR System Using Similarity Measure: Normalized L2 .....	103
Figure (4.22): Sample Retrieval CBBIR System Using Similarity Measure: Spearman .....	104
Figure (4.23): Sample Retrieval CBBIR System Using Similarity Measure: Standardized L2 .....	105
Figure (4.24): Recall Comparison between the Similarity Measures of CBBIR System (BT =20) .....	106
Figure (4.25): Performance Comparison of Similarity Measures for Different Retrieval Images .....	118
Figure (4.26): Performance Comparison in terms of Precision and Recall for Different Retrieval Systems based on BRATS Dataset .....	119
Figure (4.27): Performance Comparison of CBMIR Systems in terms of Precision ..	121
Figure (4.28): Performance Comparison of CBMIR Systems in terms of Recall .....	122

## LIST OF ABBREVIATIONS

Abbreviation	Meaning
<b>ANN</b>	Artificial Neural Networks
<b>BRAT</b>	Brain Tumor (Database)
<b>BT</b>	Brain Tumor
<b>CBBIR</b>	Content-Based Brain Image Retrieval
<b>CBIR</b>	Content-Based Image Retrieval
<b>CBMIR</b>	Content-Based Medical Image Retrieval
<b>CE-MR</b>	Contrast-Enhanced MR
<b>CHAR</b>	Convex Hull Area Ratio
<b>CSF</b>	cerebrospinal fluid
<b>CT</b>	Computed Tomography
<b>dbN</b>	where db is the surname of the wavelet and N represents the order
<b>DWT</b>	Discrete Wavelet Transform
<b>ELM</b>	Extreme Learning Machine
<b>EMRF</b>	Enhanced Markov Random Fields Approach
<b>FEMA</b>	Fuzzy Expectation Maximization Algorithm
<b>GA</b>	Genetic Algorithm
<b>GSDM</b>	Greystone Spatial Dependence Matrix
<b>GUI</b>	Graphical User Interface
<b>HSV</b>	Hue, Saturation, Value (HSV colour space)
<b>HHNN</b>	Hyperbolic Hopfield Neural Network
<b>IDE</b>	Integrated Development Environment
<b>IRMA</b>	Image Retrieval in Medical Applications
<b>ISLES</b>	Ischemic Stroke Lesion Segmentation
<b>ISLES</b>	Ischemic Stroke Lesion Segmentation
<b>KNN</b>	K Nearest Neighbors
<b>L1</b>	Manhattan Distance
<b>L2</b>	Euclidean Distance
<b>MPP</b>	Mean average Precision Project
<b>MRI</b>	Magnetic Resonance Image
<b>MRS</b>	Magnetic Resonance Spectroscopy

<b>Novel KNN</b>	Novel K Nearest Neighbors
<b>PACS</b>	Picture Archiving and Communication System
<b>PCA</b>	Principle Component Analysis
<b>PET</b>	Position Emission Tomography
<b>QBIC</b>	Query By Image Content
<b>RGB</b>	Read, Green and Blue (RGB colour space)
<b>REML</b>	Rank Error-Based Metric Learning
<b>SBIR</b>	Sketch Based Image Retrieval
<b>SOM</b>	Self Organized Map
<b>SVM</b>	Support vector Machine
<b>T<sub>1</sub></b>	T1-weighted MRI (T1)
<b>T<sub>2</sub></b>	T2- weighted MRI(T2)
<b>T<sub>2FLAIR</sub></b>	T2FLAIR- weighted, MRI with Fluid Attenuated Inversion Recovery (FLAIR)
<b>TBIR</b>	Text-Based Image Retrieval
<b>T<sub>c1</sub></b>	T1c- weighted MRI with contrast enhancement (T1c)
<b>WWW</b>	World Wide Web

# **A Content-Based Brain Tumor Images System for Classification, Retrieval and Diagnosis**

**Student Name: Muhannad Hamad Hussein**

**Supervisor**

**Dr. Sadeq AlHamouz**

## **Abstract**

Brain tumor is considered one of the most serious and life-threatening among of brains diseases. Therefore, the accurate diagnosis of brain tumor is considered crucial for the effective medical treatment of it.

Accordingly, in this thesis, we propose a Content-Based Brain Image Retrieval System (CBBIRS) that have the capability to retrieve similar pathology bearing brain magnetic resonance (MR) images from a database composed of brain MR images of four major brain diseases categories: Neoplastic Disease (brain tumor), Cerebrovascular Diseases (stroke or brain attack), Degenerative Diseases, Inflammatory or Infectious Diseases.

Since the visual characteristics of a disease carry diagnostic information and oftentimes visually similar images corresponds to the same disease category, our proposed (CBBIR) system is principally designed to assist the radiologists, neurologists, and neurosurgeons in the process of brain tumor diagnosis.

CBBIR system consists of two major phases: off-line and on-line phases. In off-line phase the feature vectors of brain MR images in the database are extracted whereas in the on-line phase, the first (k) similar brain MR images for a brain MR query image

are retrieved via KNN classification engine and using one of ensemble of similarity measures based on the query brain MR image features that discriminate its class.

Experiments were carried out on (BRATS, 2015) dataset consists of brain MR images for (126) cases. The experimental results demonstrate the effectiveness of the proposed system and show the viability of clinical implementation where it achieved a promising average precision of (98.63%) and average recall of (98.12%).

**Keywords:** Content-Based Image Retrieval, Brain tumor, K Nearest Neighbors (KNN), Feature Extraction, Classification, Similarity Metrics.

## نظام مُعْتَمَد عَلَى مُحتوى صُور وَرَم الدِّماغ لأغراض التصنيف والأسترجاع

### والتَّشخيص

اسم الطالب: مهند حمد حسين

اسم المشرف: د. صادق الحموز

### الملخص

تعتبر أورام الدماغ واحدة من أخطر أمراض الدماغ المهددة للحياة. ولذلك، يعتبر التشخيص الدقيق للورم في الدماغ أمراً حاسماً في المعالجة الطبية الفعالة له.

وفقاً لذلك، في هذه الأطروحة، نقترح نظام استرجاع صور الدماغ المعتمدة على المحتوى (CBBIRS) لدية القدرة على استرجاع صور الرنين المغناطيسي (MR) للدماغ المماثلة من الناحية الباثولوجية من قاعدة بيانات مكونة من صور الرنين المغناطيسي للدماغ تتكون من أربع فئات أمراض رئيسية هي: الأورام (أورام الدماغ)، السكتة أو النوبات الدماغية، الأمراض التنكسية، والأمراض الالتهابية (أمراض المعدية).

بما أن الخصائص البصرية للمرض تحمل معلومات تشخيصية وبما أن الصور المتماثلة بصرياً تتوافق في معظم الأحيان مع فئة المرض نفسه، فإن النظام المقترح (CBBIRS) تم تصميمه بشكل أساسي لمساعدة أطباء الأشعة و أطباء الأعصاب، وجراحي الدماغ والأعصاب في عملية تشخيص أورام الدماغ.

ويتكون نظام (CBBIRS) من مرحلتين رئيسيتين: المرحلة الفعالة و المرحلة غير الفعالة. في المرحلة غير الفعالة يتم استخراج مميزات صور الرنين المغناطيسي للدماغ الموجودة في قاعدة البيانات بينما في المرحلة الفعالة يتم استرداد أول (k) من صور الرنين المغناطيسي للدماغ

مماثلة لصورة الرنين المغناطيسي للدماغ المستعلم عنها باستخدام (KNN) كمحرك تصنيف وباستخدام واحده من مجموعة متكاملة من مقاييس التشابه بناء على مميزات صورة الرنين المغناطيسي للدماغ المستعلم عنها والتي تميز فنتها.

تم تنفيذ الاختبارات باستخدام قاعدة البيانات (BRATS,2015) والتي تتكون من مجموعة من صور الرنين المغناطيسي للدماغ لـ (126) حالة. النتائج التجريبية أثبتت فعالية النظام المقترح وتظهر جدوى تنفيذه سريريا حيث تم تحقيق دقة واحدة بمعدل (98.63%) ومتوسط استدعاء (98.12%).

**الكلمات المفتاحية:** استرجاع الصورة المعتمدة على المحتوى، ورم الدماغ، K-اقرب جار (KNN)، استخراج المميزات، المصنف، مقاييس التشابه.

# **Chapter One**

## **Introduction**

### **Background of the study and its Importance**

#### **1.1 Introduction**

The utilization of huge image databases for several applications have now become extremely realizable due to the increasing advances in the technologies that were used in manufacturing the processors and memories; which are used in storing and analyzing these image databases.

Databases that are used to store the medical imagery, satellite images, and artworks, have become attractive for more and more users and researchers in a variety of professional areas such as: medicine, architecture, geography, advertising, marketing, fashion, design, and publishing. Recently, the interest in the capabilities, and possibilities that reside in digital images is increasing dramatically; fuelled in part by the enormous growth of imaging on the World Wide Web (WWW).

The image retrieval problem is becoming recognized on a wide-scale; therefore, the search for possible solutions becomes an increasingly active area of research and development. (Lew, Sebe, Djeraba & Jain 2006) elaborated the major issues associated with classic techniques used in image indexing, which have led to the raise of interest in the approaches followed in images retrieval based on the idea of automatically-derived attribute (features) such as texture, colour, and shape. Where, it is exemplified in a technology referred to as Content-Based Image Retrieval (CBIR).

CBIR can be defined as the technique used to retrieve images from an image database based on its content or concisely, it can be defined as query by image contents (Arakeri & Reddy, 2013).

After a decade of massive researches, CBIR technology is recently moving out of the laboratory, and academic lectures, and journals into the marketplace in the form of commercial products such as: QBIC (Query By Image Content) (Flinckner, et al., 1995), and VIRAGE (Bach, et al., 1996). However, CBIR technology is still far from mature, and is not yet being employed on a large-scale.

One important application of CBIR is the medical field. Several health care institutions, and establishments have started using a variety of CBIR systems to improve, and enhance the diagnosis, and treatment processes of different diseases. In this research, we introduce a medical CBIR technique based on a combination of novel brain tumor zones segmentation, powerful feature extraction techniques and *K Nearest Neighbors* (KNN) as classification engine with an ensemble of similarity measures in order to enhance the process of the brain tumor diagnosis.

## **1.2 Research Motivation**

Several medical image retrieval systems have been proposed, developed, and implemented. However, both the accuracy and speed of these systems are still need to be enhanced, and improved. Moreover, brain tumor images retrieval systems are far from mature, due to the fact of high difficulty of designing, and development of these systems.

Our Proposed system, utilized powerful data mining technique: KNN enhancing by an ensemble of similarity measures, to build a content-based brain image retrieval

system (CBBIRS), for clinical decision support in brain tumor diagnosis. The main objectives of this research are identified as following:

- 1) Building and implementing a content-based brain medical image retrieval system (CBBIRS) for clinical decision support system for brain tumor diagnosis.
- 2) Take advantage of the merits of the data mining techniques to build a medical CBBIRS that could achieve high classification accuracy.
- 3) Develop a medical CBBIRS that shows high efficiency and viability of clinical applications.

### **1.3 Contribution**

Brain tumor Diagnostics is considered the most difficult and at the same time, the most important application of content based medical image retrieval. To be employed as a diagnostic assistant, the medical CBIR techniques need to enhance their performance, and at the same time need to be accepted by the clinicians as an effective and useful tool.

This research investigates the powerfulness KNN data mining technique with ensemble of similarity measures to refine, enhance, and improve the overall performance of medical images retrieval, used to enhance the brain tumor diseases diagnosis, and reduce the semantic gap in such a way that can be translated into medical application, and enhance clinical decision- making.

## 1.4 Problem Statement

Accurate diagnosis is essential for successful treatment, and for handling of the brain tumor. In this research, we propose a content-based brain image retrieval system CBBIRS that could retrieve similar pathology bearing magnetic resonance (MR) images of the brain from a medical database composed of brain MR images that corresponds to four major brain diseases.

The main questions in this research are identified as following:

- 1) How to build a content-based brain image retrieval system CBBIRS that has high classification accuracy?
- 2) How to employ different similarity measures in association with data mining techniques to assist neurologists, and neurosurgeons in refining the prediction process, and brain tumor cases diagnosis?
- 3) Is it possible to develop a CBBIRS have the high capability to retrieve the most similar brain tumor images in effective manner in terms of both retrieval speed and precision?
- 4) Is it possible to implement the proposed CBBIR system in hospitals for assisting the radiologist in diagnosing brain tumors in a good accuracy and speed?

## 1.5 Methodology

This thesis uses the following methodology:

1. Studying of literatures in Content Based Image Retrieval, Content Based Medical image retrieval systems, data mining and machine learning algorithms.
2. Developing a Content based medical image retrieval system that based on a KNN algorithm and a variety of similarity metrics.

3. Implement the proposed CBBIRS using Matlab 2015a as an Integrated Development Environment (IDE).
4. Experimenting the system operation (Training, Testing and Validation) using a benchmark data set of MR (Magnetic Resonance) brain images.
5. Evaluating the performance of the system, and comparing its performance with other existing CBMIR systems and models.
6. Discuss the results, give conclusions, and suggest recommendations for future work.

## **1.6 Thesis Outline:**

The rest of this thesis is organized as follows:

In Chapter II, we summarize the significant previous algorithms used to build the content based medical image retrieval systems. One portion of these literatures was used as the basis for our CBMIR system developments, whereas the other one was selected as a comparative measure of performance CBMIR system proposed in this thesis. Implementation strategies and the proposed methodology of our proposed hybrid system are explained in Chapter III.

Experimental results of the proposed system and the results of comparison with the other proposed CBMIR systems are presented in Chapter IV. Whereas the conclusions and recommendations for future work are presented in Chapter V.

## Chapter Two

### Theoretical Background and Literature Review

#### 2.1 Introduction

Since the evolution of large-scale collections of medical images available at hospitals in the early the 1990s, many difficulties were faced by the manual annotation; including huge size of image collection reaching up to thousands of images, rich content in the medical image, and human perception subjectivity.

In aim to overcome these difficulties, different image retrieval systems were suggested. The image retrieval systems can be classified according to the type and the nature of the features that are employed for the indexing process (Madugunki, Bormane, Bhadoria & Dethe 2011). Figure (2.1) depicts the detailed classification of the medical retrieval systems.

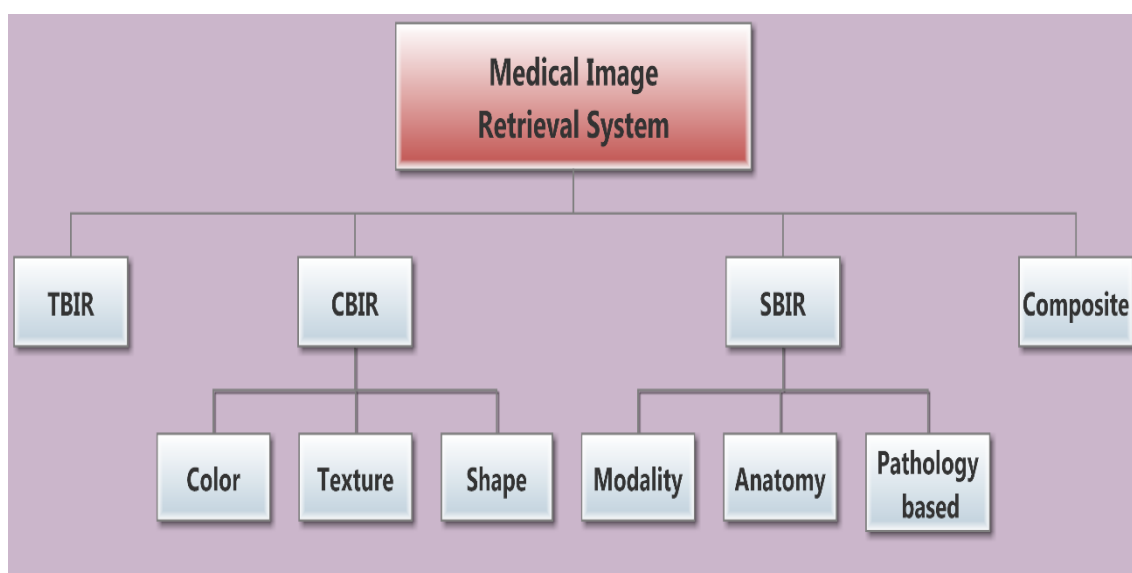


Figure 2.1: Image Retrieval Systems Classification (Madugunki, Bormane, Bhadoria & Dethe, 2011)

## **2.2 Text Based Image Retrieval**

In this type of retrieval systems, the digital images are simply indexed by text, or the metadata of the image which include: the ID number of the patient, the creation date, modified date, type of image, size of image, and any manual annotation on the content of the image itself. This type of system; when employed in image retrieval, is known as Text-Based Image Retrieval (TBIR) (Lacoste, Lim, Chevallet & Le, 2007).

These systems use the keywords and the associated text in images for querying items. Most hospitals and health care institutions used this type of systems referred to as Picture Archiving and Communication System (PACS) (Hussein, 2009). Many of the commercial systems use this retrieval technique, such as Flickr ([www.Flicker.com](http://www.Flicker.com)) and Google Images ([images.google.com](http://images.google.com)).

The core problems that associated the text based image retrieval systems reside in medical images annotations; where many of medical images annotations are hard to be expressed such as what is in the image, what does it invoke and what is it about.

On the other hand, annotations cannot be registered in complete manner and may include many spelling mistakes, or spelling differences or even weird abbreviations specifically medical ones (Müller, 2010).

## **2.3 Sketch Based Image Retrieval**

These types of systems use simple hand-drawn sketches as query items (images). Sketch Based Image Retrieval (SBIR) systems work by retrieving the images that have high similarity to a sketch made by a user, so it is called query by sketch (Yao, Li, Li,

Zhang & Ma, 2005). Typically, a sketch is a simple set of drawing lines (Arajujo, Crucianu & Gouet-Brunet, 2013).

Most of SBIR techniques mainly use the grid based or global descriptors for image matching (Eitz, Hildebrand, Boubekeur & Alexa, 2011); that means the image is divided into a regular grid and then descriptors are computed from each cell, which are then combined into a global image descriptor (Lin, Huang, Wang & Hsu, 2013).

The accuracy of this type of image retrieval is highly dependable on many factors include: The gap between the drawn sketch and the retrieved images and the different geometric transformations that may happen for both: sketch query image and the retrieved image in the database such as rotation and scaling (Abdulbaqi, Sulong & Hashem, 2014).

## **2.4 Content Based Image Retrieval**

The content-based medical image retrieval is based on the idea of indexing the medical images by their own visual content such as: texture, shape and colour instead of being manually annotated by text – based keywords (Arakeri and Reddy, 2013).

Most of content-based medical image retrieval systems were built in a very similar architecture for browsing and indexing/archiving medical images. In general, it consists of tools for visual features extraction, tools for storage and retrieval of these features, distance measurements and similarity computation, and the type of Graphical User Interface (GUI). This general system structure is shown in Figure (2.2).

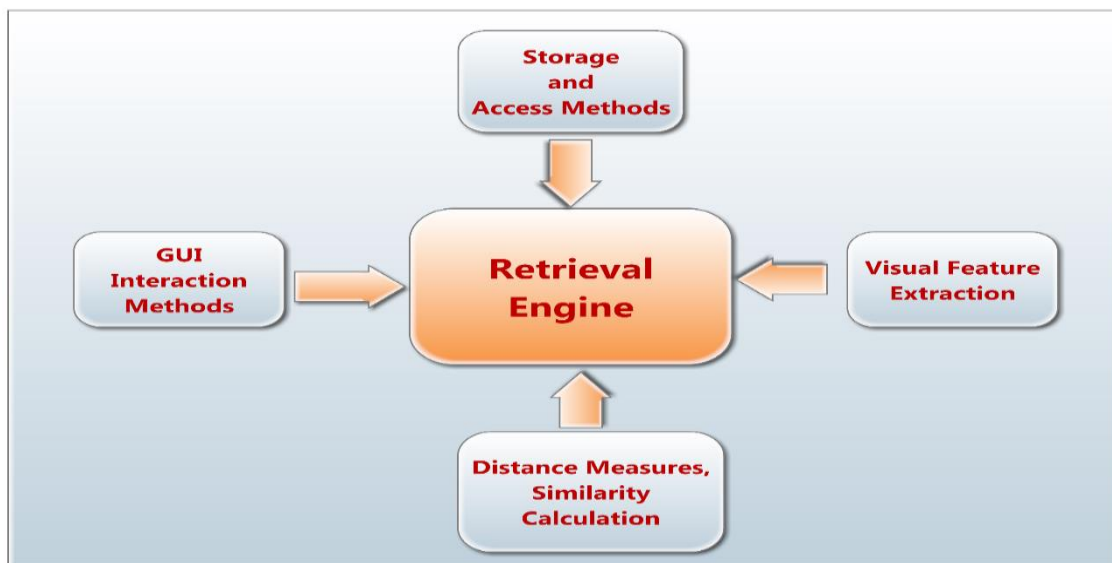


**Figure 2.2: General structure of All Content-Based Image Retrieval Systems (Müller, Michoux, Bandon & Geissbuhler, 2004).**

The algorithms used in the medical CBIR systems can be divided into three categories: Feature Extraction, Feature Selection, and Classification (Adegoke, Olarinoye, Omotayo & Olawuni, 2013).

Feature Extraction can be considered as a pre-processing step that removes the distraction variance from a specific dataset in order to enhance the performance of downstream regression estimators or classifiers (Burges, 2010).

Feature selection reduces the dimensions of the dataset that will be provided to the classification task. The overall accuracy of the CBIR system can be enhanced by increasing the number of features used in the classification task.

Various types of feature extraction techniques separately, or combined or even integrated in processing chains (Dópido, Villa, Plaza & Gamba, 2012) to improve the classification task of the medical CBIR system.

## 2.5 The Semantic Gap

The principal difference between text-based and content-based retrieval systems is that the human interaction is a requisite part of the former system. In general, humans tend to use the high-level features; or as called concepts, such as, text descriptors, specific keywords to interpret digital images, and measure their similarity, whereas the features that are automatically extracted using the computer vision tools are low-level features (low-level with respect to humans) such as colour, shape, spatial layout, and texture.

In general, there is no capability to build a direct link between the low-level features, and high-level human concepts. This is what is defined as a semantic gap (Yang & Zhu, 2012).

## 2.6 K Nearest Neighbours (KNN)

Clustering algorithms are considered one of the forms of non-linear analysis of data. The main function in the clustering process is to create subgroups; where the members of each subgroup are similar to each other and at the same time they are dissimilar to other subgroups members based on a particular similarity metric. The clustering techniques are divided into four main categories:

- **Hierarchical Clustering Techniques:**

These types of clustering approaches follow a Top-to-Bottom hierarchal way or vice versa. Initially, all data instances are put in one or different cluster(s), then, clusters are merged or divided in each iteration depending on some criterion which enhance the distinction process.

The main disadvantage of these methods is that they do not have reversible direction, namely, once the merger or division takes place, they cannot be re-assigned further on (Steinbach, Karypis & Kumar, 2000).

- **Grid-Based Clustering Techniques:**

In these types of clustering techniques; the sample space (or space of all data instances) is divided into a finite number of cells. Then, the clustering operations performed on each of the cells separately.

The processing time consumed in this type of clustering is relatively low in comparison with other clustering techniques and is dependent only on the number of cells that were created in each dimension and is independent of the number of data instances (Berkhin, 2006).

- **Partitioning-based Clustering Techniques**

In this type of clustering, a user-specified number of clusters ( $k$  clusters) are constructed out of  $n$ -samples of them by assigning one to each cluster until each cluster contains one sample at least. Thus, an iterative re-allocation is utilized to allocate samples to the defined clusters. To improve the partitioning, re-assigning data instances to other clusters in each iteration is performed.

The major disadvantage of this type of clustering resides in the dependency on initial assignments of centres where the accuracy of these methods varies according to varying initial assignment of centres (Berkhin, 2006).

Another disadvantage is that the convergence of these methods is not always assured, determining the number of clusters restricts the accuracy and the utility of these

methods. Examples of these methods: K-Means, improved K-Means and K-Medoids (Park and Jun, 2009).

- **Locality-based Clustering Techniques:**

These techniques of clustering employ the heuristic to create clusters where each cluster groups the neighbouring instances of data. An instance of data may belong to a specific cluster as long as it has more than an (k) number of instances within a specified radiuses (r) of it. Therefore, each instance in a specific cluster has (k) nearest neighbours within a radius (r) of it (Berkhin, 2006).

The key advantage of these techniques is their high capability to produce non-spherical clusters. However, they have the problem of incapability to produce good clusters; if the target data is a high-dimensional one. Examples of these techniques: KNN (Cover & Hart 1967), Novel KNN (Jivani, 2013) and the various versions of KNN.

KNN is considered as one of the most popular clustering techniques that belong to the locality-based clustering methods; that was found to be extremely effective in the field of text and documents categorization.

The core function of KNN classifier is to measure the similarity between the training data records P, and the input testing record by one of the available distance measures (Euclidean, Cosine, and Jaccard), where the KNN classifier keep the whole training dataset to perform this task.

The shorter the distance between the data points and testing vector, the more similarity we have. The final similarity score of a testing data vector being classified is the result of voting process of its Euclidean distances from the closest (nearest) K training data vectors.

Alternatively, the K-nearest neighbour classifier ranks the vectors' neighbours among the labelled training dataset vectors, and uses the class (label) of the K most similar neighbours to predict the class (label) of the new vector (Berkhin, 2006).

## **2.7 Literature Review**

A variety of techniques in this research field have been proposed and developed and several of image retrieval systems have been built for both research and commercial purposes (Kumar, Kim, Cai, Fulham & Feng, 2013).

### **2.7.1 Non-Medical Content-Based Image Retrieval**

**Mathew, Balas & Zachariah (2015)** presented a novel content based image retrieval model based on the Convex Hull Area Ratio (CHAR). The proposed technique was based on the idea of comparing the convex hull geometry of the query image to that of the database image in terms of CHAR as a relative metric.

The performance of the proposed model was evaluated by querying different images and it achieved high retrieval efficiency in terms of recall and precision.

**Qazi & Farid (2013)** proposed an efficient image retrieval approach that uses an image feature descriptors using localized multi-texton histogram. The proposed method extracts a unique feature vector for each image in the image database based on its texture, colour and shape. The proposed technique has two major stages: the image is split into small blocks of equal sizes, and then the texture orientation of each block is filtered with a set of pre-specified textons.

In the second stage, a co-occurrence relation is built from the orientation and the filtered texton image, which gives a feature vector. The feature vector of the query image is compared with the feature vectors of the stored images using the Euclidean distance metric to obtain the most similar image.

**Lee, Rhee & Kim (2012)** suggested an image retrieval approach based on a weighted combination of both colour and texture to wavelet transform depending on both spatial-colours and the statistics of second-order. The experimental results exemplified in the precision metric value, and the f-score value proved the effectiveness of the proposed image retrieval technique in the multi-resolution image search application.

### **2.7.2 Medical Content-Based Image Retrieval**

**Nangai (2015)** suggested an automatic brain tumor medical image classification based on Hyperbolic Hopfield Neural Network (HHNN) machine learning technique. The proposed classification technique consists of three major phases: Segmentation, Texture extraction, and Classification.

The segmentation is conducted using Enhanced Markov Random Fields Approach (EMRF). The experimental results of the proposed technique showed high efficiency in automatic image classification in comparison with other existing schemes.

**Esther & Sathik (2014)**, proposed an accurate and effective content based brain tumor image retrieval system. This novel retrieval system was built on two techniques: one technique is to remove the artifacts in brain image while the other used Fuzzy Expectation Maximization Algorithm (FEMA).

The proposed system used shape features as 2D-Zernike moment and used soft computing technique of Extreme Learning Machine (ELM) as the retrieval engine with ensemble of metric distances include: {Euclidean Distance, Quasi Euclidean, City Block distance and Hamming Distance}.

The experimental results reported for this systems showed high retrieval accuracy where the achieved high precision of (78%) for Chi-square distance and recall of (95.23%) for the same metric distance.

**Madheswaran & Dhas (2014)**, proposed an adroit Naïve Bayesian based sequence mining technique for the prediction of MRI brain tumor images. The proposed brain tumor retrieval system is composed of three major stages: brain MR images pre-processing, features extraction, and retrieval stage.

In the first stage, the noise in the brain MR image is removed via one filter chosen through analysing five filters. Then the spatial features of the brain MR images are extracted via Greystone Spatial Dependence Matrix (GSDM), then these extracted features are processed by joint entropy and GA technique to determine a subset of these features. In the final stage, Naïve Bayesian classifier is used in order to predict the brain MR images if it is normal, not normal (benign or malignant).

**Huang, et al. (2014)**, presented a study aimed to develop a content- based image retrieval system. For the retrieval of T<sub>1</sub>-weighted contrast-enhanced MR (CE-MR) images of the brain tumor. The system used the rank Error-based metric learning (REML) distance learning algorithm in the indexing process whereas the process of feature extraction conducted learning. The system achieved a mean average precision that

reached up to 90.8% and the precision could reach 13.1% if the top -10 medical images are retrieved by the system, which is considered a good indication of the high efficiency and feasibility of the  $T_1$ -weighted CE-MR images retrieval.

**Karthikeyan & Vembandasamy (2014)**, presented a study on the CBIR for brain tumor in magnetic resonance imaging where the main focus of the proposed system was the practical use of CBIR system for clinical purposes to differentiate between normal and abnormal brain MR image on the basis of distinctive feature.

The proposed system utilizing colour, shape and texture feature extraction techniques where in case of colour features, the proposed system used HSV colour model instead of RGB colour model. The shape features were extracted by applying segmentation or edge detection to the brain MR image into two types: Regional base and boundary base. Finally, the texture features were extracted based on statistical and structural approaches.

The support vector machine technique was used in the classification phase via dataset of (90) normal and abnormal brain MR images. The proposed system classify the abnormal brain MR image with recall of (100%) and classify the normal brain MR images with recall of (96%).

**Singh (2014)**, proposed a new approach for brain tumor detection based on the KNN classification algorithm as a classifier whereas the K-means clustering was used as a segmentation tool. The main principle goal of the proposed system is to segment the brain MRI images effectively to enhance the identification of brain tumor. The proposed system achieved an 87.0% accuracy using only textural features.

**Chitari & Bag (2014)**, suggested a brain tumor detection system in aim of reducing the effort needed by radiologists to detect any abnormality found in an MRI image and classify property. The principle idea of the system is to find the lesion present in MRI image and to classify them. The system consists of three stages: image pre-processing, the feature extraction, and KNN classification algorithm. The system achieved an accuracy of 97.3% which is considered better than other classification technique.

**Arakeri & Reddy (2013)**, proposed an intelligent content- based retrieval for brain tumor diagnosis purposes. The system retrieves magnetic resonance images that bear the same pathology of the brain from 820 MR data set of medical images.

The system design assists the radiologist in the process of diagnosis of brain tumor by using a clustering technique with principle component analysis (PCA). The KD-tree clustering technique groups sub – class features into clusters depending on the modified K- means then the reduced feature set is then indexed utilization a KD-tree. The experimental results proved the effectiveness of the system and the high viability of clinical application.

**Arakeri & Reddy (2012)**, suggested a two- level hierarchical CBMIR system for brain tumor. The proposed CBMIR system addresses the problem of misalignment of magnetic resonance image slices and the problem of semantic gap that happened due to the gap between the extracted low-level feature of MRI image and the high level features of brain tumor.

Several set of texture and rotation invariant shape features are employed to distinguish between brain tumors at each level. The experimental results show a promising retrieval results exemplified by the high achieved precision of 97% and recall of 95.78% in a comparable retrieval time.

**Yang, et al. (2012)**, presented a content-based image retrieval technique for T<sub>1</sub>-weight contrast-enhanced MRI (CE-MRI) images of brain tumors in aim of enhancing the diagnosis assistance. The proposed system built was based on margin information descriptor (MRI) that has the capability to describe the characteristics of the tissues that surround a tumor area. That led to more specific representation of image contents.

The indexing and retrieving of images is conducted depending on the maximum mean average precision project (MPP) distance metric learning algorithm. The experimental results of the tested proposed system proved its high retrieval performance through mean averaged precision of 87.3% and a precision of 89.3% when the top 10 images are retrieval by the system.

**Keysers, Ney, Wein & Lehmann (2003)**, developed a sustained effort in the field of CBIR of X-ray medical images in aim of supporting the medical diagnosis in hospitals and called it the Image Retrieval in Medical Applications (IRMA) project. The proposed technique was divided into seven interdependent stages: in the first stage, the medical images were cauterized and grouped based on global features. In the second stage, the geometry and contrast are used to build the registration. In the third stage, the local features are extracted. In the fourth stage, the feature selection is conducted depending on the query and category. In the fifth stage, multi-scale indexing, and semantic knowledge

identification is performed. In the final stage, the retrieval is done based on the previous stages.

**Marchiori, et al. (2001)**, present a new model for CBIR that especially targeted for the medical field by first predicting the disease class of the query image where the CBIR system is customized to retrieve only the very similar image with the same diagnosis. The system was evaluated by eight medical doctors, where the average diagnosis accuracy increased from 32.5% to 64.6%.

## Chapter Three

### Proposed CBBIR System Algorithm: Implementation and Methodology

#### 3.1 Introduction

The image retrieval problem is becoming recognized on a wide-scale; therefore, the search for possible solutions becomes an increasingly active area of research and development. (Lew, Sebe, Djeraba & Jain, 2006) have elaborated the major issues that are associated with classic techniques used for image indexing, which have led to the raise of interest in the approaches followed in images retrieval, based on the idea of automatically-derived attribute (features) such as texture, colour, and shape. Where, it is exemplified in a technology referred to as Content-Based Image Retrieval (CBIR).

CBIR can be defined as the technique used to retrieve images from an image database based on its content or concisely, it can be defined as query by image contents. (Arakeri & Reddy, 2013).

One important application of CBIR is the medical field. Several health care institutions and establishments have started using a variety of CBIR systems to improve and enhance the diagnosis and treatment processes of different diseases. In this research, we introduce a medical CBIR technique based on the *K Nearest Neighbors* (KNN) algorithm, and ensemble of similarity measures and prediction refining to enhance the process of the brain tumor diagnosis.

Our proposed system; Content-Based Brain Image Retrieval (CBBIR) system, the implementation consists of two phases: On-Line and Off-Line Phases.

### 3.2 The Proposed CBBIR System Framework

The general block diagram of the proposed CBBIRS for the diagnosis of brain tumor is shown in Figure (3.1).

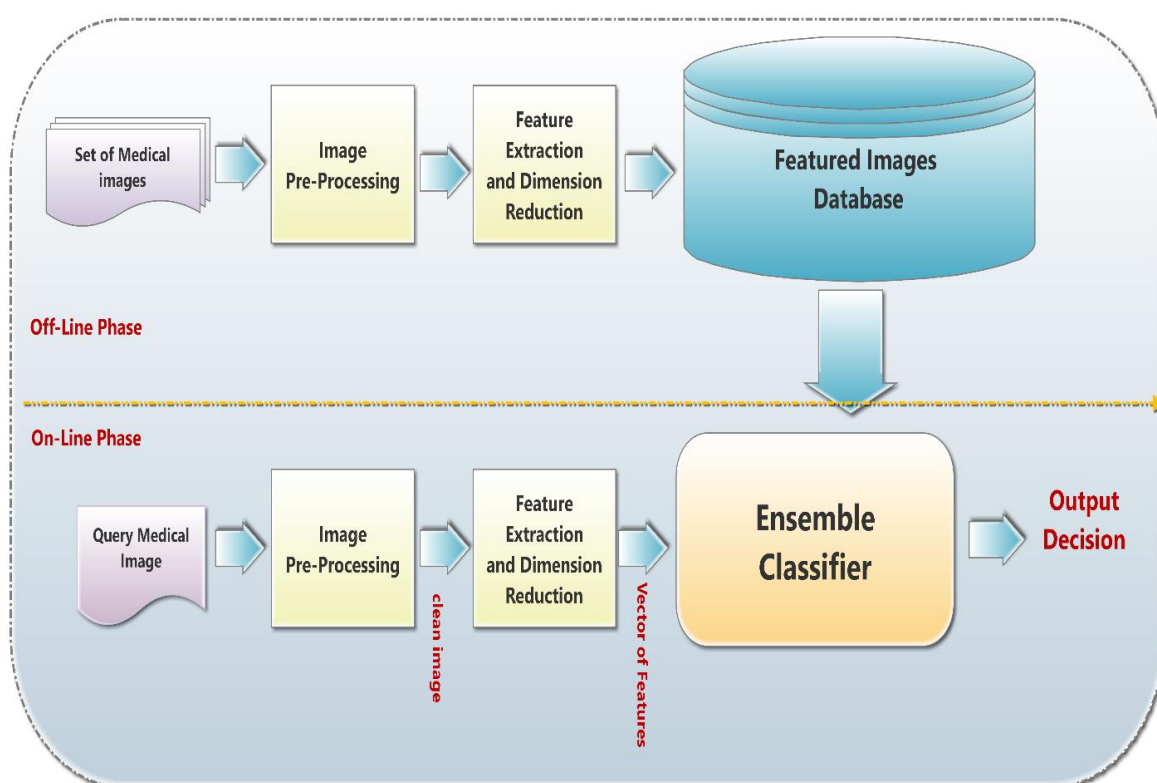


**Figure (3.1): Framework of the proposed CBBIRS**

As shown in Figure (3.1), our proposed CBBIR system consists of two major phases: Database building (off-line) phase and image query processing (on-line) phase. In the off-line phase, the MR images of brain (belong to four brain diseases) stored in the image database are pre-processed by image de-noising and automatic brain tumor zones segmentation. The processed MR brain images are then processed in seek of

features extraction that will be collected to compose a feature vectors database that will be used in the classification stage in the on-line phase.

Similarly, in the on-line phase, the MR brain query image is pre-processed and then processed to extract the query vector of features that will be compared with feature vectors in the features database using ensemble of different types of similarity metrics including Euclidian, Chi-Square, Chebychev, Cosine, Correlation, Spearman, Relative Deviation, Minkowski, Cityblock, Mahalanobis, and Normalized Euclidian.

The addition of ensemble of similarity metrics will enhance the diagnosis process in finding the similarity between different brain diseases including brain tumor and refining the prediction results. The database is indexed using the KNN classifier using the most similar pathology bearing MR images of brain tumor of the MR brain image database. The classification process and the ensemble of similarity measures is illustrated in Figure (3.2).

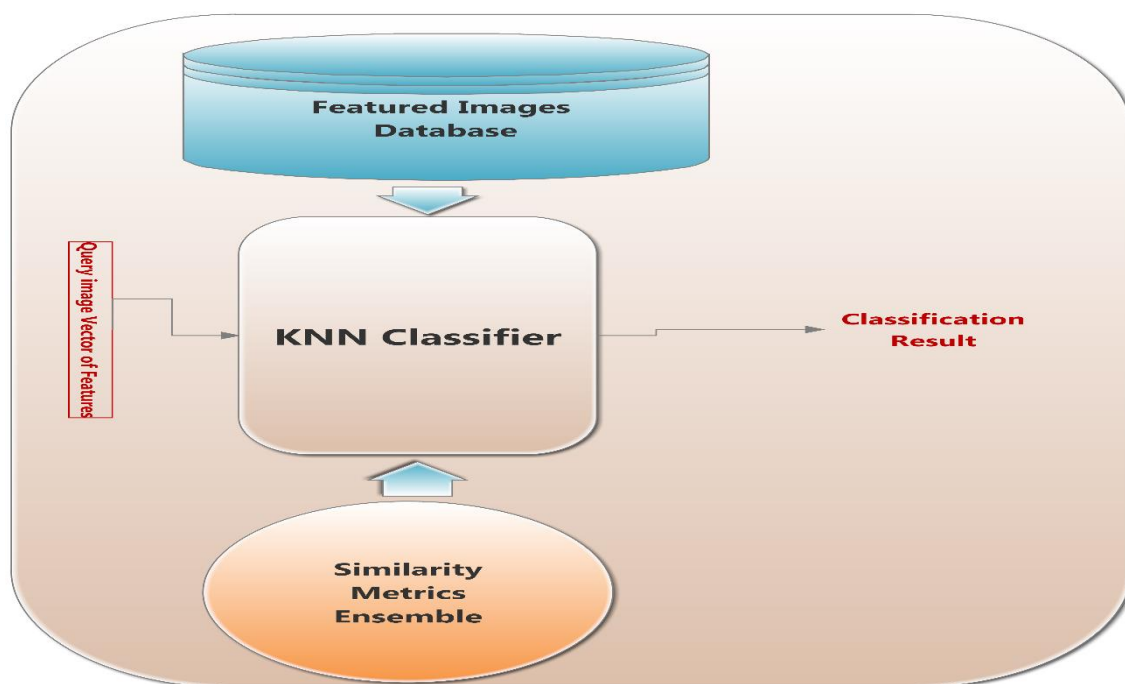


**Figure (3.2): Framework of Proposed Retrieval Engine**

### 3.3 PHASE (1): Brain MRI Dataset Pre-Processing

Although this phase is the first step in our system implementation, it is of essential importance to the next phases of CBBIR system. In this phase, we pre-process the raw brain MR images not only in terms of dataset collection and noise removal, but in terms of MR image regional processing in order to enhance the process of colour, shape and texture features extraction. This phase consists of major stages that are explained in the following subsections.

#### 3.3.1 Brain MRI Dataset Collection

Our data set consists of MR brain images of (126) patients diagnosed in one of four brain diseases categories: (1) Neoplastic disease or brain tumor which represent the core of our proposed CBIR system. (2) Cerebrovascular disease (stroke or brain attack) (3) Degenerative diseases and (4) Inflammatory or infectious diseases.

The patients' ages were in the range of (20 -95) years. The images were acquired from the **Ischemic Stroke Lesion Segmentation (ISLES)** (<http://www.isles-challenge.org/>) which is a challenge (2015) that aim to provide a public dataset that reflects the diversity of the problem and a platform for a fair and direct comparison of methods with suitable evaluation measures. Thus, the scientific progress in the field of medical image processing is promoted.

We give each brain MR image a number corresponds to the band that the brain disease belongs to, namely, the brain MR images that belong to the brain tumor band take number from [1 to 100], for example if the brain MR image has the number of [37] then it belongs to brain tumor (patient case is brain tumor). Now, we give a number

between [101 to 200] to each MR brain image that was classified as cerebrovascular brain disease, and a number between [201 to 300] to each MR image that belongs to degenerative brain disease. Finally, we give a number between [301 to 400] to each brain MR image that is diagnosed as inflammatory or infectious disease.

Accordingly, we have encoded the available brain MR images according to the category of brain disease that the image belongs to. Table (3.1) illustrates the range of numbers and the corresponding disease category.

**Table (3.1). The Range of Numbers and the Corresponding Disease Category**

<b>NO</b>	<b>Brain Disease category</b>	<b>Range</b>
1	Neoplastic disease or brain tumor	1-100
2	Cerebrovascular disease (stroke or brain attack)	101-200
3	Degenerative diseases	201-300
4	Inflammatory or infectious diseases.	301-400

### 3.3.2 Brain MRI Dataset Noise Removal

The Magnetic Resonance Images (MRI) are often corrupted by the noise added to them during the process of image acquisition. The important information that exists in the image which makes the process of image analysis a difficult task.

We proposed to use a median filter and low-pass filter to enhance the quality of MR images. The use of median filter leads to smooth edges of the image, which improves the perceptibility of structures in the brain.

### 3.3.3 Why Magnetic Resonance Imaging (MRI)

Magnetic Resonance Imaging is the most broadly used modality for the diagnosis of brain diseases in general and for brain tumors in particular where it is considered as the most broadly used modality for brain tumor analysis (DeAgelis, 2001 and Wen, et al., 2010).

Measuring the size and the shape of tumor by a segmentation method is considered the best way of brain tumor diagnosis. However; Segmentation is often done totally in a manual manner; a very monotonous and time consuming task.

Since MRI is a non- invasive technique, this will yield good soft tissue contrast. Other imaging modalities can be used along with MRI in order to obtain an enhanced view and more exact information; such as Computed Tomography (CT), Magnetic Resonance Spectroscopy (MRS), and Position Emission Tomography (PET).

However, MRI remains the most accepted standard. Therefore, in this thesis, we will use MRI images in the process of medical images retrieval. One of the properties of MRI images that make it a very versatile tool is the possibility to produce noticeably different types of tissues contracts varying excitation and times of repetition.

Due to the appearance and the nature of brain tumors, one sequence of MRI is not adequate to segment the whole tumor entirely including all its sub regions (regions inside a tumor and around it). Currently, a variety of MRI sequences for diagnosis and portraying purposes of tumor zones (Bauer, Wiest, Nolte & Reyes, 2013).

These sequences include:  $T_1$ -weighted MRI ( $T_1$ ) and  $T_2$ - weighted MRI with contrast enhancement ( $T_{c1}$ ),  $T_2$ - weighted MRI ( $T_2$ ) and  $T_2$ - weighted MRI with Fluid Attenuated Inversion Recovery ( $T_{2FLAIR}$ ) ( Bauer, Wiest, Nolte, & Reyes, 2013).

### 3.3.3.1 What is Image Contrast?

Contrast is defined as the separation between the darkest and brightest areas of an image. Increasing contrast leads to an increase in the separation between dark and bright regions, making shadows darker and highlights brighter. Figure (3.3) illustrate this concept (Tang, Peli & Acton, 2003).



**Figure (3.3): The effect of contrast increasing**

Whereas the decreasing contrast brings the shadows up and the highlights down to make them closer to one another as shown in Figure (3.4).

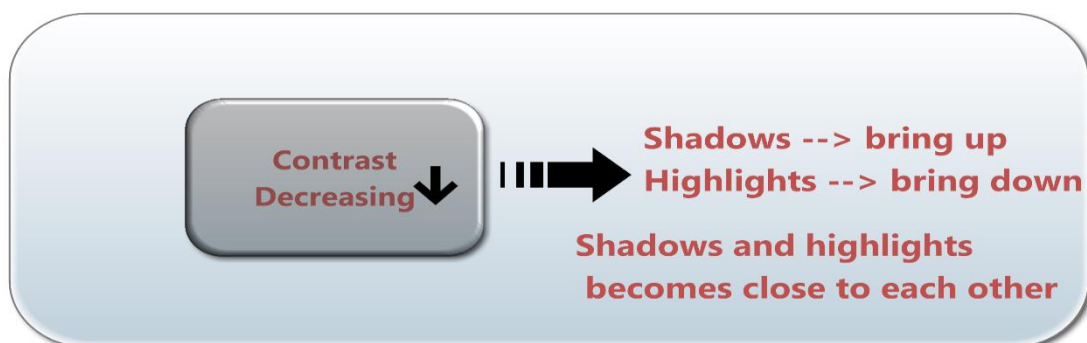


**Figure (3.4): The Effect of Contrast Decreasing**

Adding contrast usually adds "pop" and makes an image look more vibrant while decreasing the contrast can make an image look duller (Tang, Peli & Acton, 2003).

### 3.3.4 What is the Difference between MRI scans: $T_1$ , $T_{1c}$ , $T_2$ and $T_{2FLAIR}$ ?

MR images can be acquired with several techniques (pulse sequences) and acquisition parameters (echo time, TE, repetition time TR) resulting in different image contrasts. The four image types mentioned in the above question belong to the most common MR acquisitions (Bauer, Wiest, Nolte, & Reyes, 2013):

**$T_1$ -weighted MRI:** In this type, the image contrast is based predominantly on the  $T_1$  (longitudinal) relaxation time of a tissue, tissue with short  $T_1$  relaxation time appears brighter (hyper intense).  $T_1$ -weighted is considered the most commonly used sequence in aim of structural analysis and it make the annotation of healthy tissues possible in easy manner.

**$T_2$ -weighted MRI:** an image contrast is based predominantly on the  $T_2$  (transverse) relaxation-time of a tissue where tissues with long  $T_2$  relaxation time appears brighter (hyper intense).

**$T_{1c}$ -weighted MRI:** after administration of contrast media: many tumors show signal enhancement after administration of contrast agent; administration means that not long  $T_2$  and not short  $T_1$ , We control the contrast to achieve best signal enhancement).

**$T_{2FLAIR}$  MRI:** Attenuated Inversion-Recovery MRI: bright signal of the CSF (cerebrospinal fluid) is suppressed which allows a better detection of small hyper intense lesions. The effect of increasing CSF on the small lesions detection as shown in Figure (3.5)

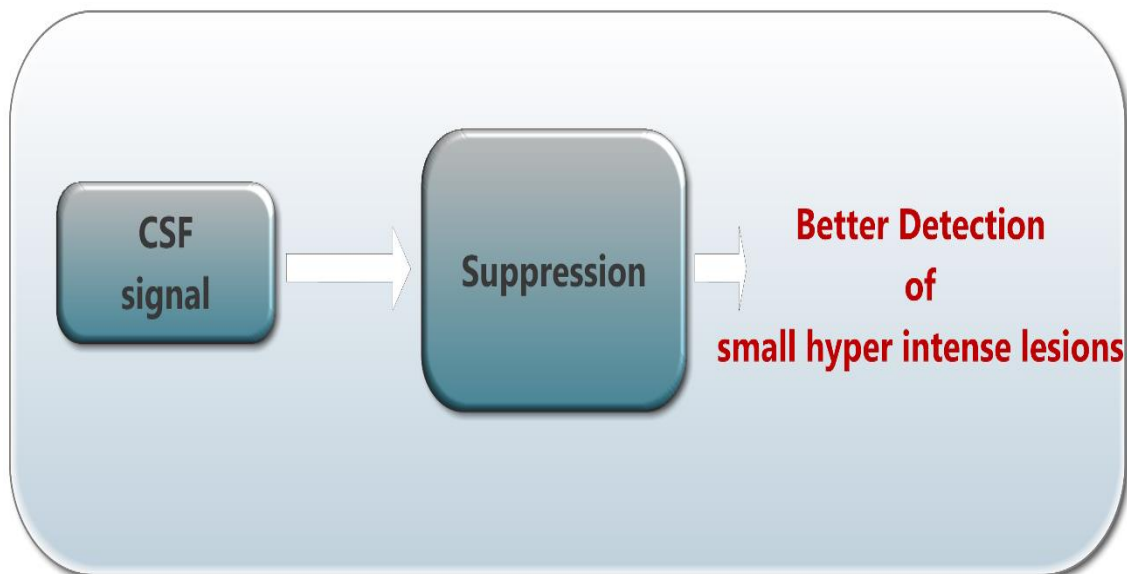


**Figure (3.5): Steps of Attenuated Inversion-Recovery MRI mechanism**

Segmentation of tumors in a manual manner will probably be the most successful if several (or better all) of these images are combined and better identification will be obtained if all of MRI types are combined altogether.

In our thesis, we overly all types of the MRI images sequences for each patient.

Figure (3.6) elaborate the importance of this step

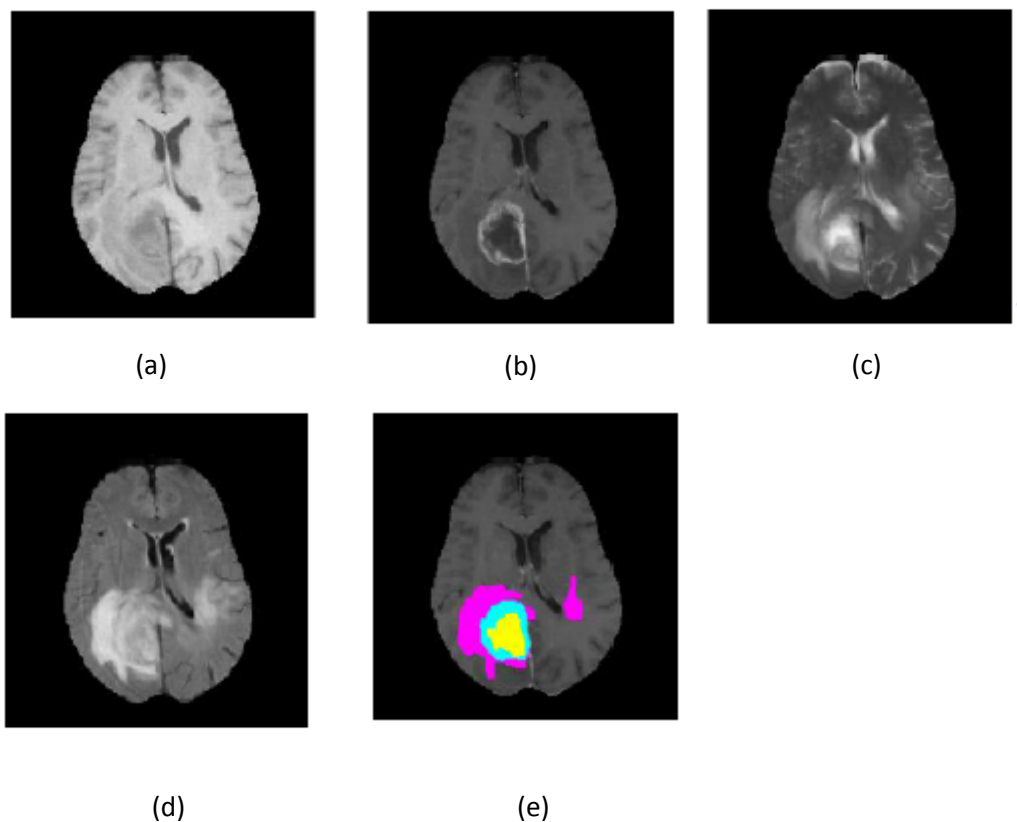


**Figure (3.6): One axial slice of an MR image of a high-grade glioma patient.**

**From left to right: (a) T<sub>1</sub>-weighted image (b) T<sub>1c</sub>-weighted image (c) T<sub>2</sub>-weighted image (d) T<sub>2FLAIR</sub>-weighted image (e) manual segmentation into necrotic (yellow), active (green), edema (pink) tumor compartments.**

The overlaying process enable us to enhance the contrast agent accumulation which in turn make the borders of the tumor brighter. Therefore; in this sequence of MRI images, the necrotic and the active tumor regions can be identified easily.

The edema that surrounds the tumor zone appears bright whereas T<sub>2</sub> flair makes the separation of edema region from the cerebrospinal fluid (CSF) due to the fact that the free water signal has been suppressed.

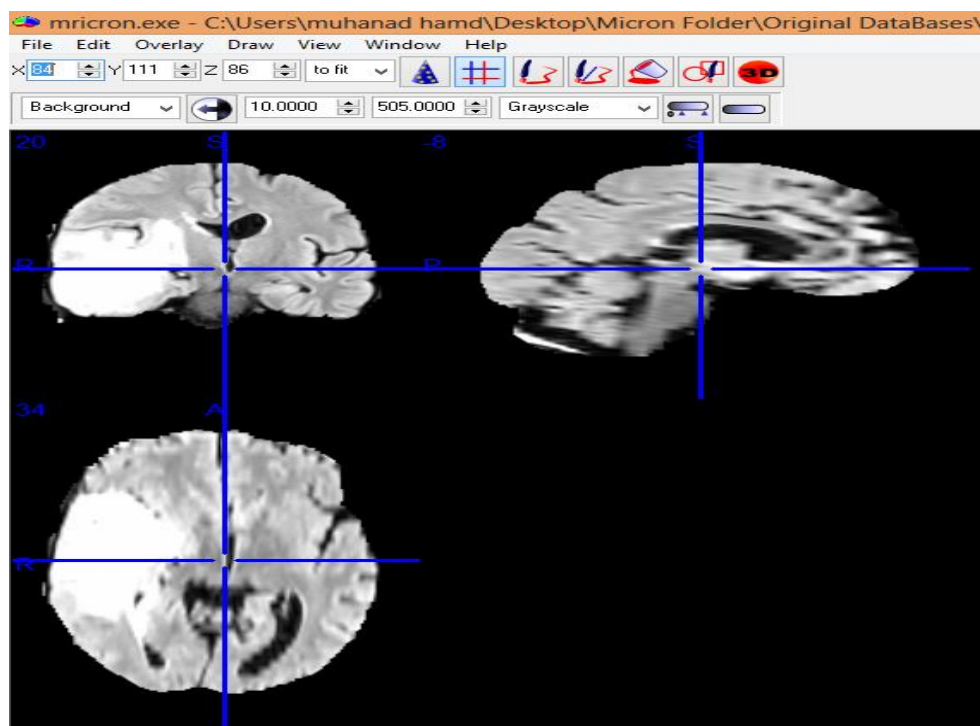
### **3.3.5 Magnetic Resonance Images Viewing and Overlaying**

BRAT 2015 and BART 2013 databases contain MRI images in {'.mha'} form and each patient has Four MRI sequence (T<sub>1</sub>, T<sub>1C</sub>, T<sub>2</sub>, T<sub>2flair</sub>) which creates the need for special software that can open and view these types of MR images and at the same time enables you to overlay them in order to obtain more enhanced view of brain tumor.

In order to view and overlay our MRI images, we used MRICron (available online at: <http://www.mccauslandcenter.sc.edu/mricron/>) to allow the view of medical images, and overlay multiple regions of interest at the same time.

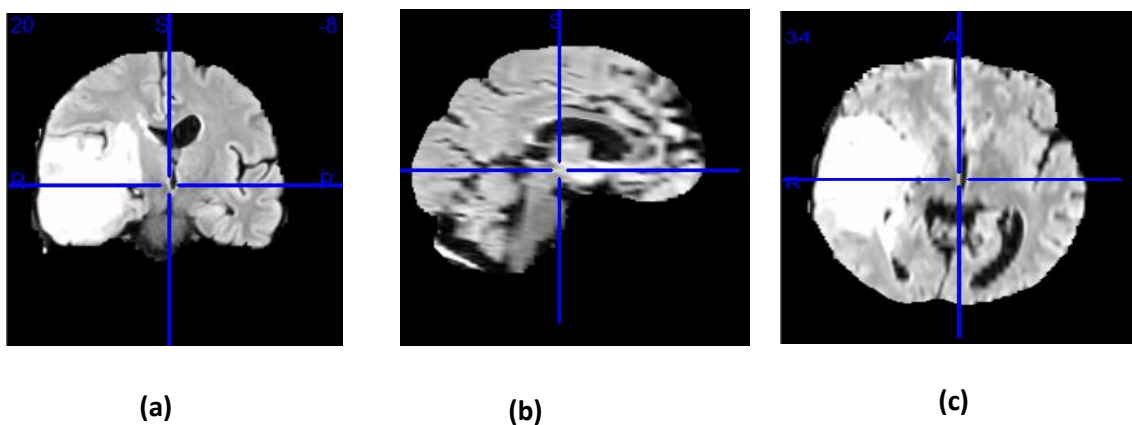
Using the software, we have the capability to expand the MR image from its medical format {'.nifti' or '.mha.'} available in BRAT 2015 and BART 2013 databases to {'.BMP', '.JPEG', '.PNG' or '.TIF' } formats.

Figure (3.7) shows the main (home) window of MRICron CAD that shows one of our MR images (brain tumor case).



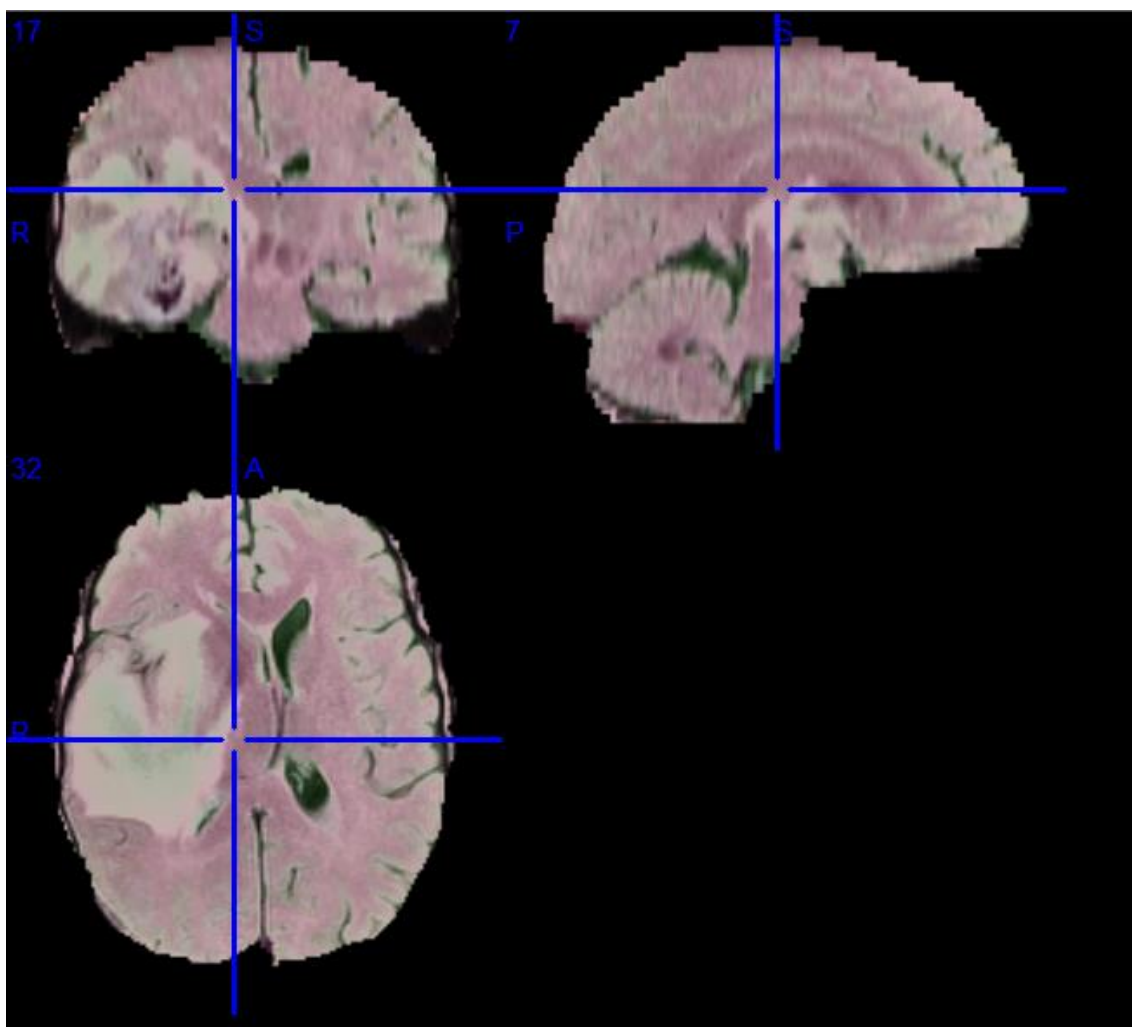
**Figure (3.7): Axial, Coronal and Sagittal Displays of the Brain MR Image**

Figure (3.7) shows the Axial, Coronal and Sagittal displays of the brain MR image under consideration. For more detailed view, Figure (3.8) shows these types of MR image displays.



**Figure (3.8): (a) Coronal (b) Sagittal (c) Axial Displays**

We use the axial MRI display and convert it to {'.BMP'} format via MRIcron CAD. Now, the next stage is to overlay the different types of MR image, namely, {T<sub>1</sub>, T<sub>2</sub>, T<sub>1c</sub>, and FLAIR} in one enhanced MR image. Then, we extract the axial view and convert it to '.BMP' file format as shown in Figure (3.9).



**Figure (3.9): The final View of an overlay Brain Tumor MRI Image**

Figure (3.10) illustrates the process of overlying using MRIcron software where the MRI image is called and viewed in its sequences and finally after overlaying the brain tumor and its zones and boundaries appears distinguished in an enough manner.

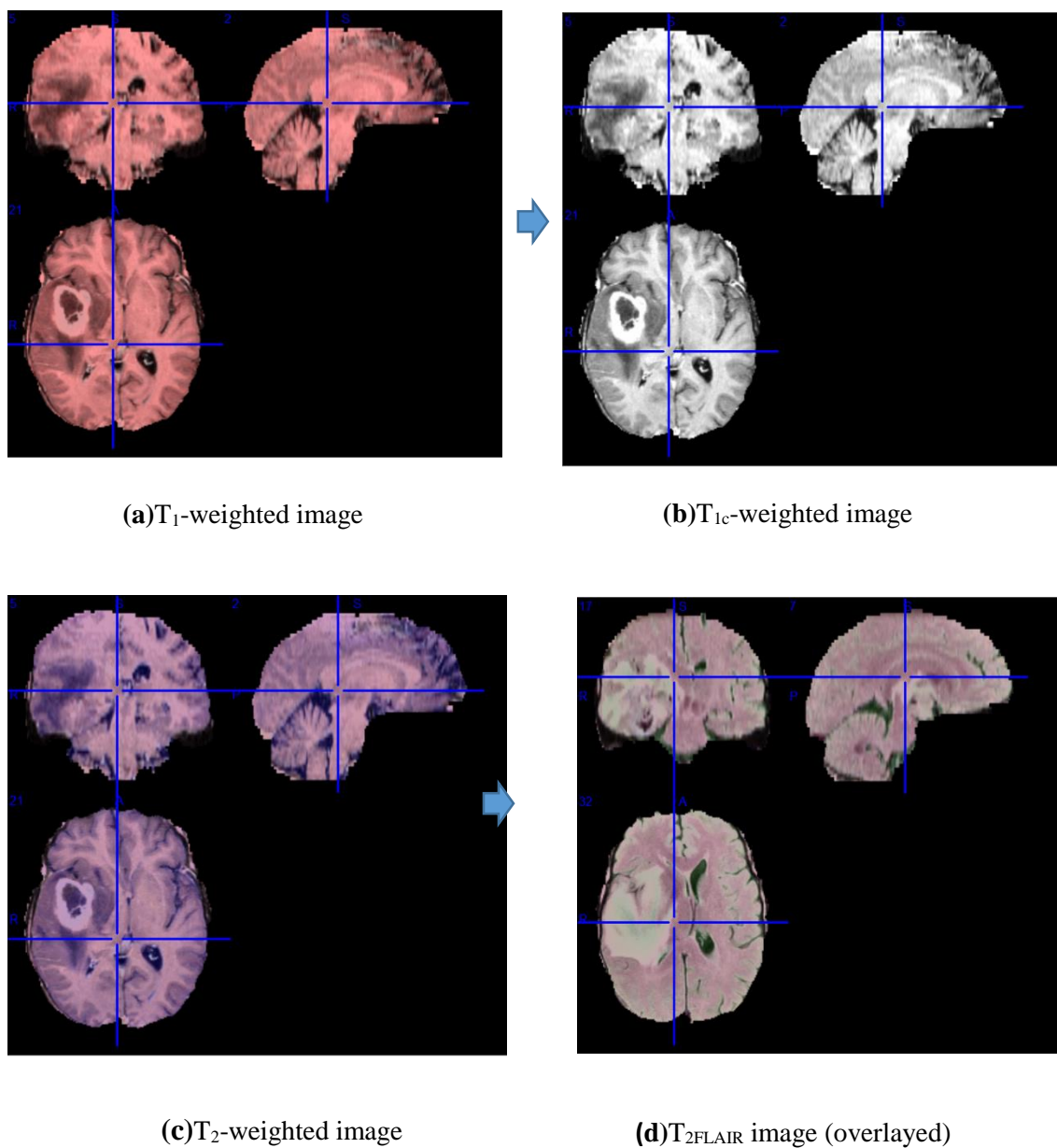


**Figure (3.10):** (a)  $T_1$  weighted MRI image layer (b)  $T_{1c}$  weighted MRI image layer  
 (c)  $T_2$  weighted layer (d)  $T_{2FLAIR}$  MRI image layer (final overlay image)

Moreover, MRICron enables us to see the "big view" or viewing a series of slices of the currently open MRI volume. As illustrated below in Figure (3.11)



**Figure (3.11): The Slices of a Brain Tumor MR Volume Image**

In order to create the database that will be used in our proposed CBMIR system, All MRI will have viewed, overlaid and then converted from {'. mha'} medical image file extension to {'.bmp'} image file extension. As shown in Figure (3.12).

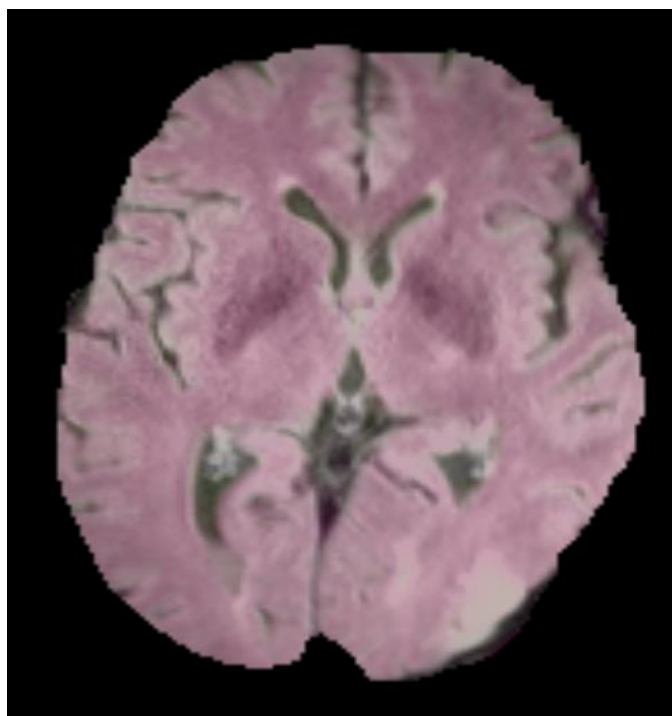


**Figure (3.12): The '.bmp' Format of Final Brain MR Image.**

To simplify the classification task, and in order to make it a dynamic duty, many proposed techniques and algorithms are fully automatic; which often use machine learning techniques. As noted above the zones of brain tumor were segmented manually. In addition, it is much easier for the human eye to different between the colour amount then the gray scale amount in an image.

In medical radiology, the clinically useful information can be extracted out of variations in the highly localized regions of the MR image (Arakeri & Reddy, 2012). Therefore, in our research, and in order to obtain enhanced performance in the process of content based medical image retrieval, we let the MRI images of our database to undergoes an automatic segmentation using colour substitution and quantization with specific set of colours.

That means we quantized the image colours into specific set of colours used to represent the MRI image; which giving us a more bounded view of brain tumor zones and more distinguished view. Figure (3.13) elaborates this idea, where we use three levels of quantization, and test our proposed CBMIR system using each quantization level and compare the resulted performance, then we choose the best level that yields the best performance.

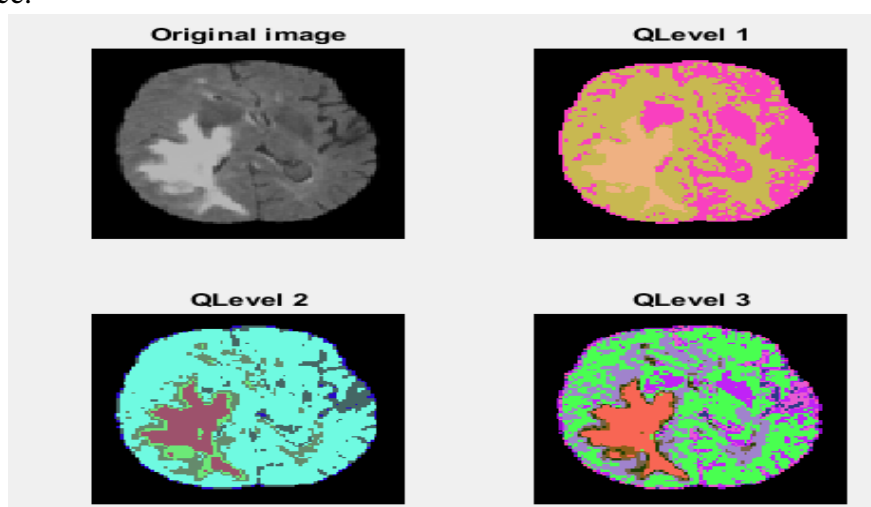


**Figure (3.13): Brain Tumor Automatic Zones Segmentation in Three (n) Levels**

### **3.4 Features Extraction and Dimensions Reduction**

In our thesis, we have used a novel hybrid combination of colour, shape and texture features extraction techniques which in turn lead us to high competitive retrieval performance.

#### **3.4.1 Colour Features Extraction**

This type of features descriptor is considered the most straightforward one that is widely used in CBIR systems due to its simplicity (Chary, Lakshmi & Sunitha, 2012).

Colour is considered a robust descriptor that leads to high simplification in the process of objects identification of a query image (Gonzalez, Woods & Eddins, 2004). In addition, it is also considered as one of the most important visual features that are most frequently used by content based image retrieval in general and content based medical image retrieval in particular.

In case of medical images, the participation of colour element is excessively limited since the majority of medical images come in grey scale. Therefore, the choice of colour features that best describe the MR images is a hard task in our situation. In our research, we have used colour histogram, colour sets, colour moments and colour correlogram to represent the colour features of a brain MR image. On the other hand, we highly depended on the texture features in order to identify the brain tumor, rather than colour features even though it play an important role in the classification phase.

Once the suitable colour space have been selected, an efficient colour descriptor should be appropriately chosen in order to represent the colour of both global and regional areas of the MR image under consideration.

A variety of colour descriptors have been suggested, implemented and realized for various representation schemes such as: Colour Moments (Stricker & Orengo ,1995), Colour Texture Moments (Yu, Li, Zhang & Feng, 2002), Colour Edge (Gevers & Stokman ,2003), Colour Histograms (Ouyang & Tan, 2002), Colour Texture (Guan & Wada ,2002) and Colour Correlograms (Moghaddam, Khajoie & Rouhi, 2003).

In our research, we have used: Normalized Colour Histogram, Colour Moments and Correlograms as colour features extractors where they represent adequate descriptors of the colour contents of the brain MR image and in an accurate manner that is suitable to this type of difficult and colour-constrained MR images. The following sections discuss these descriptors in more detail.

#### **3.4.1.1 Colour Sets**

Colour sets are proposed by (Smith & Change, 1997) as an approximation to colour histogram to facilitate fast search over image databases of large scale. Colour sets can be defined as a selection of colours from the quantized colour space (Rui, Huang & Chang, 1999).

Originally, our database is in RGB colour model, but in order to reduce the size of features set, all colours are quantized into 64 (4x4x4) colours in the RGB colour space first. This step is important before colour moments or colour correlogram extraction as if the number of quantized colours increases, the retrieval speed will be decreased.

### 3.4.1.2 Colour Histogram

The colour features extraction out of image content requires an appropriate colour space and efficacious colour descriptors. The main goal of proper colour space is to make the colour specification more smoothly and more accurate (Wei, Li & Wilson, 2005).

Each colour in the colour space is represented by a single point in a coordinate system where the different colours are defined as the linear combination of the bases of the coordinate system.

A variety of colour spaces have been proposed and implemented depending on the application under consideration. Such as RGB, HSV, YCbCr, XYZ, YIQ, YuV,  $L^*a^*b$ ,  $U^*V^*W$ ,  $L^*V^*W$ ,  $L^*u^*v$ ,  $I_1I_2I_3$ , HSL, and rgb (Shih & Liu, 2005).

In general, there is no agreement on the best colour space to be used in the content based image retrieval. However, a proper colour system is needed to ensure one essential issue: Perceptual Uniformity. We will use the (HSV) colour model instead of Red, Green, and Blue (RGB) colour model due to the fact that the HSV colour model is more close to the human perceptual than RGB model

Although RGB colour space is broadly used as a system for colour image representation, it is not appropriate to be used in CBIR systems since it is perceptually non-uniform. Moreover, it is a device- dependent colour system (Gevers, 2001).

The most considerably used technique is the conversion from one colour representation to an appropriate one via equations that are used to transform from one colour space to another.

Frequently, RGB colour space is converted to HSV, CIE L\*a\*b or CIE L\*u\*v colour spaces that have high perceptual uniformity (Li and Yuen, 2002). Figure (3.14) shows the most of available colour spaces and the most perceptual uniform ones that can be efficiently used in the content based image retrieval systems.

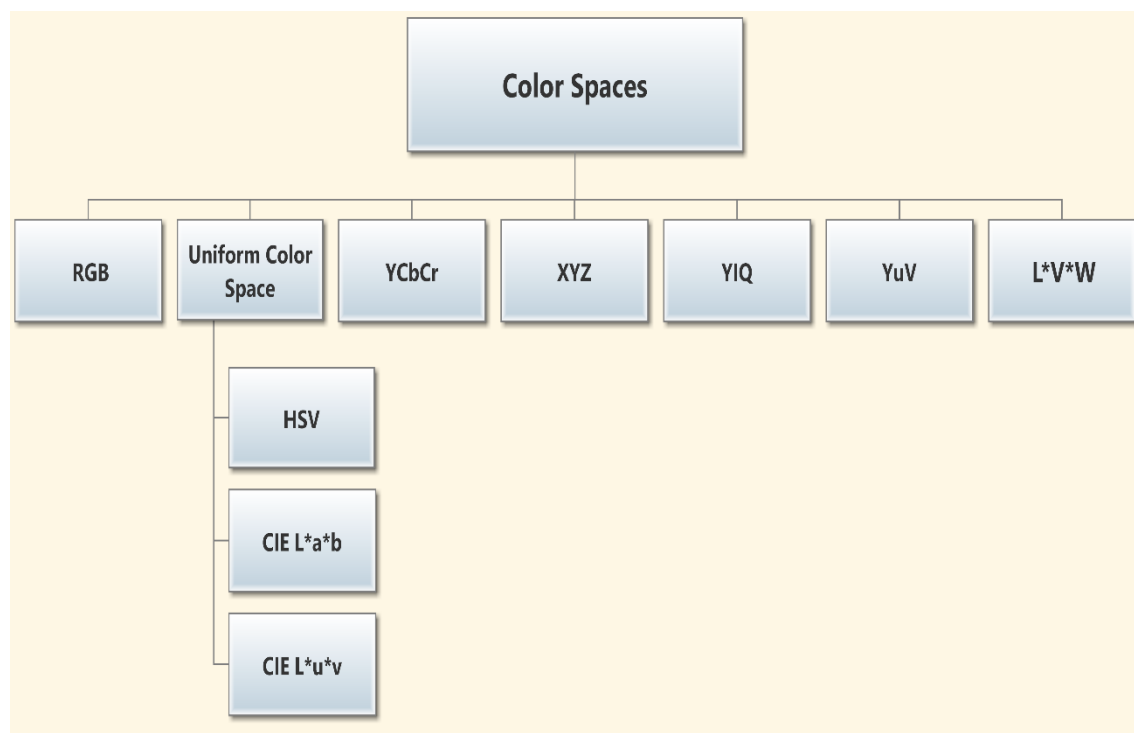


**Figure (3.14): Colour Spaces**

HSV colour space is the most intuitive colour system that describes a particular colour by its hue, saturation and brightness value components. This type of colour representation is very advantageous in interactive colour selection and manipulation.

On the other hand, both of CIE L\*u\*v and CIE L\*a\*b colour spaces are perceptually uniform colour systems that ease the similarity metrics utilization for colour comparison purposes (Haeghen, et al., 2000).

As we mentioned before, we use the MR brain images which have not a broad variation of colour. Therefore, we use the most proper colour space that can ease the duty of similarity metrics and it is more similar to the human perception of colour namely, HSV colour space. That means, in our proposed CBBIR system we will consider the Hue, Saturation, and Value (HSV model). Hue is a saturated colour on the outer rim of the colour wheel. Saturation is the amount of white added to the colour. 0% means that the colour (at V=100%) is totally white; 100% means totally saturated with no white added. Value is the brightness of the colour. 0% means totally dark or black; 100% means full brightness.

- **RGB Colour Model**

Originally, most of our MRI brain images are in RGB model. Where, the colours of each pixel are expressed by the combination of R, G, B components where the brightness value  $I = R+G+B$  components and the range of each colour components value is:  $[0, 1, 2, \dots, 255]$  (Shaik, et al., 2015). Since the colour information is highly sensitive to the brightness values of the pixel, each colour component value can be normalized with the brightness value ( $I$ ) as follows (Shaik, et al., 2015):

$$r = \frac{R}{I}$$

$$g = \frac{G}{I}$$

$$b = \frac{B}{I}$$

Where  $r + g + b = 1$ ;

(3.1)

- **HSV Colour Model**

HSV colour space is more similar to the human brain perception of colour. The hue of the colour (H) is a measure of the spectral composition of colour and it is represented by an angle that varies from (0° to 360°).

Whereas, the saturation (S) refers to the degree of purity of colours and varies from (0 to 1). The darkness degree of a colour is given by the value (V) which ranges from (0 up to 1) too.

In our feature extraction process, we first converted all RGB MRI images into HSV colour model via the following equations (Wang & Yuan, 2001):

$$H1 = \cos^{-1} \left[ \frac{0.5[(R - G) + (R - B)]}{\sqrt{(R - G)^2 + (R - B)(G - B)}} \right] \quad (3.2)$$

$$H = H1 \text{ if } B \leq G,$$

$$H = 360^\circ - H1 \text{ if } B > G$$

$$S = \frac{\text{Max}(R, G, B) - \text{Min}(R, G, B)}{\text{Max}(R, G, B)} \quad (3.3)$$

$$V = \frac{\text{Max}(R, G, B)}{255} \quad (3.4)$$

Figure (3.15) illustrate HSV colour space model in Cartesian and polar coordinates definition (Shen, Zhou, Teng & Wang, 2015).

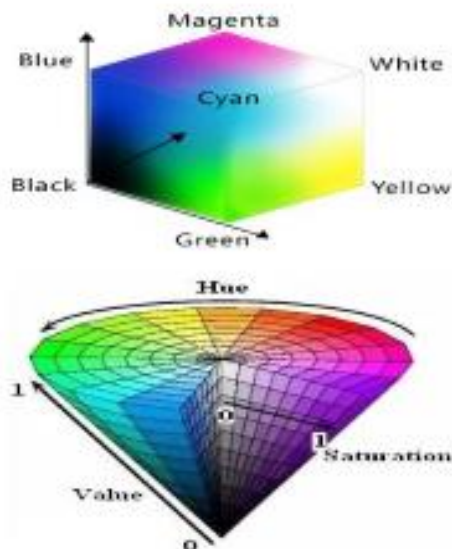


**Figure (3.15): (a) RGB Colour Space (b) HSV Colour Space.**

Hue (H) is determined by dominate wavelength of visible light that is reflected by an object. Hue parameter is described by the angle that can rotates 360 degrees around the centre in the polar coordinate system.

Whereas the Saturation (S) represents the brightness degree of the colour, therefore, it reflects the colours shade, which ranges from 0 to 1. That means, the higher the degree of saturation the deeper the colour is, therefore, as a corresponding result, when saturation is zero, then there only left grey scale (Ibraheem, Hasan, Khan & Mishra, 2012).

The brightness Value (V) plays an important role in describing the grey scalar by representing the brightness of the original image. V takes value between 0 and 1, where

the greater coefficient of the colour, the much brightness of the object is. (Ibraheem, et al., 2012).

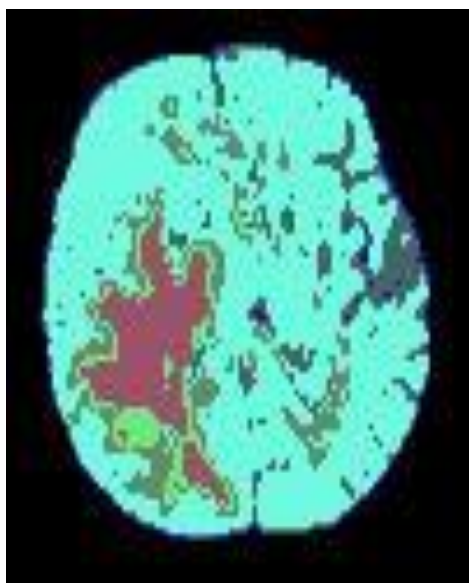
### 3.4.1.3 Normalized HSV Colour Histogram

To introduce the concept of normalized colour histogram we used in our proposed CBIR system, let us first define the colour histogram of an image.

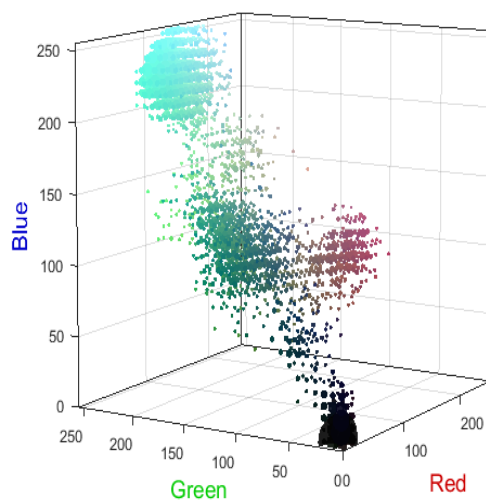
If the colours of an image  $\mathbf{I}$  are mapped into a discrete colour space composed of  $(n)$  colours, then the colour histogram of this image  $\mathbf{H}(\mathbf{I})$  is defined as the vector:  $[\mathbf{h}_{c1}, \mathbf{h}_{c2}, \dots, \mathbf{h}_{cn}]$ , where each element  $\mathbf{h}_{ck}$  represents the probability of the colour  $\mathbf{C}_k$  existence in the image (Sebe, & Lew,2001).

Therefore, the colour histogram is considered a tool that can represents the distribution of the number of pixels dedicated for each quantized colour bin which is relatively an efficient representation of colour content of an image. The colour histogram have the capability to characterize the global and regional distribution of colours in an image.

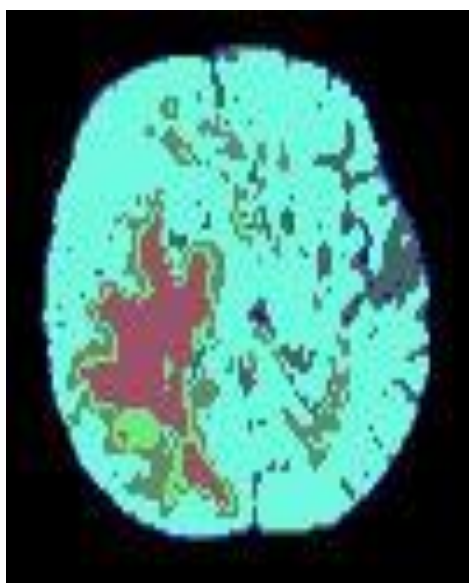
Moreover, it is invariant to the rotation about view axis. In order to elaborate the concept of colour distribution, Figure(3.16) and Figure(3.17) show the RGB and HSV distributions respectively implemented in MATLAB for two Brain MR images (belongs to our database) corresponds to: Brain Tumor MR image and the other for other brain disease.



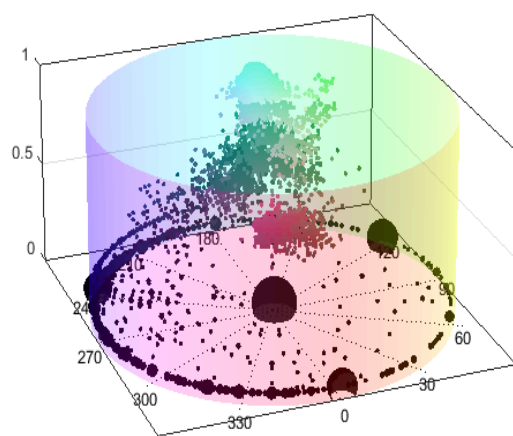
(a)



(b)

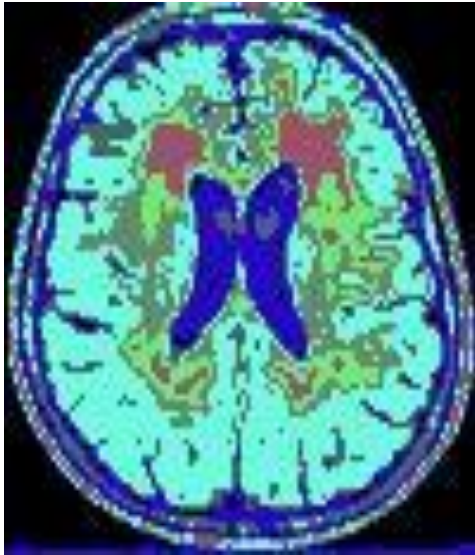


(c)

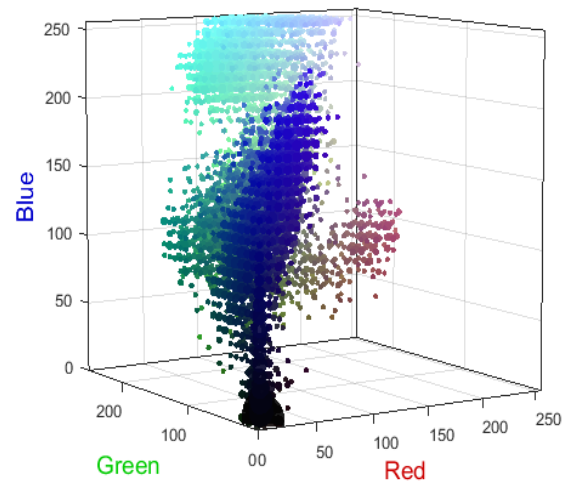


(d)

**Figure (3.16): RGB and HSV Colour Distribution of Brain Tumor MR Image**



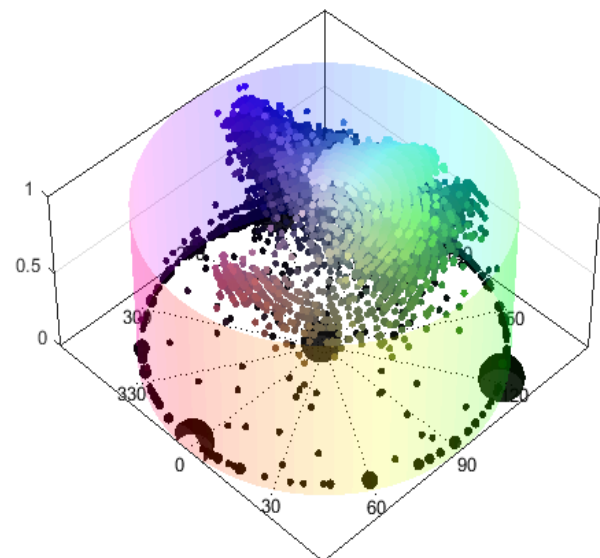
(a)



(b)



(c)



(d)

**Figure (3.17): RGB and HSV Colour Distribution of Brain Disease MR Image**

As we noted in Figures (3.16) and (3.17) above, the colour distribution for the brain tumor is different than that of brain disease either RGB colour space or HSV colour space different, the difference in colour content of an image will enable our proposed CBBMIR system to distinguish brain tumor images than non-brain tumor ones.

The histograms can depict the colour distribution as they appear in images regions, and since it is a discrete distribution, it can be represented as feature vectors in M-dimensions. In our research, we use the quantized HSV histogram, where the hue component is quantized to (8) levels whereas Saturation and brightness values are quantized into (2) levels respectively.

#### 3.4.1.4 HSV Histogram Normalization

The brain MR images are composed of different regions with different sizes, thus, in order to compare the regions of an image that have different sizes, we use the histogram normalization which can make the comparison more standard and return back to one reference level (Smith,1997).

Figure (3.18) shows a couple of brain tumor MR images where the tumor is in different region size in each one, which will reflect different colours distributions,

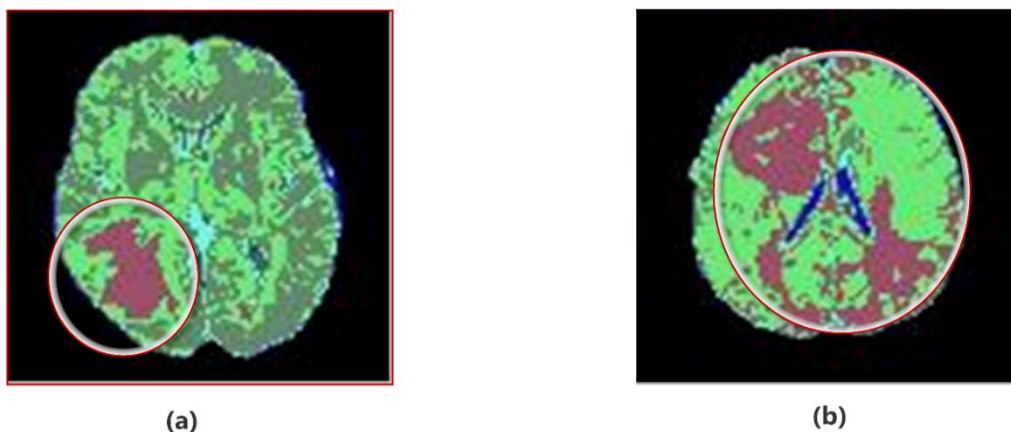


**Figure (3.18): The Tumor Regions in Brain MR Images (a) Small Region (b) Wide Region**

However, when the histogram is normalized it returns both regions to a reference level when the histograms of both images will be compared by one of similarity measures. Histogram normalization is given by the following equation:

$$\mathbf{h}^r = \frac{\mathbf{h}}{(\sum_{d=0}^{D-1} |h[d]|^r)^{1/r}} \quad (3.5)$$

Where  $r = 1$ , or  $2$ .

The major effect of normalization is the reduction in dimensionality of feature space (dimensionality of features dataset). In order to elaborate the concept of normalized histogram, let us assume that we have two histograms ( $h_0$ ,  $h_1$ ) composed of just two bins (colour bins) as shown in Figure (3.19) (Smith, 1997).

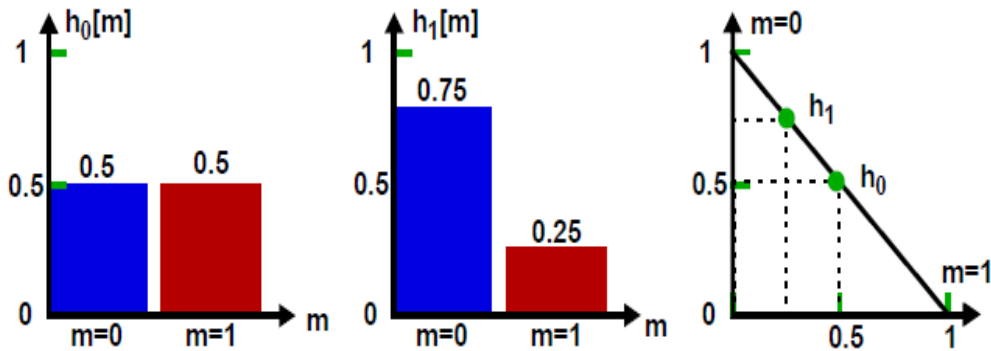


**Figure (3.19): Two Bins Normalized Histograms ( $h_0$ ,  $h_1$ ) with ( $r = 1$ )**

We note that the feature points for all two-bin histograms (where it is normalized with  $r = 1$ ) lie on one-line segment which gives the conclusion that if we have an element of a histogram, then the other is easily determined via the line segment.

In our research, we normalized the histogram with ( $r = 1$ ) which is suitable to our limited colour set that we have used to represent the brain MR image. During our

features extraction process, we use HSV model for the grey scalar MRI images; we establish the normalized HSV colour model for each MRI image.

However; we encounter a problem of ( $\frac{0}{0}$ ) division that a result of being same of saturation (represented by H component) and the darkness (represented by V component) Value for some regions in the brain MRI equal to zero. This was expected since all brain MRI images have saturation and darkness values close to or equal to zero.

### **3.4.1.5 Colour Moments**

In order to overcome the quantization effects of the colour histogram, we have used the colour moments proposed by (Stricker & Orengo, 1995) as feature vectors for image retrieval.

Any colour distribution can be characterized in terms of its moments and at the same time most of information is focused on the low-order moments, namely, first moment (mean), and second moment or the standard deviation or variance (Jau-Ling & Ling-Hwei, 2002). Therefore, in our research, we have used the colour moments in the process of feature construction.

Since a probability distribution is uniquely characterized by its moments (Stricker & Orengo, 1995), the colour distribution of the R, G and B colour components of a MR image can be represented respectively by its colour moments (Jau-Ling & Ling-Hwei, 2002).

The first colour moment of the  $i^{th}$  colour component where  $i = 1, 2 \text{ or } 3$ , is given by moments (Jau-Ling & Ling-Hwei, 2002):

$$M_i^1 = \frac{1}{N} \sum_{j=1}^N P_{i,j} \quad (3.6)$$

Where,  $P_{i,j}$  represents the colour value of the  $i^{th}$  colour component of the  $j^{th}$  image pixel and N represents the total number of the image pixels.

Now, the  $h^{th}$  moment, where h can take values of:  $\{h = 2, 3, \dots\}$  of the  $i^{th}$  colour component is given mathematically as moments (Jau-Ling & Ling-Hwei, 2002) :

$$M_i^h = \left( \frac{1}{N} \sum_{j=1}^N (P_{i,j} - M_i^1)^h \right)^{1/h} \quad (3.7)$$

### 3.4.1.6 Colour Correlograms

The colour histogram, colour sets and colour moments can contain only the information of each pixel in the MR image, however, the local relationship among the neighbouring pixels is not involved.

In other words, although colour histograms can describe the colour distribution of the MR image efficiently and it is easy to compute and at the same time it is insensitive to small changes in the viewing positions that may occur to MR images, colour histogram give us any spatial information of the image colours.

Therefore, in addition to colour histogram image feature, we have used the colour correlogram; first proposed by (Huang, Kumar, Mitra, Zhu & Zabih, 1997). This feature enables us to describe the global distribution of the local spatial correlation of colours that means, this feature enables us to express how the spatial correlation of pairs of colours changes with distance along the image itself.

A Correlogram of an image can be defined as a table indexed by colour pairs, where the  $k^{th}$  entry of this table for  $\langle i, j \rangle$  will determine the probability of finding a pixel of colour  $j$  at a distance  $k$  from a pixel of colour  $i$  in the image.

This colour feature is considered robust in tolerating large changes in appearance of the same scene that may happen due to changes in viewing positions or changes that may occur in the background scene (Huang et.al., 1997).

### 3.4.2 Shape Features Extraction

In comparison to other low features as texture and colour, shape features representation is considered much more efficient in semantically characterizing the image content (Ha, Kim & Choi, 2008). However, the major challenging task of any shape descriptor is to extract and represent the shape information in accurate manner.

This task becomes more challengeable and even more complicated when the invariance is required after the target image undergoes a number of possible transformation such as shifting, scaling or rotation.

Shape descriptors are essentially built based on *Edge Detection*. Where edge detection can be defined as locating and identification of shape discontinuities in an image under consideration (Desai, Pujari & Goudar, 2012).

The discontinuities of an image are the sharp and sudden changes in pixel intensity which identifies the boundaries of different objects in a particular scene.

A variety of conventional methods for edge detection exist which has a general core idea that involves the convolving of the target image with a two dimensional filter designed to have a sensitivity to large gradient in the image while returning values of zero (no changes) in uniform regions (Desai, et al.,2012).

The boundaries between regions in an image are defined by edges which assists in image segmentation tasks and objects recognition. Edges have the high capability to show where the shadows fall in an image or any other distinguishable changes in the intensity of an image.

Edge detection is considered fundamental for low-level image processing, and the obvious edges are essential for higher level image processing either the image is medical one or not (Datta, Joshi, Li & Wang, 2008).

The classical edge detection techniques and algorithms such as: Canny edge detector, Laplacian of Gaussian (LOG), gradient-based edge detectors, zero-crossing detection suffer from limitations reveal when it is implemented in real-world applications (Desai, et al., 2012).

With attractive properties associated with multi-scale and time-frequency localization, wavelet transforms proved its high efficiency in feature extraction and representation in image compression, encoding, and other image processing fields especially edge detection.

Wavelet transforms are multi-resolution image decomposition tools that represent the image features via a variety of channels created by different frequency sub bands at different multi-scale. It is a well-known technique in analysing one and two dimensional signals. The core idea of wavelet-based shape features is the high sensitivity to local contrast changes such as edges, corners and region boundaries.

For all reasons that we have mentioned above, in our research, we have used two dimensional discrete wavelet transforms as edge detectors in such a way for a given MR brain query image, an edge map is obtained by using wavelet decomposition. Then, shape feature vector is constructed using the moment invariants.

Wavelet transform is used to represent the local shape of brain tumor in a vector of features. Therefore, the identification of the most similar shapes from the database will be easier by taking into account the fine edges of the tumor shape of other brain disease

shape. In our research, we have used 'Coiflets' wavelet functions family, which is a near symmetric wavelet function used widely in CBIR systems. (Beylkin, Coifman & Rokhlin, 1991).

Wavelets are continuous and real in their nature and at the same time they have the least Root Mean Square Error (RMSE) which makes it more appropriate for detecting discontinuities and any break down points that may appear in the brain MR image; which may help us in finding an edge of an image.

### **3.4.2.1 Wavelet Moments**

A wavelet is defined as a signal or waveform of limited time duration that has an average value of zero. Wavelets have varying frequency and they inherently are irregular and asymmetric (Desai, Pujari & Goudar 2012).

A wavelet can be applied on one dimensional signals such as audio signals and on two dimensional signals such as images. The core reason for using wavelet transforms in edge detection is the high possibility of selecting the size of details required for an edge to be detected (Desai, Pujari & Goudar 2012).

In case of image processing, wavelet transform is performed separately in two directions: vertical and horizontal. Therefore, the details along the vertical and horizontal directions are identified in separate manners.

The 2D (dimensional) discrete wavelet transform (DWT) decomposes the image into four sub images: one is called approximate and the other three sub images along vertical, horizontal and diagonal directions and called details. Figure (3.20) shows the sub

images that resulted from the 2D wavelet transform before we apply it on a brain MR image (Desai, Pujari & Goudar 2012).

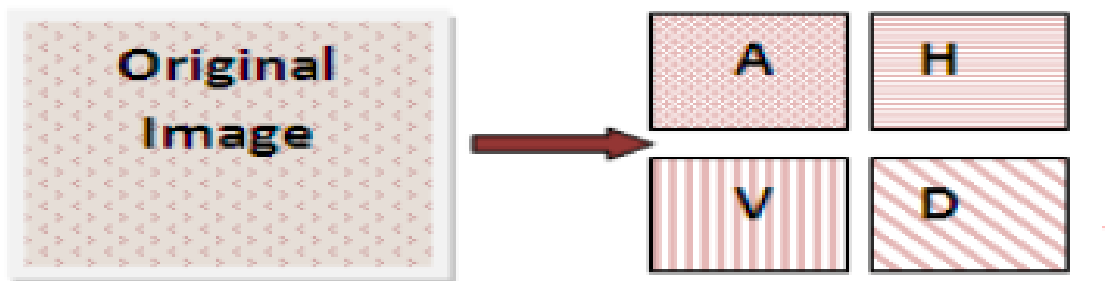


**Figure (3.20): Wavelet Decomposition of an Image (Desai, Pujari & Goudar 2012)**

Figure (3.21) shows these sub images for a MR image undergoing one type of 2D discrete wavelet transforms.

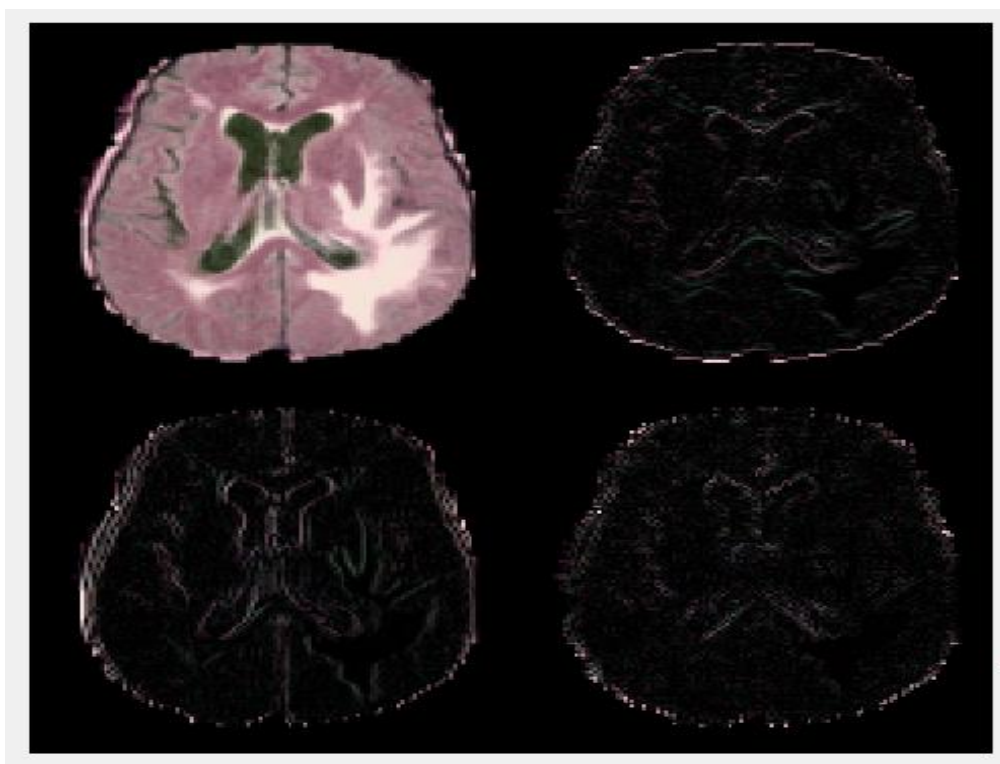


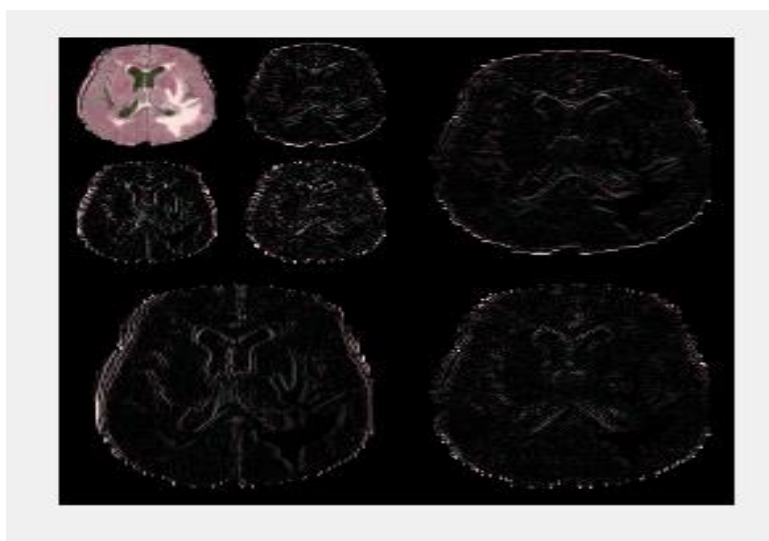
**Figure (3.21): 2D Discrete Wavelet Transform of Brain MR Image**

As shown in Figure (3.21) above, the approximate sub image is the image that looks similar to the original brain MR image except it is only  $\frac{1}{4}$  of the original size whereas the details sub images are the images resulted in horizontal, vertical and diagonal directions.

A 2D wavelet transform is considered an extension of the 1D wavelet transform in both directions: horizontal and vertical, therefore, the resulting sub images resulted from an octave (or single iteration of DWT) are labeled as approximation which represent the smooth version of the original brain MR image.

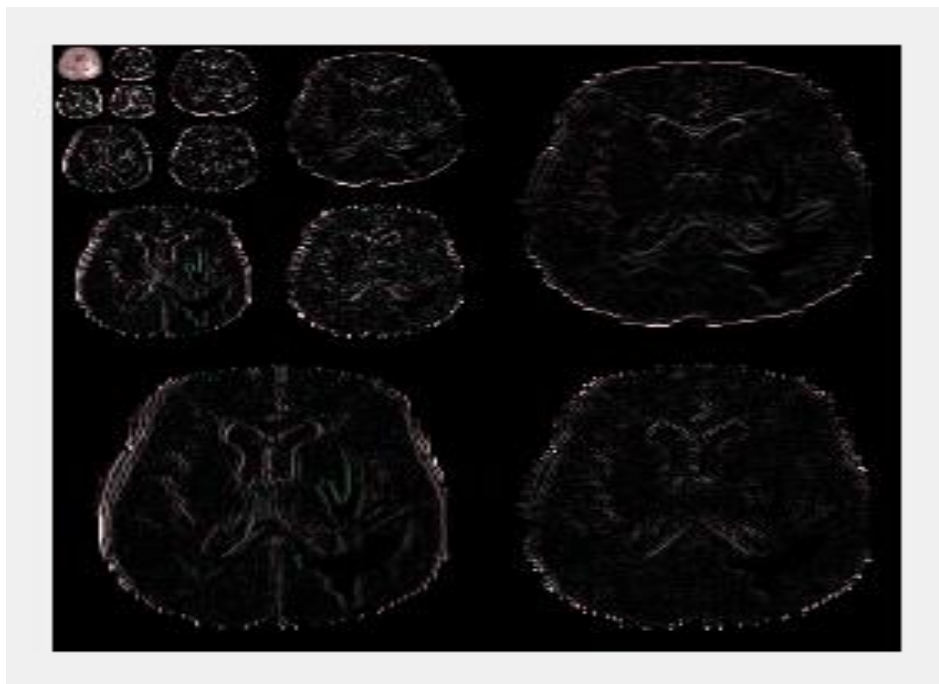
According to the filters designed to generate each sub image, the Horizontal sub image preserves the horizontal edge details along the horizontal direction while the Vertical sub image preserves the vertical ones, and the diagonal sub image preserves the diagonal edge details; which are dramatically influenced by noise.

This process can be repeated continuously by putting the approximation sub image through another set of low pass and high pass filters that construct the discrete wavelet transform which lead to multi-resolution analysis of the brain MR image as elaborated in Figure (3.22).



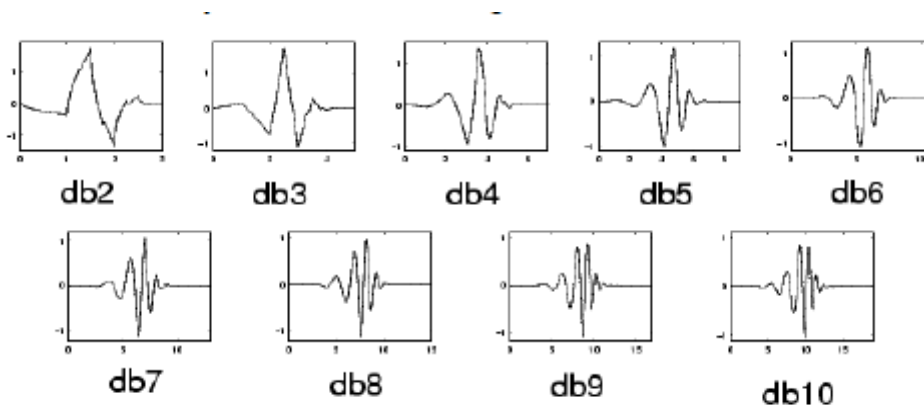
**Figure (3.22): Discrete Wavelet Transform (Level 2) of a brain MR image**

Figure (3.23) shows the discrete wavelet transform for the same brain MR image, but for (level = 4).



**Figure (3.23): Discrete Wavelet Transform (Level 4) of a Brain MR Image**

Daubechies wavelets are one of the many families of orthogonal wavelets that defines a discrete wavelet transform. The names of the Daubechies family wavelets are written as: dbN, where db is the surname of the wavelet and N represents the order. The db1 wavelet is similar to Haar wavelet (used to decompose brain MR images in Figures



**Figure (3.24): Daubechies Wavelets Family (Desai, Pujari & Goudar 2012)**

(3.22) and (3.23) above. The nine member's functions of this family are shown in Figure (3.24).

Another wavelet family that we utilize in our research is Coiflets wavelet

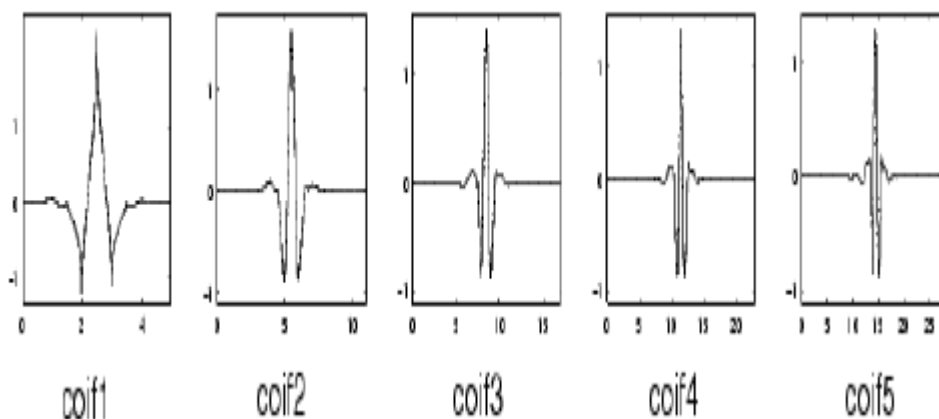


**Figure (3.25): Coiflet wavelets family (Desai, Pujari & Goudar 2012)**

functions that have both orthogonal and bi-orthogonal properties. Coiflet wavelet family is shown in Figure (3.25)

Our proposed system uses these types of wavelets for image decomposition, where the query brain MR image is converted to gray scale image. The resulted grey scale MR image is decomposed using wavelets into 4 components: Approximate, vertical, horizontal and diagonal and for four levels of decompositions.

Approximation component contains only smoother version of the original brain MR image or alternative rows and columns of it. The other components (V, H, D) yield the other prominent edge information. However, in order to obtain all strong and weak edge information, we have used all four components.

Coiflets wavelet family proved its high performance in our proposed system, thus we adopt it as shape descriptor. Figure (3.26) shows a brain MR image decomposed by Coiflets wavelet at four levels.

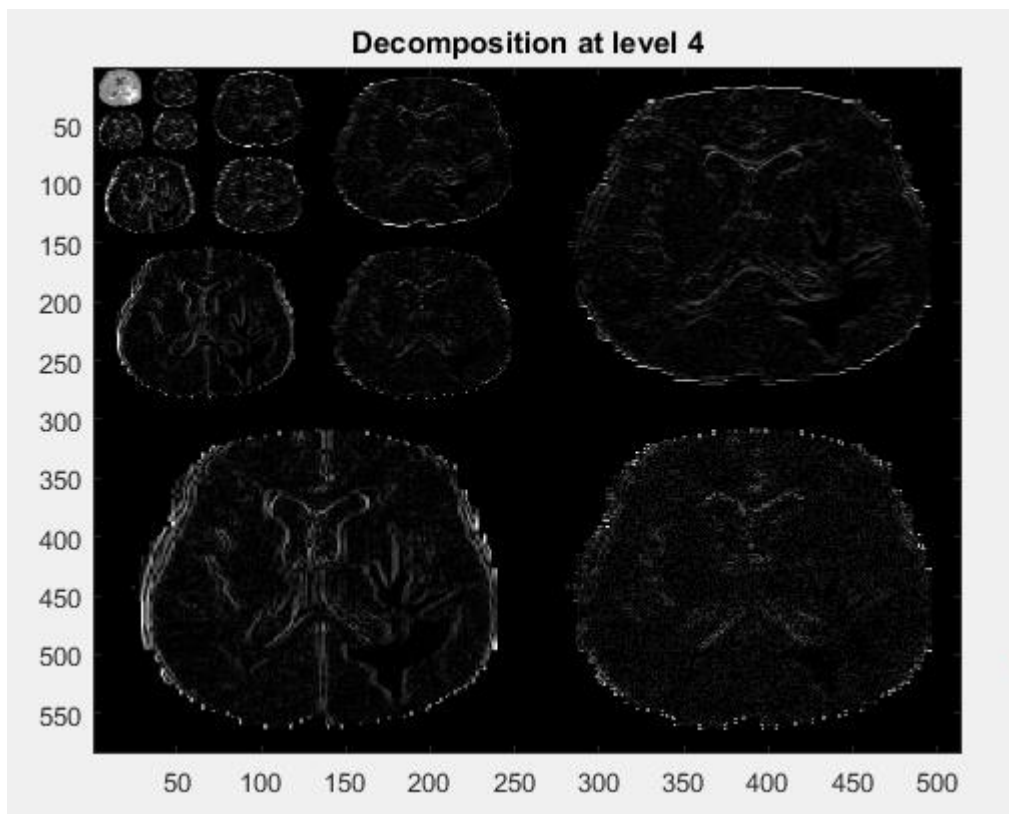


**Figure (3.26): A Brain MR Image Decomposed by Coiflet Wavelet at level 4**

As can be noted from Figure (3.26) above, the edges in the MR image can be obviously determined which proves the high efficiency of the wavelets as shape descriptor.

### 3.4.3 Texture Features Extraction

Tissues are expected to be homogenous and are consistent through the whole organ tissues. Therefore, the information that can be got from the texture can be used to distinguish tissues from each other, especially, to differentiate the normal brain tissues from the tumor ones. The extracted texture features provide perceptual representation of the image texture which will enhance the process of retrieving the most similar images from the database of medical images.

The rapid successes and developments that have been achieved by the wavelet transforms in the field of image processing have yielded an alternative multi-resolution to be proposed majorly for an enhanced resolution in orientation and in aliasing effects avoidance.

In the last twenty years, many oriented band-pass multi-resolution transforms have been proposed, implemented, and realized with an increasingly interest such as: Steerable Pyramids (Simoncelli,et.al.,1992), Complex valued wavelets (Gross & Koch,1995), (Portilla, et.al.,1996), (Kingsbury, 2001), Contourlets (Do & Vetterli,2005), Curvelets (Starck,, Candès & Donoho, 2002) and Gabor multiresolution (Gross & Koch,1995), (Nestares, Navarro, Portilla & Taberner, 1998), (Fischer,et.al, 2007).

In our research, the local texture features of the brain tumor zones and the rest of normal tissues around it in magnetic resonance image are extracted using Log-Gabor filter. Since Log-Gabor filter is a modified version of Gabor filter, we will discuss Gabor filter and its shortcomings that forced us to use Log-Gabor filter.

### 3.4.3.1 Gabor Filter

A Gabor filter is often used in face recognition and face detection applications. In contrary to Canny edge detector, it is more comfortable to adjust the filter parameters in order to avoid the over detection (Kang, Lei, Lin & Li, 2014).

A Gabor filter is a Gaussian function multiplied by a complex exponential function, which is expressed mathematically for two dimensions as (Arakeri, & Reddy 2013).

(3.8)

$$g(x, y) = \frac{1}{2\pi\sigma_x\sigma_y} \exp\left(-\frac{1}{2} * \left( \frac{x^2}{\sigma_x^2} + \frac{y^2}{\sigma_y^2} \right) + 2\pi jWx\right)$$

Where;

W: the modulation frequency,

$\sigma_x^2$  and  $\sigma_y^2$  are the variances along x and y directions respectively.

Which has the following Fourier transform:

$$G(u, v) = \exp\left(\frac{1}{2} \left( \frac{(u - F_0)^2}{\sigma_u^2} + \frac{v^2}{\sigma_v^2} \right)\right) \quad (3.9)$$

Where;

$u, v$  are the polar coordinates in the frequency domain.

Outstandingly enough, it is being found by a pioneer paper of (Daugman ,1985), that this family of Gabor functions has the capability to well describe the two dimensional field profile of the simple cells that exist in the mammalian visual cortex.

That means the perception of the visual system of humans can be simulated through image analysis utilizing these functions. This was a motivator for us and for other researchers to use Gabor filter in a wide spectrum of applications such as image segmentation (Weldon, Higgins & Dunn, 1996), object tracking (Arróspide & Salgado,2013), image data retrieval (Manjunath & Ma ,1996), texture-based image retrieval (Han & Ma ,2007). All of these situations are strictly related to the image texture analysis issues.

Generally speaking, the core idea of Gabor filter is to provide a frequency description of the image but in localized manner. Therefore, in order to grasp all frequency content of the texture pattern of the brain MR image, a bank of filters built in different frequencies is required. This idea can be mathematically explained as:

If  $g(x, y)$  represents the mother generating function for the Gabor filter family, this function represent the mother that under particular modifications produce the family of Gabor filter functions. Set of functions can be created and we will denoted as  $g(x, y)_{m,n}$  by rotating and scaling  $g(x, y)$  function:

$$g_{m,n} = a^{-2m}g(x', y') \quad (3.10)$$

Where

$$x' = a^{-m}(xcos(\theta_n) + ysin(\theta_n) ) \quad (3.11)$$

$$y' = a^{-m}(-xsin(\theta_n) + ycos(\theta_n) ) \quad (3.12)$$

Where  $a > 1$ ;

If we assuming a bank of filter with  $K$  orientations and  $N$  different scales.  $\{m=0\dots, N-1\}$ ,  $\{n= 0\dots, K-1\}$ . Each filter describes a frequency  $F_m$  which given mathematically as:

$$F_m = a^{-m}F_0 \quad (3.13)$$

Note that  $a^{-m}$  determines the scales and an angle  $\theta_n = \frac{n\pi}{K}$  determine the orientations.

The frequency response of Gabor filter will guide the texture analysis of the brain MR image through orientations and scales, thus the frequency response of Gabor filter is given by:

$$G(u, v)_{m,n} = \exp\left\{-\frac{1}{2} \left[ \frac{(u-u_{m,n})_r^2}{a^{-2m}\sigma_u^2} + \frac{(v-v_{m,n})_r^2}{a^{-2m}\sigma_v^2} \right]\right\} \quad (3.14)$$

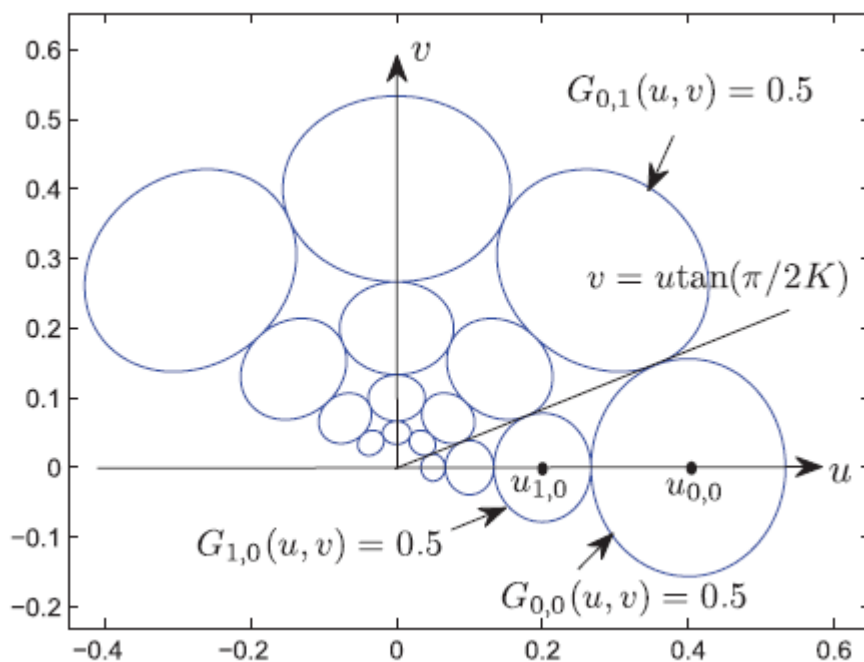
Where  $(u_{m,n}, v_{m,n})$  represents the spatial frequencies of the sinusoidal carrier, namely,  $u_{m,n} = F_m \cos(\theta_n)$ ,  $v_{m,n} = F_m \sin(\theta_n)$  and  $r$  indicates the rotation.

Therefore the terms:  $(u - u_{m,n})_r^2$  and  $(v - v_{m,n})_r^2$  given by the following equations:

$$(u - u_{m,n})_r^2 = ((u - u_{m,n}) \cos(\theta_n) + (v - v_{m,n}) \sin(\theta_n))^2 \quad (3.15)$$

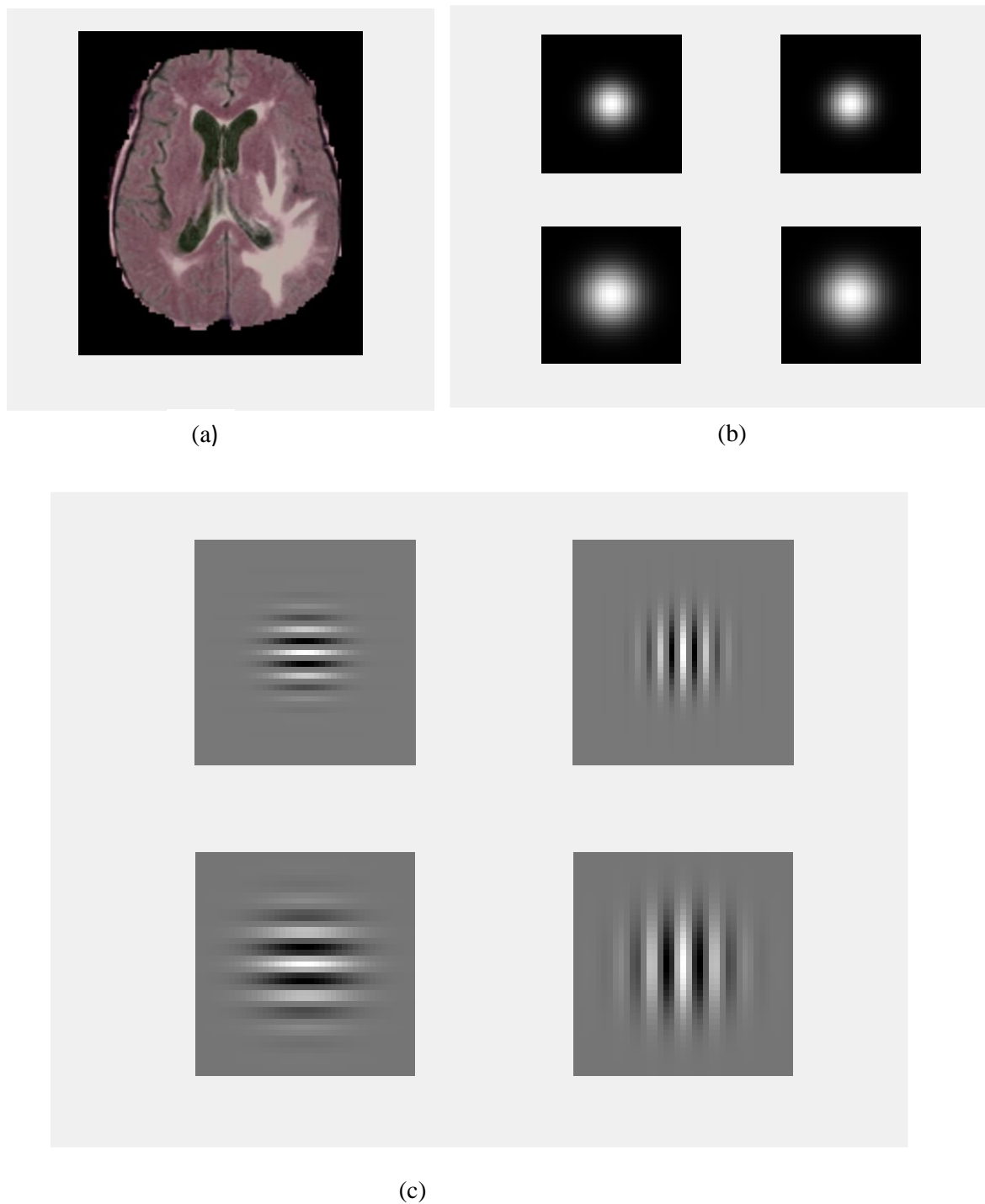
$$(v - v_{m,n})_r^2 = (-(u - u_{m,n}) \sin(\theta_n) + (v - v_{m,n}) \cos(\theta_n))^2 \quad (3.16)$$

Figure (3.27) elaborates the frequency response of the Gabor filter bank.

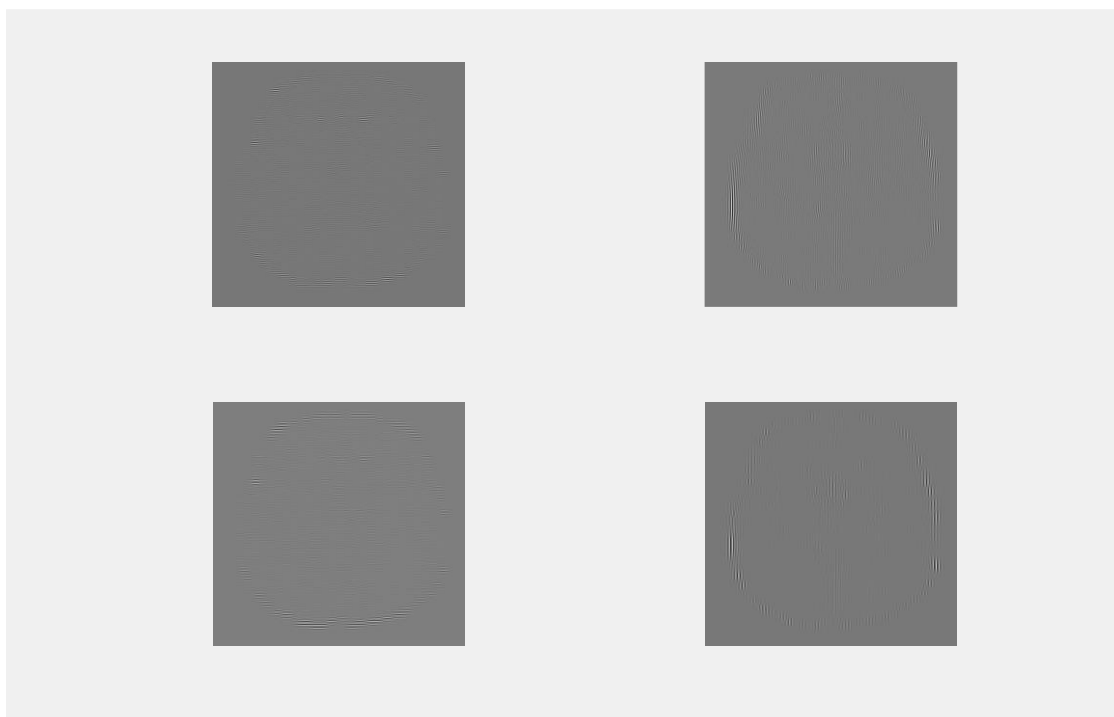


**Figure (3.27): Frequency response of the Gabor filter bank. The contours represent the Half-Peak Magnitude of the Filter Responses in the Gabor filter family. The Filter Parameters used here are:  $K=4$ ,  $N=4$ , and  $F0=0.4$**

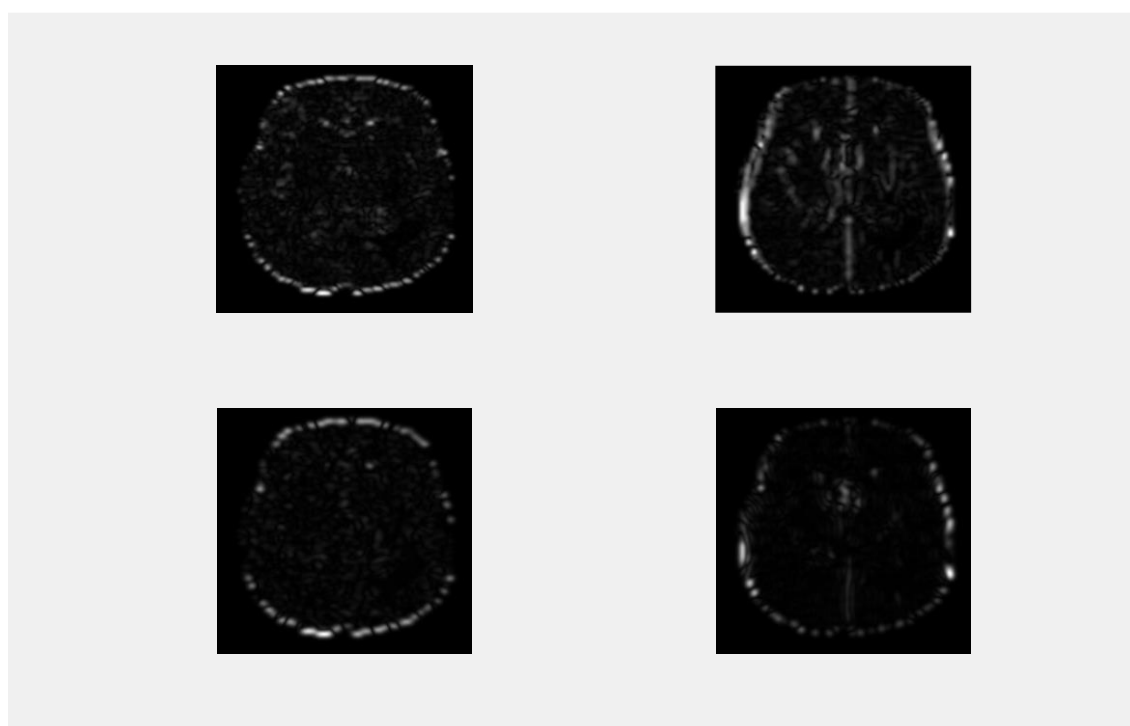
Figures (3.28) and (3.29) elaborates the texture analysis utilizing 2x2 Gabor filter that have two scales and two orientations values for a given brain MR image.



**Figure (3.28): Real parts of 2x2 Gabor Filter**



(a)



(b)

**Figure (3.29): Magnitudes of 2x2 Gabor Filter**

### 3.4.3.2 Log-Gabor Filter

Although Gabor filters have been utilized in comprehensive manner for a wide range of applications, they have a number of drawbacks.

First, Gabor filter is considered as one-octave bandwidth, that means it is constrained to one octave bandwidth and beyond this bandwidth, a too high DC component is expected. Therefore, in order to cover a wide spectrum, a large number of filter is needed.

Moreover, as suggested by (Field, 1987), a natural image have an amplitude that falls off in average by a factor of nearly ( $1/f$ ). This property of natural images is in contract to the properties of Gabor filters where a wide extent of the Gabor response concentrates on the lower frequencies which in turn yields a redundancy in the information given by the filters.

In addition, the high frequency tail of the natural image which include MR image in our case is not captured. A good alternative to Gabor filter is Log-Gabor filter that was introduced by Field in his well-known paper (Field, 1987).

Thus, based on these important drawbacks of Gabor filter, in our research, we have used Log-Gabor filter instead of Gabor filter which lead to an effective enhancement in the overall performance of the proposed CBBIR system.

The frequency response of Log-Gabor filter is given by (Nixon & Aguado, 2012) in the following mathematical expression in polar coordinate:

(3.17)

$$LG(f, \theta)_{m,n} = \exp\left\{-\frac{\left(\log\left(\frac{f}{Fm}\right)\right)^2}{2(\log(\beta))^2}\right\} \exp\left\{\frac{-(\theta - \theta n)}{2\sigma\theta^2}\right\}$$

And in the log axis (Fischer et al., 2007);

$$LG(\rho, \theta)_{m,n} = \exp\left\{-\frac{(\rho - \rho m)^2}{2(\sigma_\rho^2)}\right\} \exp\left\{\frac{-(\theta - \theta n)}{2\sigma\theta^2}\right\} \quad (3.18)$$

Where,  $\rho = \log(f)$ ,  $\rho m = \log Fm$ ,  $\sigma_\rho^2 = (\log\beta)^2$ . the  $\beta$  parameter determines the band width of the Log-Gabor filter.

### 3.4.3.3 Feature Extraction based on Log-Gabor Filter

Roughly speaking, there are many strategies that can be taken in order to define a feature vector out of Log-Gabor filtering. (Nava, Escalante-Ramírez, & Cristóbal, 2011) discussed some of them which includes the use of thresholded Gabor features, grating cell operator features, raw Gabor responses, and Gabor energy features.

In our thesis, we will use Gabor energy features which combine the responses of symmetric and antisymmetric Log -Gabor filter. Since these features yield a very large vector which is as large as the size of the MR image, we use the statistical moments to represent it.

In our thesis, we have used the Gabor mean square energy and the Gabor mean amplitude for each filter scale and orientation.

### **3.5 Classification and Retrieval Phase**

The classification phase will determine the class of the given query MR brain image based on the class features (attributes) extracted out of the query MR brain image.

To overcome the limited generalization performance of using a single classifier, we use ensemble of similarity measures to enhance and refine the class prediction for the given brain MR query image.

KNN is computationally efficient where the key computational operations is lied in the process of sorting of the training documents in order to find the K closest neighbours for the test record.

In addition, an KNN classifier can be used in a dynamic environment where frequent additions of records to the training records collection is required, where the insertion and incorporation of new training records is considered easy duty with respect to the KNN classifier.

#### **3.5.1 K Nearest Neighbour (KNN) Classification Engine**

To demonstrate the way by which KNN classifier works; let's consider an example of classifying a new item (query item) among a number of known items. Figure (3.30) depicts the items with plus and minus signs, and the query item is represented in a red circle.

Our task is to classify (predict) the label of a red-circled item. Based on a selected number K of its closest (nearest neighbours) so, the query item will be classified as a plus (+) or a minus (-) sign.

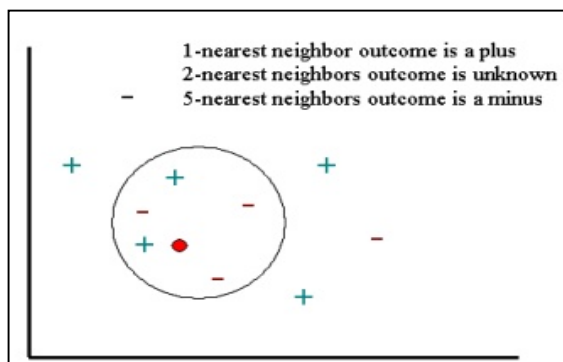


**Figure (3.30): K Nearest Neighbor Classification**

The idea behind KNN classifier is as follows: Let's first take the case when the selected nearest neighbours is  $K=1$ , or 1-nearest neighbour, it is obvious that KNN classifier will predict the label of the query item with a plus (+) since the plus sign is the closest point to it.

If we increase the number of nearest neighbours to 2, namely, 2-nearest neighbours, in this case, the KNN classifier has not the ability to classify the label of query item since the first closest item is plus and the second closest item is minus and both have the same number of votes (scores) in the voting process, so choosing  $K$  as an (even) number in KNN classification is not allowed.

As a final step, let's increase the number of nearest neighbour's  $K$  to 5 or 5-nearest neighbours. Now, we have defined the region of nearest neighbour which is indicated by a black circle in Figure (3.30). Since we have 2 plus signs and 3 minus signs, then the voting will be biased toward minus sign. Consequently, KNN classifier will assign a minus sign to the label of the query item.

The basic KNN algorithm works in the following pseudo-code (Seidl & Kriegel, 1998):

START

1. Input:  $D = \{(R_1, \text{label}_1), \dots, (R_N, \text{label}_N)\}$
2.  $R = (r_1, r_2, \dots, r_n)$  // new feature vector to be classified
3. //  $d(R_i, R)$  the distance between  $R_i$  and  $R$
4. For each labelled feature vector  $(R_i, \text{label}_i)$ , calculate  $d(R_i, R)$
5. Order  $d(R_i, R)$  in ascending order, ( $i = 1, \dots, N$ )
6. Choose the  $(k)$  nearest records to  $R$ :  $D_r^k$
7. Assign to  $R$  the most frequent class in  $D_r^k$

END

### 3.5.2 Similarity Metrics

KNN classifiers and all of clustering techniques that belongs to the locality-based clustering techniques depend on the distance between the query sample and the training data samples to predict its class (type of brain disease). Therefore; to make the prediction, a metric for measuring the distance is defined.

Now, the first important question is what are the properties that make the distance a metric?

In order to answer this question, let us define the following:

A distance  $d: X \times X \rightarrow \mathbb{R}^+$  is a bivariate operator, which means it takes in two arguments  $a \in X$  and  $b \in X$  that maps to  $\mathbb{R}^+ = [0, \infty)$ , then this distance  $d$  is a metric if:

$$(R1) : d(a, b) \geq 0 \quad (\text{non-negativity})$$

$$(R2) : d(a, b) = 0 \text{ if and only if } a = b \quad (\text{identity})$$

$$(R3) : d(a, b) = d(b, a) \quad (\text{Symmetry})$$

$$(R4) : d(a, b) \leq d(a, c) + d(c, b) \quad (\text{triangle inequality})$$

A distance that satisfies (R1), (R3), and (R4) (but not necessarily (R2)) is called a pseudo-metric. And if a distance satisfies (R1), (R2), and (R4) (but not necessarily (R3)) is called a quasi-metric (Phillips, 2013).

We now enumerate a series of distances that we have used as similarity metrics in this research.

If we define two vectors  $a$  and  $b$  where  $a = [a_1, a_2, \dots, a_d]$  and  $b = [b_1, b_2, \dots, b_d]$ . Now a  $L_p$  distances are defines as (Phillips, 2013):

$$d_p(a, b) = \|a - b\|_p = \left( \sum_{i=1}^d (|a_i - b_i|)^p \right)^{1/p} \quad (3.19)$$

Then, the most common distance is  $L_2$  distance which is defined if  $p = 2$  in above equation:

$$d_2(a, b) = \|a - b\|_2 = \left( \sum_{i=1}^d (|a_i - b_i|)^2 \right)^{1/2} \quad (3.20)$$

This type of distance measures is interpreted as *Euclidian Distance*. Or “straight-line’ distance between two points or vectors since if we draw a line between two points, then its length measures the Euclidian distance (Phillips, 2013) as shown in Figure (3.31).

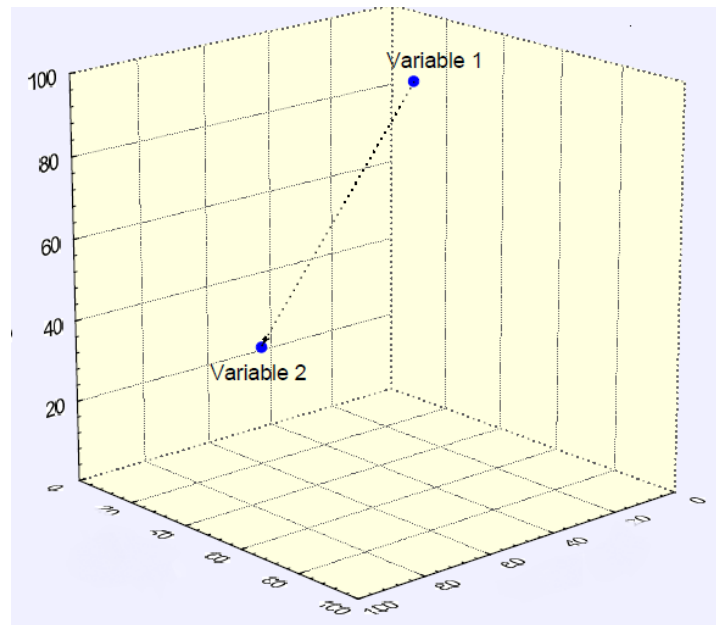


**Figure (3.31): L2 Distance Between Two Points (Phillips, 2013)**

Another common distance derived of  $L_p$  that we also used in our similarity ensemble is  $L_1$  where  $p=1$ , or (Phillips ,2013) :

$$d_1(a, b) = \|a - b\| = \sum_i |a_i - b_i| \quad (3.21)$$

Which is also known as “Manhattan “distance since it is the sum of lengths on each coordinate axis.

Now, the normalized Euclidian distance is defined as the Euclidian distance between two vectors divided by the number of vector components as (Phillips, 2013):

$$d = \frac{d_E}{\sqrt{n}} \quad (3.22)$$

Where  $n$ : is the number of vector components.

Another generalized metric distance that we used in our research is the Minkowski distance given by (Teknomo, 2006; Viriyavisuthisakul, et al., 2015):

$$d_{ij} = \sqrt[\psi]{\sum_{k=1}^n |a_{ik} - b_{jk}|^\psi} \quad (3.23)$$

When  $\psi=1$  Mincowiski distance becomes Cityblock distance and when  $\psi=2$ , it becomes the Euclidean distance that discussed above. Now, when  $\psi=\infty$  (taking the limit), then this distance is called Chebyshev metric distance (Teknomo, 2006).

We also used Pearson’s Correlation coefficient as metric distance that is given by (Prasad, et al., 2006):

$$r = \frac{1}{n} \sum_{i=1}^n \left( \frac{x_i - \bar{x}}{\sigma_x} \right) \left( \frac{y_i - \bar{y}}{\sigma_y} \right) \quad (3.24)$$

The Pearson distance is then defined as  $d_p = 1 - r$ . In which  $\bar{x}$  and  $\bar{y}$  are the sample mean of x and y respectively, and  $\sigma_x$ ,  $\sigma_y$  are the sample standard deviation of x and y.

Pearson distance is considered a measure for how well a straight line can be fitted to a scatter plot of x and y. If all the points in the scatter plot lie on a straight line, the Pearson correlation coefficient is either +1 or -1, depending on whether the slope of line is positive or negative. If it equals to zero, there is no correlation between x and y. As the Pearson correlation coefficient falls between [-1, 1], the Pearson distance lies between [0, 2] (Prasad, et al., 2006).

On the other hand, as in the case of the Pearson correlation, a distance measure corresponding to the Spearman rank correlation can be defined as (Prasad, Babu & Ahson, 2006):

$$d_s = 1 - r_s \quad (3.25)$$

Where  $r_s$  is the Spearman rank correlation. The Spearman rank correlation is an example of a non-parametric similarity measure. It is useful because it is more robust against outliers than the Pearson correlation (Prasad, et al., 2006). To calculate the Spearman rank correlation, each data value is replaced by their rank if the data in each vector is ordered by their value. Then the Pearson correlation between the two rank vectors instead of the data vectors is calculated. Finally, the cosine metric distance is given mathematically by (Prasad, et al., 2006):

$$d = \frac{\sum_{i=1}^n x_i y_i}{\sum_{i=1}^n x_i \sum_{i=1}^n y_i} \quad (3.26)$$

Where x and y are the vectors of n components.

## Chapter Four

### Experimental Results

#### 4.1 Introduction

As mentioned before, the experiments for this chapter were performed for (126) cases, each of which contained a magnetic resonance of four sequences:  $\{T_1, T_{1c}, T_2, \text{ and } T_{2\text{FLAIR}}\}$  with verified and untreated brain diseases that were divided into four bands. These magnetic resonance images were acquired from BRATS 2015 and BRATS 2013 databases. An image processing engine was used to generate features database of (126 x 91) dimensions.

This chapter presents discussion of experimental results obtained from testing our proposed CBBIR system mentioned in chapter three. Our system is implemented using MATLAB 2015a as a powerful integrated development environment and windows 8.1 platform with Intel Core i3 2Due CPU 2.5 GHz with RAM 4.0GB.

#### 4.2 Retrieval Parameters

Several parameters were used when we conducted our experiments in aim of finding the “optimal “classification model which in turn leads to the “optimal “content based medical image retrieval.

These retrieval parameters include: the number of retrieval images per query MR image and the type of used similarity measure. Different combination of these parameters will lead the experimental results toward the optimal number of retrieval image that can be used with the best similarity measure.

### 4.3 The Graphical User Interface of Our Proposed CBBIR System

The graphical user interface (GUI) of our proposed CBBIR system consists of two main phases: (1) Off-line phase (MRI features database Creator) and (2) On-line phase which consists of Retrieved MR images Display Panel and CBBIR Retrieval Engine as shown in the Figure (4.1).

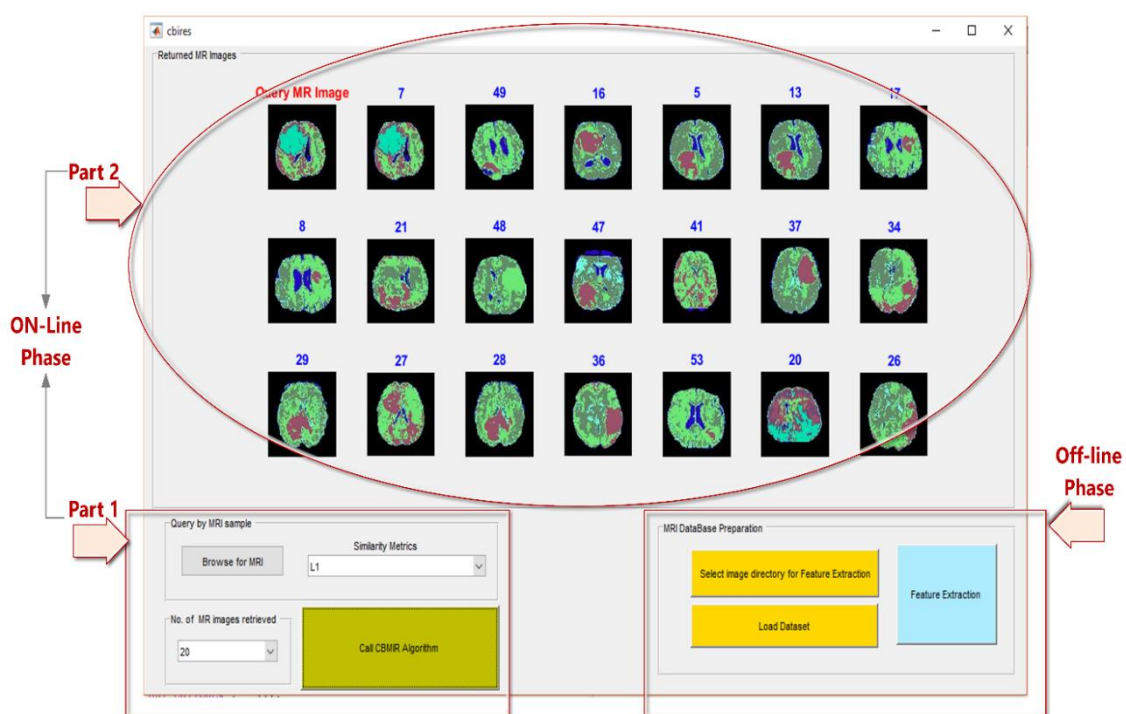


**Figure (4.1): The Graphical User Interface (GUI) of Our Proposed CBBIR System.**

Figure (4.1) shows the GUI of our proposed CBBIR along with the retrieval experimental results for a given query brain MR image and for a given similarity measure.

It can be seen from Figure (4.1) that our proposed CBBIR system retrieves the brain tumor MRI images in response to a brain tumor query image.

With the help of GUI of our proposed system, the end user can friendly select an MR and can browse for query brain MR image and at the same time the end user can

choose a particular similarity measure and can choose the number of MR images to be retrieved out of our database.

As shown in the Figure (4.1), the retrieved MR images are ranked by the degree of similarity to the query feature vector (where each MRI has as feature vector).

Our proposed CBBIR GUI works as follows: First, for each MR image in the database, a feature vector characterizing some image properties is calculated and stored in a feature database as shown in Figure (4.2).

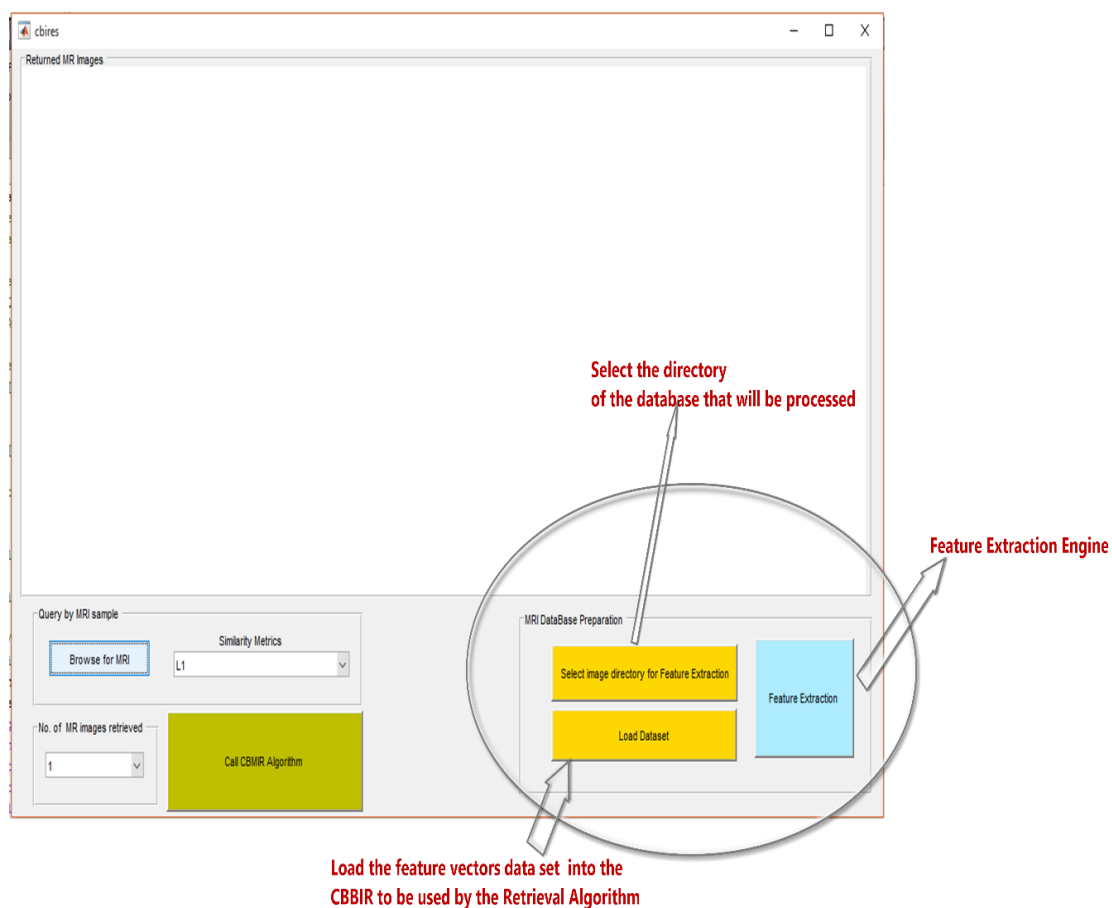


**Figure (4.2): The Features Extraction Engine of the proposed CBBIR GUI**

Second, the user selects a MR query image by press on: Browse for MRI icon in the second part of the GUI of our proposed system and select the number of retrieved images and the type of the similarity measure. This part of GUI is illustrated in the Figure (4.3) below:

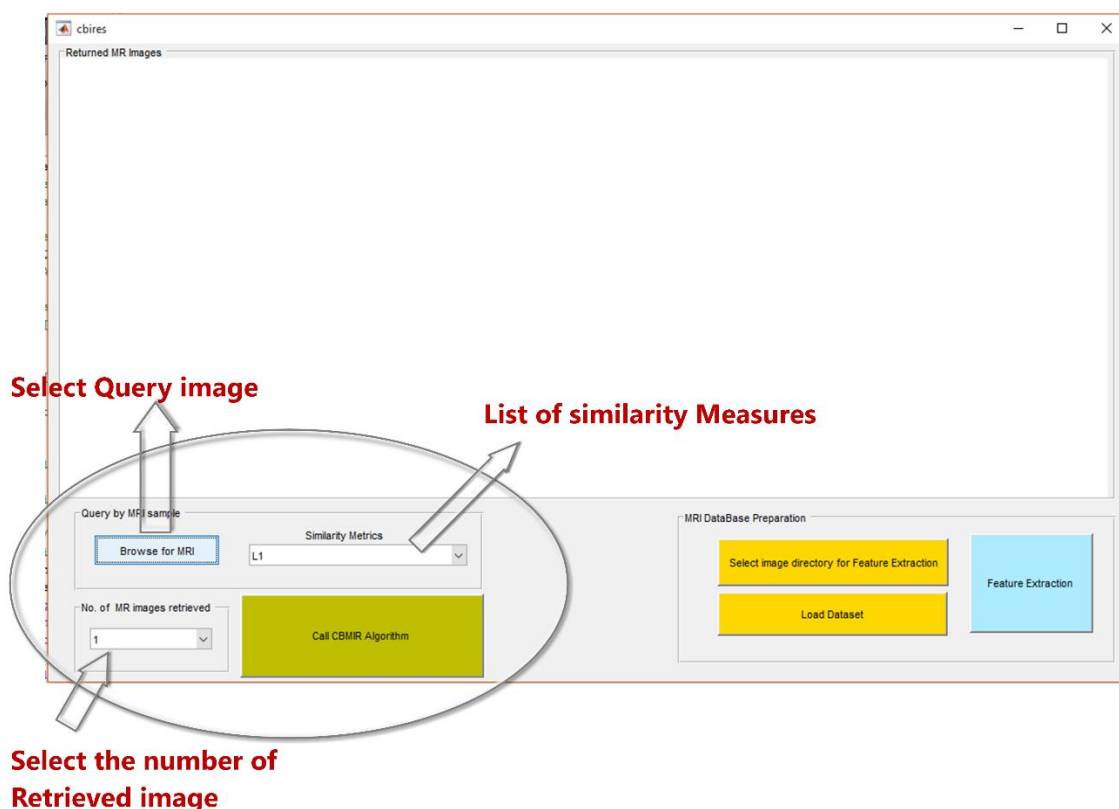


**Figure (4.3): The CBBIR Retrieval Engine of the proposed CBBIR GUI**

Given a query MR image, its feature vector is evaluated and then compared to the feature vectors in the features database then according to the chosen number of retrieved images (N), The top “N” most similar MRI images are retrieved and displayed in response to both: query MR image and similarity measure associated with the number of the patient case at the top of the retrieved images as shown in Figure (4.4).

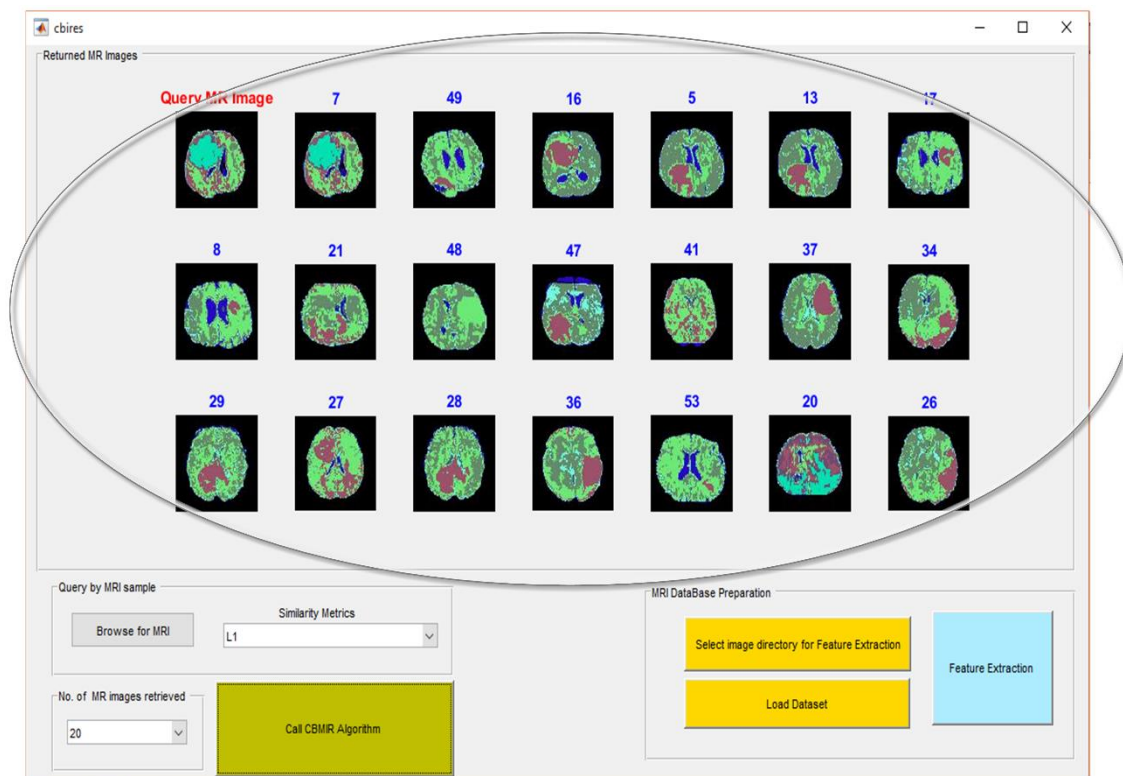


**Figure (4.4): The Top (N =20) Retrieved Brain MR Images**

After the retrieval process is done, the neurologists, or neurosurgeons can then study the characteristics of the retrieved MR images and can also compare it with the patient case which will assist the neurologists, or neurosurgeons in the process of making case-based decision.

#### 4.4 CBBIR System: Experimental Results and Performance Analysis

This section is dedicated to evaluate the effectiveness of our proposed CBBIR retrieval system, where we evaluate the similarity metrics in terms of precision and recall in retrieving images that are relevant to twenty example MR image queries.

The effectiveness of any image content retrieval system is estimated via overall retrieval performance in terms of overall precision and recall.

The overall performance is performed inherently by considering each image as query image and measures the retrieval outcome and report the overall average which equals precision (or recall) for each query image divided by the number of query images used in the process of performance evaluation (Maheswari, 2013).

Generally speaking, recall is defined as the ratio of relevant items retrieved to the total number in the database. Therefore, it measures the ability of the retrieval system to present all relevant items and it given by the following mathematical formula:

$$Recall = \frac{NO. of Relevant retrieved images}{Total number of relevant images in database} \quad (4.1)$$

Whereas, the precision is the ratio of relevant items retrieved to the total number of items retrieved, and it measures the capability of the retrieval system to present only the relevant items. Precision of retrieval system is evaluated by the following mathematical formula:

$$Precision = \frac{NO. of Relevant retrieved images}{Total number of retrieved images} \quad (4.2)$$

In order to elaborate the recall and precision concepts, let us assume that our database has total brain MR images of (126) and it contains (20) brain tumor MR images in particular, Now, let us assume that we run a retrieval system for top (20) brain tumor MR images. Then, if the retrieval system retrieves (17) brain tumor MR images correctly and the other images belongs to other brain diseases, then the precision equal to  $(17/20 = 0.8500)$  that means we have (15%) false negative error. Now, the recall equals the total number of brain tumor MR images that really exist in the database which is in our case equal to (20) and since the retrieval system was capable to retrieved all relevant images in the original database, that means recall equals to  $(20/20 = 100\%)$ .

Therefore, in order to measure the performance of our proposed system we create two databases: one database contains (20) brain tumor MR images and the other one contains (53) brain tumor MR images, in this way we can ensure that our proposed system can deals with large databases effectively as it small one and we can ensure the performance of the similarity measures and the efficiency of KNN classification technique.

#### **4.4.1 CBBIR System Performance Analysis: Precision**

As mentioned in previous section, *Precision* is one of the performance measures that we have used to evaluate the retrieval performance and effectiveness of our proposed CBBIR system in two stages.

In the first stage, the experimental results and their associated performance analysis in terms of precision for each similarity measures (we have 10 similarity measures) are evaluated based on two database structures: (1) Database composed of (126) MRI image includes (53) brain tumor cases and (2) Database composed of (96)

MRI image includes (20) brain tumor cases where the number of retrieved MR images is (20).

Then, in the second stage, we have run our proposed CBBIR system using the first database structure, namely, (126 (total) and 53 (Brain Tumor)) to retrieve different number of MR images: {5, 10, 15} where the precision is calculated for the best similarity measures that yield the best performance in first stage.

We will use the abbreviation of BT to stands for number of brain tumor cases in the database under consideration.

The retrieval precisions and the overall retrieval precision of the twenty random-selected sample of query brain tumor MR images are listed in table (4.1) to table (4.10) based on the first structure of database and for (10) similarity measures, where the number of retrieved MR images for each query brain tumor image was twenty (20). As shown in Table (4.1).

**Table (4.1): Precision of CBBIR System (BT =53), Similarity Measure: L1**

Patient No.(Query MRI)	Brain Tumor	Non-Brain Tumor	Precision
1	13	7	65%
5	20	0	100%
7	20	0	100%
13	20	0	100%
14	20	0	100%
19	20	0	100%
20	19	1	95%
22	20	0	100%
24	16	4	80%
25	20	0	100%
27	20	0	100%
28	20	0	100%
29	20	0	100%
30	20	0	100%
37	20	0	100%
38	20	0	100%
40	20	0	100%
41	20	0	100%
46	20	0	100%
50	20	0	100%
<b>Average Precision</b>			<b>97%</b>

Table (4.2): Precision of CBBIR System (BT =53), Similarity Measure: L2

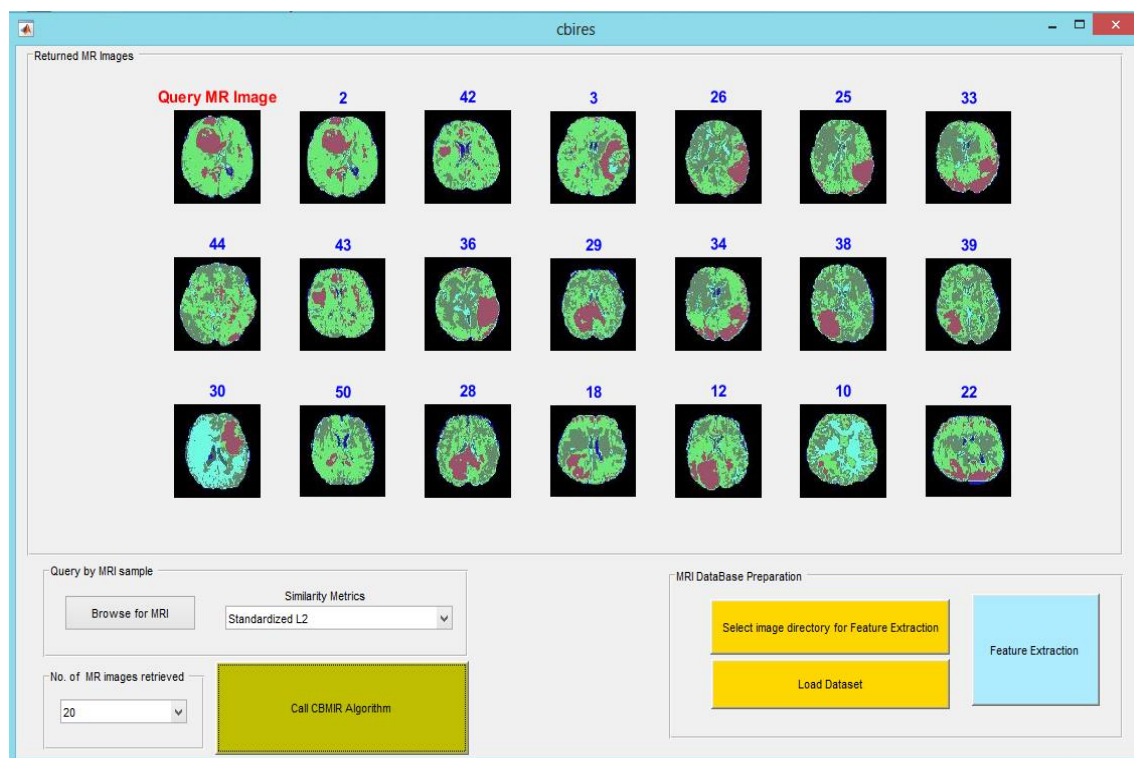
Patient No.(Query MRI)	Brain Tumor	Non-Brain Tumor	Precision
1	13	7	65%
5	20	0	100%
7	20	0	100%
13	20	0	100%
14	20	0	100%
19	20	0	100%
20	20	0	100%
22	20	0	100%
24	17	3	85%
25	20	0	100%
27	20	0	100%
28	20	0	100%
29	20	0	100%
30	20	0	100%
37	20	0	100%
38	20	0	100%
40	20	0	100%
41	20	0	100%
46	20	0	100%
50	20	0	100%
<b>Average Precision</b>			<b>97.5%</b>



Figure (4.5): Sample Retrieval CBBIR System Using Similarity Measure: L2

**Table (4.3): Precision of CBBIR System (BT =53), Similarity Measure: Standardized L2**

Patient No.(Query MRI)	Brain Tumor	Non-Brain Tumor	Precision
1	13	7	65%
5	20	0	100%
7	20	0	100%
13	19	1	95%
14	20	0	100%
19	20	0	100%
20	19	1	95%
22	20	0	100%
24	14	6	70%
25	20	0	100%
27	20	0	100%
28	20	0	100%
29	20	0	100%
30	18	2	90%
37	20	0	100%
38	20	0	100%
40	19	1	95%
41	19	1	95%
46	19	1	95%
50	19	1	95%
<b>Average Precision</b>			<b>94.75%</b>



**Figure (4.6): Sample Retrieval CBBIR System Using Similarity Measure: Standardized L2**

Table (4.4): Precision of CBBIR System (BT =53), Similarity Measure: Cityblock

Patient No.(Query MRI)	Brain Tumor	Non-Brain Tumor	Precision
1	13	7	65%
5	20	0	100%
7	20	0	100%
13	20	0	100%
14	20	0	100%
19	20	0	100%
20	20	0	100%
22	20	0	100%
24	15	5	75%
25	20	0	100%
27	20	0	100%
28	20	0	100%
29	20	0	100%
30	20	0	100%
37	20	0	100%
38	20	0	100%
40	20	0	100%
41	20	0	100%
46	20	0	100%
50	20	0	100%
<b>Average Precision</b>			<b>97%</b>



Figure (4.7): Sample Retrieval CBBIR System Using Similarity Measure: Cityblock

Table (4.5): Precision of CBBIR System (BT =53), Similarity Measure: Minkowski

Patient No.(Query MRI)	Brain Tumor	Non-Brain Tumor	Precision
1	13	7	65%
5	20	0	100%
7	20	0	100%
13	20	0	100%
14	20	0	100%
19	20	0	100%
20	20	0	100%
22	20	0	100%
24	17	3	85%
25	20	0	100%
27	20	0	100%
28	20	0	100%
29	20	0	100%
30	20	0	100%
37	20	0	100%
38	20	0	100%
40	20	0	100%
41	20	0	100%
46	20	0	100%
50	20	0	100%
<b>Average Precision</b>			<b>97.5%</b>



Figure (4.8): Sample Retrieval CBBIR System Using Similarity Measure: Minkowski

**Table (4.6): Precision of CBBIR System (BT =53), Similarity Measure: Chebychev**

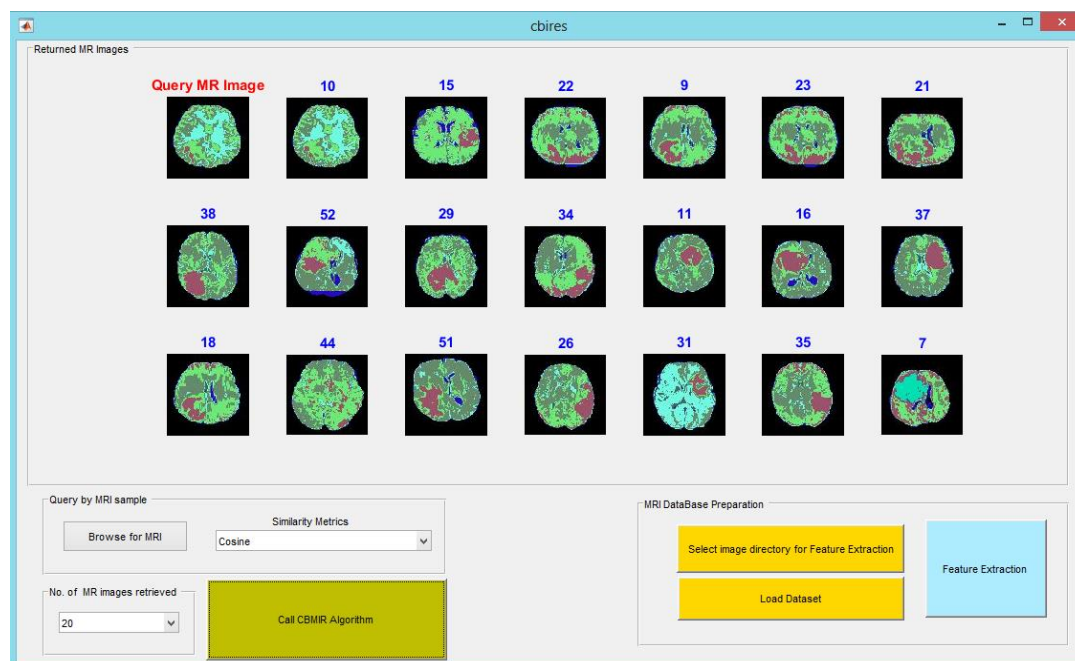
Patient No.(Query MRI)	Brain Tumor	Non-Brain Tumor	Precision
1	15	5	75%
5	20	0	100%
7	20	0	100%
13	20	0	100%
14	20	0	100%
19	20	0	100%
20	18	2	90%
22	20	0	100%
24	16	4	80%
25	20	0	100%
27	20	0	100%
28	20	0	100%
29	20	0	100%
30	20	0	100%
37	20	0	100%
38	20	0	100%
40	20	0	100%
41	20	0	100%
46	18	2	90%
50	20	0	100%
<b>Average Precision</b>			<b>96.75%</b>



**Figure (4.9): Sample Retrieval CBBIR System Using Similarity Measure: Chebychev**

**Table (4.7): Precision of CBBIR System (BT =53), Similarity Measure: Cosine**

Patient No.(Query MRI)	Brain Tumor	Non-Brain Tumor	Precision
1	20	0	100%
5	20	0	100%
7	20	0	100%
13	20	0	100%
14	20	0	100%
19	20	0	100%
20	20	0	100%
22	20	0	100%
24	19	1	95%
25	20	0	100%
27	20	0	100%
28	20	0	100%
29	20	0	100%
30	20	0	100%
37	20	0	100%
38	20	0	100%
40	20	0	100%
41	20	0	100%
46	20	0	100%
50	20	0	100%
<b>Average Precision</b>			<b>99.75%</b>

**Figure (4.10): Sample Retrieval CBBIR System Using Similarity Measure: Cosine**

**Table (4.8): Precision of CBBIR System (BT =53), Similarity Measure: Correlation**

Patient No.(Query MRI)	Brain Tumor	Non-Brain Tumor	Precision
1	20	0	100%
5	20	0	100%
7	20	0	100%
13	20	0	100%
14	20	0	100%
19	20	0	100%
20	20	0	100%
22	20	0	100%
24	19	1	95%
25	20	0	100%
27	20	0	100%
28	20	0	100%
29	20	0	100%
30	20	0	100%
37	20	0	100%
38	20	0	100%
40	20	0	100%
41	20	0	100%
46	20	0	100%
50	20	0	100%
<b>Average Precision</b>			<b>99.75%</b>

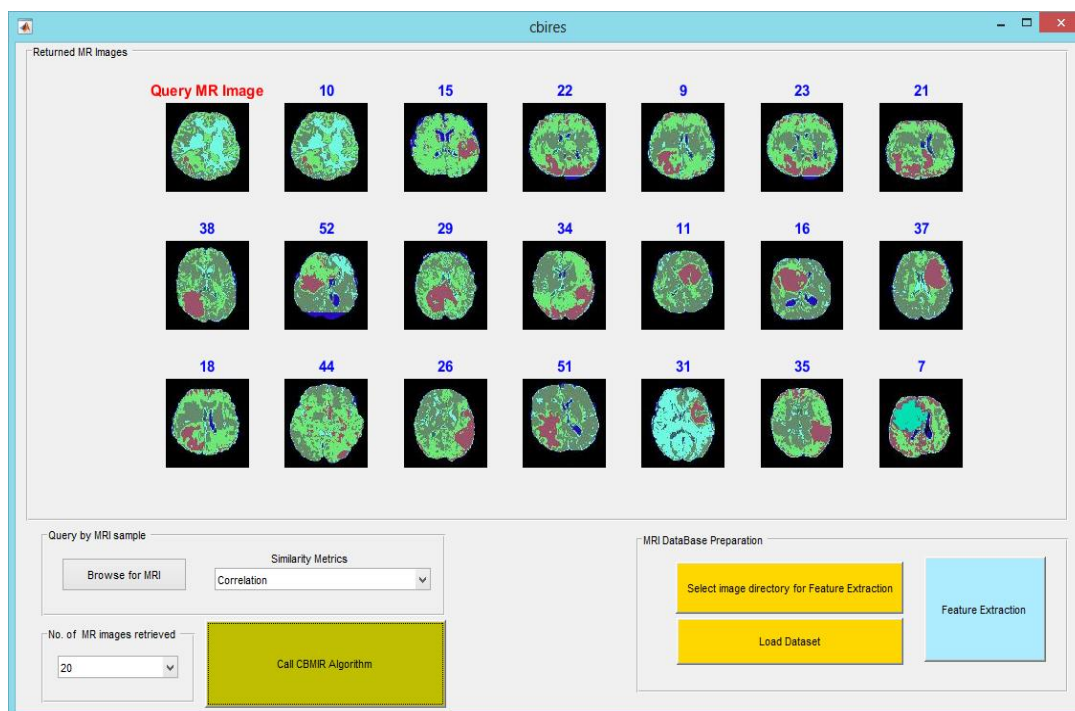


**Figure (4.11): Sample Retrieval CBBIR System Using Similarity Measure: Correlation**

**Table (4.9): Precision of CBBIR System (BT =53), Similarity Measure: Spearman**

Patient No.(Query MRI)	Brain Tumor	Non-Brain Tumor	Precision
1	8	12	40%
5	20	0	100%
7	20	0	100%
13	18	2	90%
14	17	3	85%
19	16	4	80%
20	18	2	90%
22	20	0	100%
24	7	13	35%
25	16	4	80%
27	17	3	85%
28	17	3	85%
29	20	0	100%
30	11	9	55%
37	20	0	100%
38	15	5	75%
40	18	2	90%
41	17	3	85%
46	14	6	70%
50	16	4	80%
<b>Average Precision</b>			<b>81.25%</b>



**Figure (4.12): Sample Retrieval CBBIR System Using Similarity Measure: Spearman**

**Table (4.10): Precision of CBBIR System (BT =53), Similarity Measure: Normalized L2**

Patient No.(Query MRI)	Brain Tumor	Non-Brain Tumor	Precision
1	13	7	65%
5	20	0	100%
7	20	0	100%
13	20	0	100%
14	20	0	100%
19	20	0	100%
20	20	0	100%
22	20	0	100%
24	17	3	85%
25	20	0	100%
27	20	0	100%
28	20	0	100%
29	20	0	100%
30	20	0	100%
37	20	0	100%
38	20	0	100%
40	20	0	100%
41	20	0	100%
46	20	0	100%
50	20	0	100%
<b>Average Precision</b>			<b>97.5%</b>



**Figure (4.13): Sample Retrieval CBBIR System Using Similarity Measure: Normalized L2**

In our research, we have used ten similarity measures in order to determine the best similarity measure for brain tumor detection. To investigate these similarity measures we have compared the overall average precision when the proposed system run on the same sample and compare the precision values as shown in Figure (4.14).

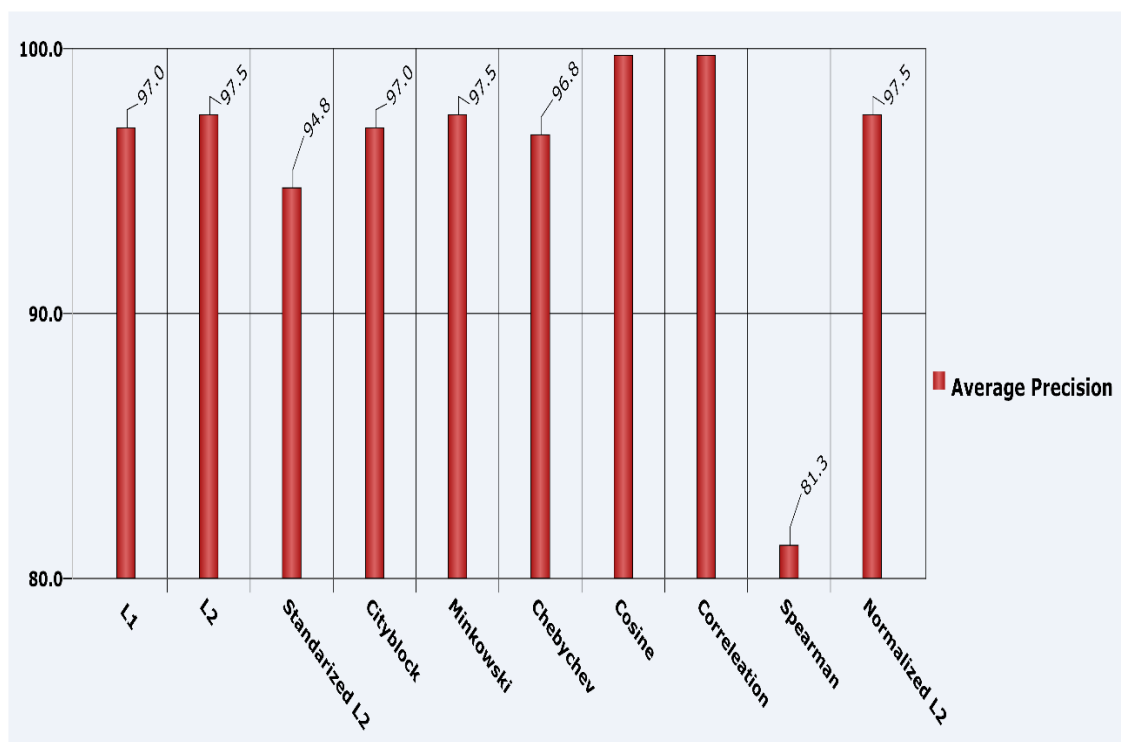


**Figure (4.14): Precision Comparison between the Similarity Measures of CBBIR System (BT =53)**

As shown in Figure (4.14), *Correlation* and *Cosine* similarity measures have the highest achieved precision, that means they have the highest capability to discriminate the features of different brain MR images.

This is expected since the *Cosine* similarity and *correlation* (or as called *Pearson correlation*) similarity can all be viewed as variants on the inner product, namely, they are versions of inner products that can result if the image under consideration undergoes different ways of centring and magnitude variations.

To elaborate this idea, let us assume that we represent our MR images as two vectors  $X$  and  $Y$  where we want to measure the similarity between them. Then, a basic similarity function would be the inner product or:

$$Inner(x, y) = \sum_i x_i y_i = \langle x, y \rangle \quad (4.3)$$

This equation means that if  $X$  tends to be high where  $Y$  is also high, and low where  $Y$  is low, then the inner product will be high, which means that the vectors are more similar. However, the inner product is unbounded and there is one way to make it bounded between -1 and +1 namely; it can be divided by the vectors' L2 norms, which will give us the Cosine similarity measure or:

$$CosineSim(x, y) = \frac{\sum_i x_i y_i}{\sqrt{\sum_i x_i^2} \sqrt{\sum_i y_i^2}} = \frac{\langle x, y \rangle}{\|x\| \|y\|} \quad (4.4)$$

Now, if  $X$  and  $Y$  are non-negative, the cosine similarity is bounded between 0 and 1. The cosine can be interpreted as the cosine of the angle between two vectors  $X$  and  $Y$ . However, The Cosine similarity measure is not invariant to shifts (shift in MR image), namely, if the pixels of  $X$  are shifted by one or  $X+1$  then the cosine similarity will change its value.

Now, Pearson Correlation is invariant to shift. Let  $\bar{X}$  and  $\bar{Y}$  be the means of  $X$  and  $Y$  vectors respectively. Then, the similarity between  $X$  and  $Y$  is not invariant if these vectors undergoes some sort of shifting (since it depends on means not on the vector itself).

Pearson Correlation (or correlation similarity) given as:

$$Correlation(x, y) = \frac{\sum(x_i - \bar{X})(y_i - \bar{y})}{\sqrt{\sum_i(x_i - \bar{X})^2}\sqrt{\sum_i(y_i - \bar{y})^2}} = \frac{\langle x - \bar{X}, y - \bar{Y} \rangle}{\|x - \bar{X}\| \|y - \bar{Y}\|} \quad (4.5)$$

Or

$$Correlation(x, y) = CosineSim((x_i - \bar{X})(y_i - \bar{y})) \quad (4.6)$$

As shown in the equations above, the correlation similarity is just the cosine similarity between centred versions of X and Y and are bounded between -1 and 1. However, it is invariant to changes in both scale and locations of X and Y pixels.

Since the Brain lesions can be thought of as vectors that have similar means and features, then the cosine and correlation similarity measures will yield the best recognition results.

The usual way to derive the Pearson's correlation is the normalized form of the covariance which in turn represents the centred average of the inner product (inner product alone represent no normalization). Mathematically given by:

$$Cov(x, y) = \frac{\sum(x_i - \bar{X})(y_i - \bar{y})}{n} = \frac{\langle x - \bar{X}, y - \bar{Y} \rangle}{n} \quad (4.7)$$

Next section will discuss the performance of our proposed CBBIR system in terms of Recall.

#### 4.4.2 CBBIR System Performance Analysis: Recall

The retrieval precisions and the overall retrieval recall of the twenty random-selected sample of query brain tumor MR images are listed in table (4.11) up to table (4.20) based on the second structure of database and for (10) similarity measures, where the number of retrieved MR images for each query brain tumor image was twenty (20).

**Table (4.11): Recall of CBBIR System (BT =20), Similarity Measure: L1**

Patient No.(Query MRI)	Brain Tumor	Non-Brain Tumor	Recall
1	9	11	45%
2	20	0	100%
3	18	2	90%
4	14		70%
5	18	6	90%
13	17	2	85%
16	17	3	85%
17	18	3	90%
19	18	2	90%
22	18	2	90%
25	18	2	90%
28	18	2	90%
30	18	2	90%
31	16	4	80%
33	18	2	90%
35	18	2	90%
39	18	2	90%
40	17	3	85%
44	16	4	80%
53	17	3	85%
<b>Average recall</b>			<b>85.25%</b>

Table (4.12): Recall of CBBIR System (BT =20), Similarity Measure: L2

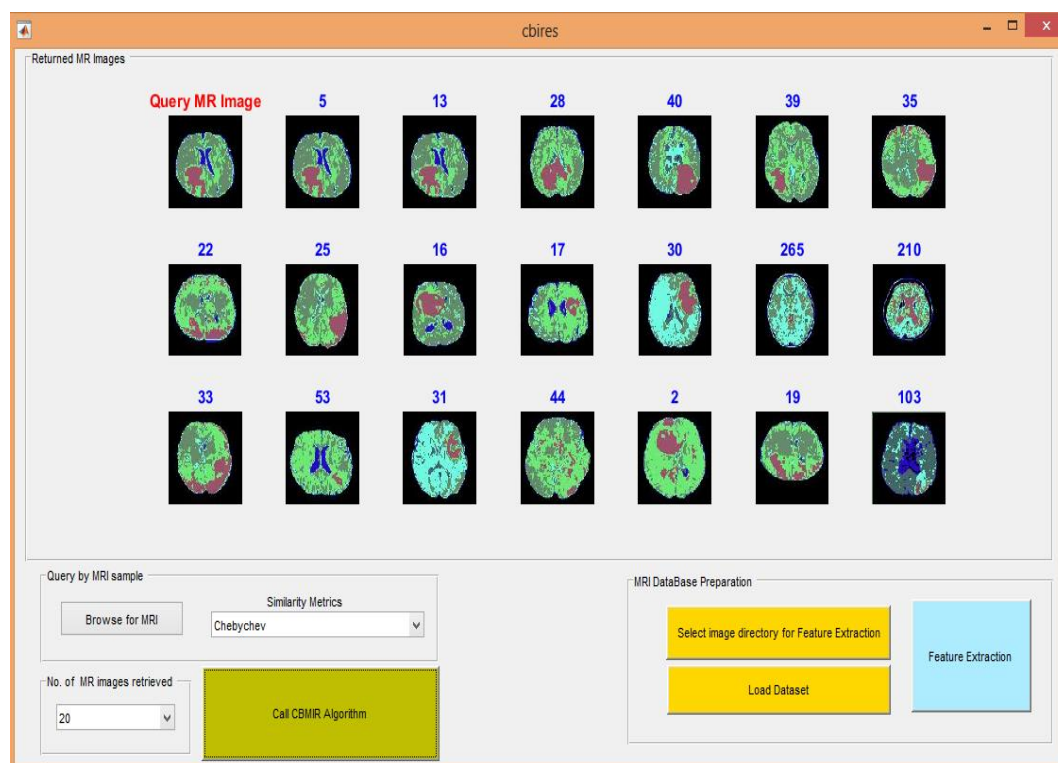
Patient No.(Query MRI)	Brain Tumor	Non-Brain Tumor	Recall
1	9	11	45%
2	18	2	90%
3	19	1	95%
4	10	10	50%
5	17	3	85%
13	17	3	85%
16	17	3	85%
17	18	2	90%
19	18	2	90%
22	18	2	90%
25	18	2	90%
28	18	2	90%
30	18	2	90%
31	16	4	80%
33	17	3	85%
35	18	2	90%
39	18	2	90%
40	18	2	90%
44	18	2	90%
53	16	4	80%
<b>Average recall</b>			<b>84%</b>



Figure (4.15): Sample Retrieval CBBIR System Using Similarity Measure: L2

**Table (4.13): Recall of CBBIR System (BT =20), Similarity Measure: Chebyshev**

Patient No.(Query MRI)	Brain Tumor	Non-Brain Tumor	Recall
1	9	11	45%
2	18	2	90%
3	18	2	90%
4	9	11	45%
5	17	3	85%
13	17	3	85%
16	17	3	85%
17	17	3	85%
19	17	3	85%
22	18	2	90%
25	17	3	85%
28	18	2	90%
30	18	2	90%
31	17	3	85%
33	17	3	85%
35	17	3	85%
39	17	3	85%
40	17	3	85%
44	18	2	90%
53	17	3	85%
<b>Average recall</b>			<b>82.5%</b>



**Figure (4.16): Sample Retrieval CBBIR System Using Similarity Measure: Chebyshev**

**Table (4.14): Recall of CBBIR System (BT =20), Similarity Measure: CityBlock**

Patient No.(Query MRI)	Brain Tumor	Non-Brain Tumor	Recall
1	9	11	45%
2	18	2	90%
3	19	1	95%
4	11	9	55%
5	18	2	90%
13	18	2	90%
16	17	3	90%
17	18	2	90%
19	18	2	90%
22	18	2	90%
25	18	2	90%
28	18	2	90%
30	18	2	90%
31	16	4	80%
33	18	2	90%
35	18	2	90%
39	18	2	90%
40	18	2	90%
44	18	2	90%
53	17	3	85%
<b>Average recall</b>			<b>85.25%</b>



**Figure (4.17): Sample Retrieval CBBIR System Using Similarity Measure: Cityblock**

**Table (4.15): Recall of CBBIR System (BT =20), Similarity Measure: Correlation**

Patient No.(Query MRI)	Brain Tumor	Non-Brain Tumor	Recall
1	18	2	90%
2	20	0	100%
3	20	0	100%
4	19	1	95%
5	19	1	95%
13	19	1	95%
16	19	1	95%
17	20	0	100%
19	20	0	100%
22	20	0	100%
25	20	0	100%
28	20	0	100%
30	20	0	100%
31	19	1	95%
33	20	0	100%
35	20	0	100%
39	20	0	100%
40	20	0	100%
44	20	0	100%
53	19	1	95%
<b>Average recall</b>			<b>98%</b>



**Figure (4.18): Sample Retrieval CBBIR System Using Similarity Measure: Correlation**

**Table (4.16): Recall of CBBIR System (BT =20), Similarity Measure: Cosine**

Patient No.(Query MRI)	Brain Tumor	Non-Brain Tumor	Recall
1	18	2	90%
2	20	0	100%
3	20	0	100%
4	19	1	95%
5	19	1	95%
13	19	1	95%
16	19	1	95%
17	20	0	100%
19	20	0	100%
22	20	0	100%
25	20	0	100%
28	20	0	100%
30	20	0	100%
31	19	1	95%
33	20	0	100%
35	20	0	100%
39	20	0	100%
40	20	0	100%
44	20	0	100%
53	19	1	95%
<b>Average recall</b>			<b>98%</b>

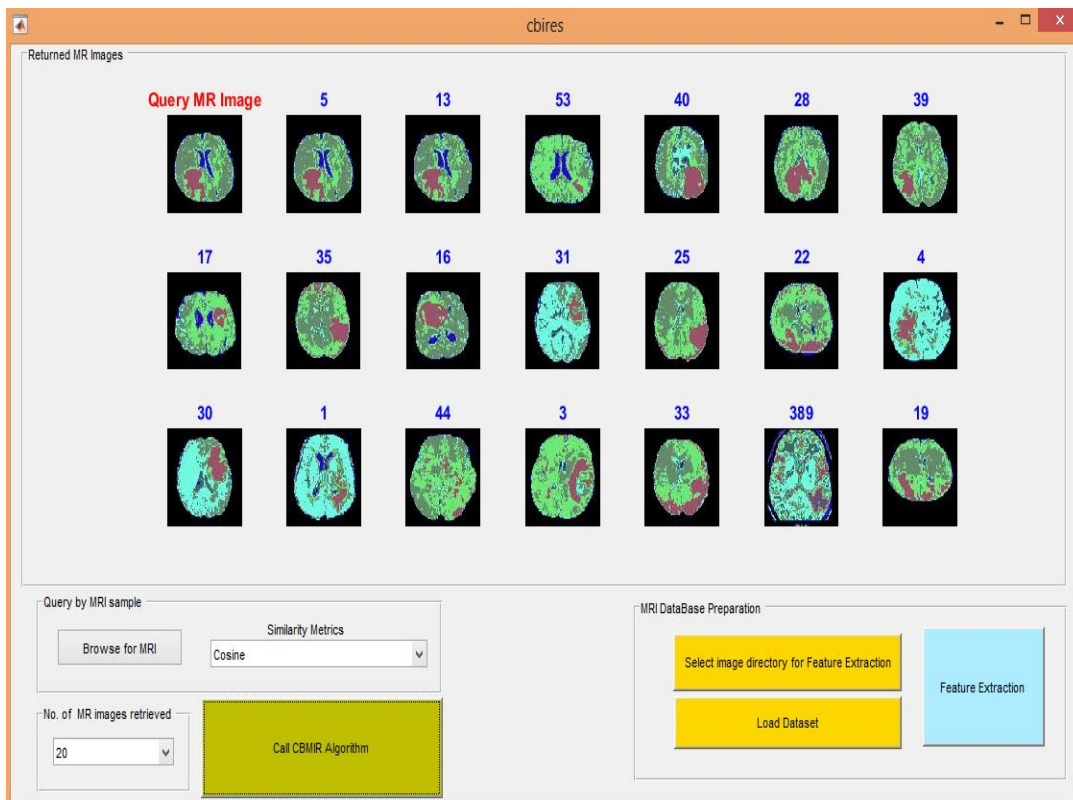


**Figure (4.19): Sample Retrieval CBBIR System Using Similarity Measure: Cosine**

Table (4.17): Recall of CBBIR System (BT =20), Similarity Measure: Minkowski

Patient No.(Query MRI)	Brain Tumor	Non-Brain Tumor	Recall
1	9	11	45%
2	18	2	90%
3	19	1	95%
4	10	10	50%
5	17	3	85%
13	17	3	85%
16	17	3	85%
17	18	2	90%
19	18	2	90%
22	18	2	90%
25	18	2	90%
28	18	2	90%
30	18	2	90%
31	16	4	80%
33	17	3	85%
35	18	2	90%
39	18	2	90%
40	18	2	90%
44	18	2	90%
53	16	4	80%
<b>Average recall</b>			<b>84%</b>

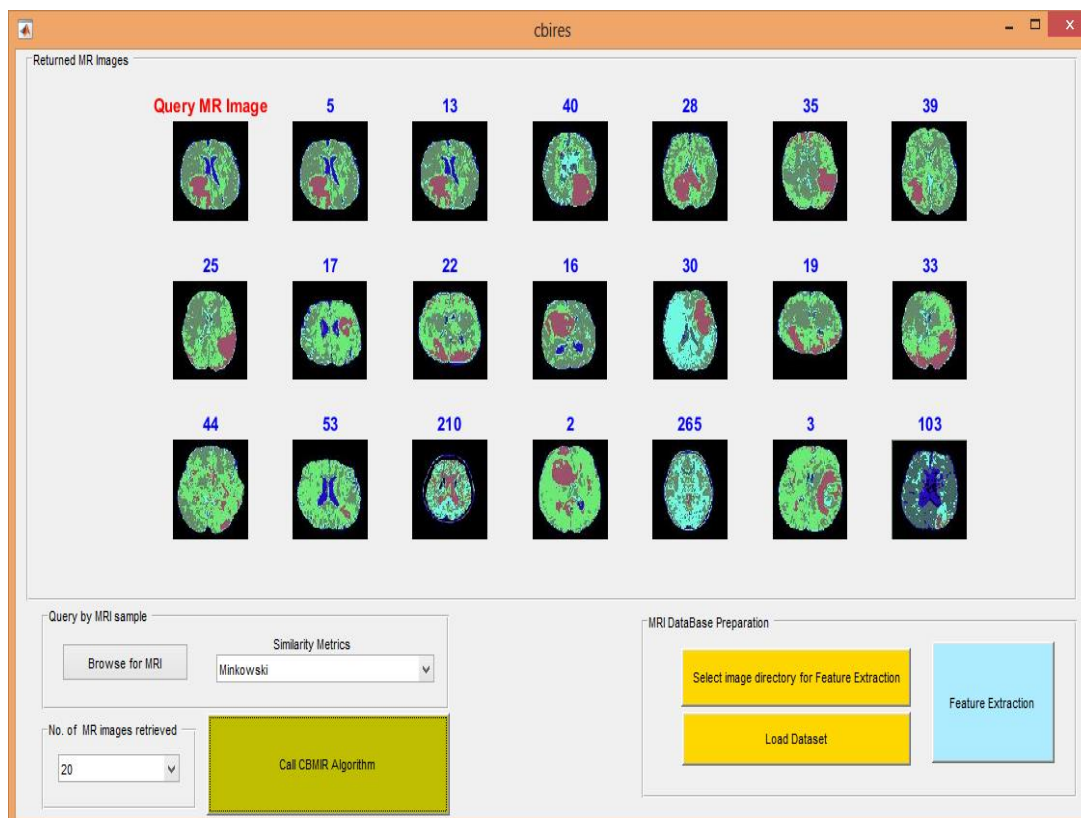


Figure (4.20): Sample Retrieval CBBIR System Using Similarity Measure: Minkowski

**Table (4.18): Recall of CBBIR System (BT =20), Similarity Measure: Normalized L2**

Patient No.(Query MRI)	Brain Tumor	Non-Brain Tumor	Recall
1	9	11	45%
2	18	2	90%
3	19	1	95%
4	10	10	50%
5	17	3	85%
13	17	3	85%
16	17	3	85%
17	18	2	90%
19	18	2	90%
22	18	2	90%
25	18	2	90%
28	18	2	90%
30	18	2	90%
31	16	4	80%
33	17	3	85%
35	18	2	90%
39	18	2	90%
40	18	2	90%
44	18	2	90%
53	16	4	80%
<b>Average recall</b>			<b>84%</b>

**Figure (4.21): Sample Retrieval CBBIR System Using Similarity Measure: Normalized L2**

**Table (4.19): Recall of CBBIR System (BT =20), Similarity Measure: Spearman**

Patient No.(Query MRI)	Brain Tumor	Non-Brain Tumor	Recall
1	8	12	40%
2	9	11	45%
3	10	10	50%
4	7	13	35%
5	13	7	65%
13	14	6	70%
16	14	6	70%
17	12	8	60%
19	10	10	50%
22	9	11	45%
25	9	11	45%
28	10	10	50%
30	9	11	45%
31	4	16	20%
33	12	8	60%
35	8	12	40%
39	7	13	35%
40	12	8	60%
44	8	12	40%
53	12	8	60%
<b>Average recall</b>			<b>49.25%</b>

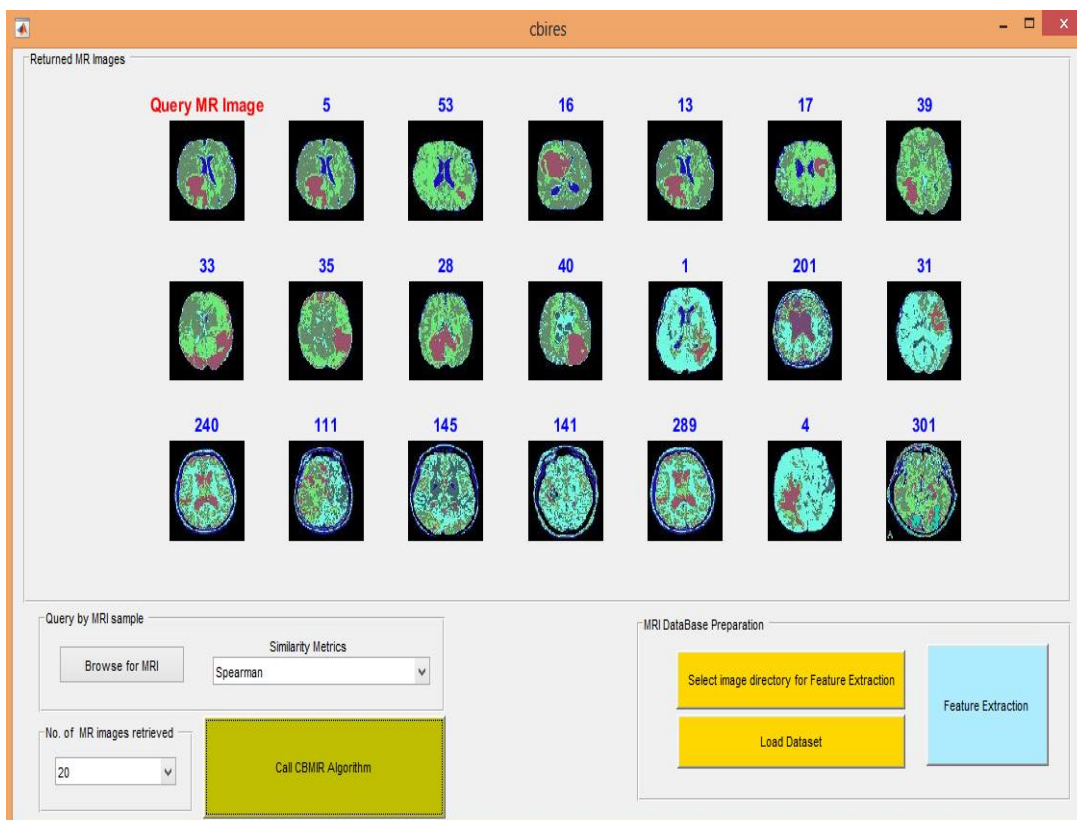


**Figure (4.22): Sample Retrieval CBBIR System Using Similarity Measure: Spearman**

**Table (4.20): Recall of CBBIR System (BT =20), Similarity Measure: Standardized L2**

Patient No.(Query MRI)	Brain Tumor	Non-Brain Tumor	Recall
1	9	11	45%
2	18	2	90%
3	16	4	80%
4	12	8	60%
5	13	7	65%
13	12	8	60%
16	13	7	65%
17	13	7	65%
19	15	5	75%
22	15	5	75%
25	16	4	80%
28	16	4	80%
30	16	4	80%
31	13	7	65%
33	16	4	80%
35	16	4	80%
39	15	5	75%
40	13	7	65%
44	13	7	65%
53	14	6	70%
<b>Average recall</b>			<b>71%</b>



**Figure (4.23): Sample Retrieval CBBIR System Using Similarity Measure: Standardized L2**

Now, in order to investigate the average recall of our proposed CBBIR system using the different similarity measures, we have compared the overall average recall when the proposed system run on the same sample and compare the recall values as shown in Figure (4.24).

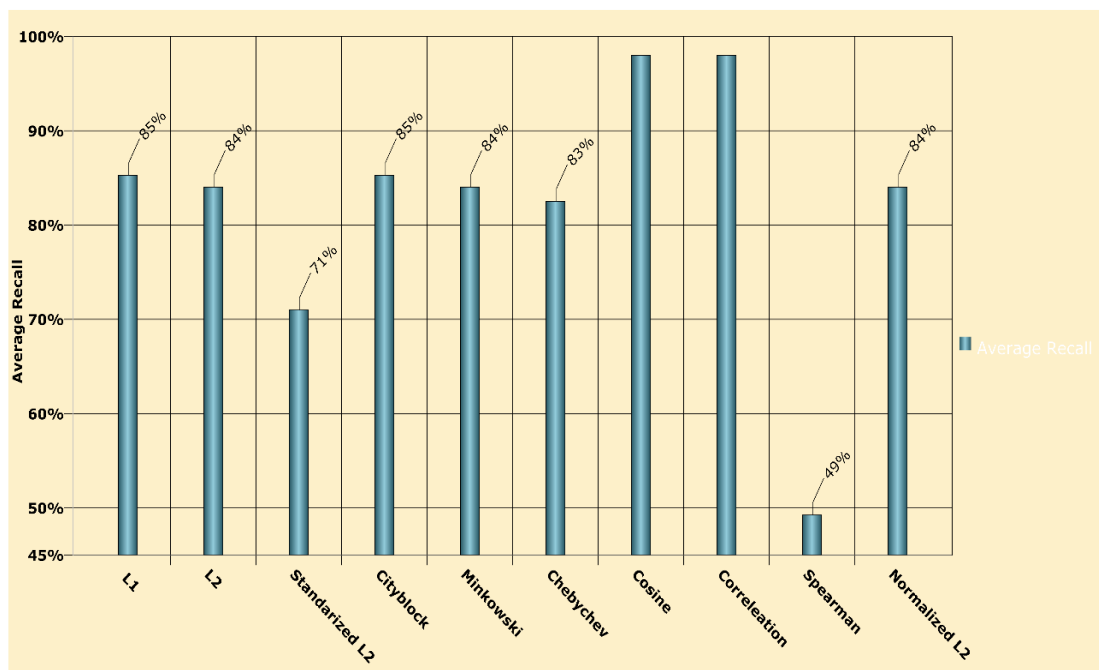


**Figure (4.24): Recall Comparison between the Similarity Measures of CBBIR System (BT =20)**

As shown in Figure (4.24), *Cosine* and *Correlation* have achieved high recall performance for brain tumor MR image recognition which is a powerful indicator that the most suitable similarity measures for this band of brain disease detection is the *Cosine* and *Correlation* distance metrics.

Even though that most of similarity measures achieved high precision performance, they achieve low level of recall performance. Therefore, as a conclusion of this research, *cosine* and *correlation* similarity measures are the best similarity measures that have the highest capability in retrieving the most similar patient cases in case of brain tumor.

## **4.5 Comparison of Similarity Measures for Different Number of Retrieved Images.**

The performance of our proposed CBBIR system depends on four basic building blocks: Automatic brain tumor segmentation, feature extraction techniques, classification technique, and the used similarity measure. In this section, we elaborate the effect of varying the number of retrieved brain MR images on the overall precision of the proposed system. Then we deduce the optimal number of retrieved images that we recommend to be chosen via our system implementation.

Therefore, Tables (4.21) to (4.30) list the average precision for our similarity measures when the number of retrieval images per query image is **{5, 10, 15}**. Then a graphical comparison between similarity measures retrieval performance shows the general tendency of these measures.

**Table (4.21): Precision of CBBIR System (BT =53), Similarity Measure: L1**

Patient No.(Query MRI)	Brain Tumor	Non-Brain Tumor	Precision
1	5	0	100%
2	5	0	100%
3	5	0	100%
4	5	0	100%
5	5	0	100%
13	5	0	100%
16	5	0	100%
17	5	0	100%
19	5	0	100%
22	5	0	100%
25	5	0	100%
28	5	0	100%
30	5	0	100%
31	5	0	100%
33	5	0	100%
35	5	0	100%
39	5	0	100%
40	5	0	100%
44	5	0	100%
53	5	0	100%
<b>Average Precision</b>			<b>100%</b>
Patient No.(Query MRI)	Brain Tumor	Non-Brain Tumor	Precision
1	7	3	70%
2	10	0	100%
3	10	0	100%
4	9	1	90%
5	10	0	100%
13	10	0	100%
16	10	0	100%
17	10	0	100%
19	10	0	100%
22	10	0	100%
25	10	0	100%
28	10	0	100%
30	10	0	100%
31	8	2	80%
33	10	0	100%
35	10	0	100%
39	10	0	100%
40	10	0	100%
44	10	0	100%
53	10	0	100%
<b>Average Precision</b>			<b>97%</b>
Patient No.(Query MRI)	Brain Tumor	Non-Brain Tumor	Precision
1	9	6	60%
2	15	0	100%
3	15	0	100%
4	12	3	80%
5	13	2	86.67%
13	13	2	86.67%
16	13	2	86.67%
17	14	1	93.33%
19	14	1	93.33%
22	15	0	100%
25	14	1	93.33%
28	14	1	93.33%
30	14	1	93.33%
31	13	2	86.67%
33	14	1	93.33%
35	14	1	93.33%
39	14	1	93.33%
40	13	2	86.67%
44	15	0	100%
53	15	0	100%
<b>Average Precision</b>			<b>91%</b>

**Table (4.22): Precision of CBBIR System (BT =53), Similarity Measure: L2**

Patient No.(Query MRI)	Brain Tumor	Non-Brain Tumor	Precision
1	3	2	60%
2	5	0	100%
3	5	0	100%
4	5	0	100%
5	5	0	100%
13	5	0	100%
16	5	0	100%
17	5	0	100%
19	5	0	100%
22	5	0	100%
25	5	0	100%
28	5	0	100%
30	5	0	100%
31	5	0	100%
33	5	0	100%
35	5	0	100%
39	5	0	100%
40	5	0	100%
44	5	0	100%
53	5	0	100%
<b>Average Precision</b>			<b>98%</b>
Patient No.(Query MRI)	Brain Tumor	Non-Brain Tumor	Precision
1	3	2	60%
2	5	0	100%
3	5	0	100%
4	5	0	100%
5	5	0	100%
13	5	0	100%
16	5	0	100%
17	5	0	100%
19	5	0	100%
22	5	0	100%
25	5	0	100%
28	5	0	100%
30	5	0	100%
31	5	0	100%
33	5	0	100%
35	5	0	100%
39	5	0	100%
40	5	0	100%
44	5	0	100%
53	5	0	100%
<b>Average Precision</b>			<b>98%</b>
Patient No.(Query MRI)	Brain Tumor	Non-Brain Tumor	Precision
1	3	2	60%
2	5	0	100%
3	5	0	100%
4	5	0	100%
5	5	0	100%
13	5	0	100%
16	5	0	100%
17	5	0	100%
19	5	0	100%
22	5	0	100%
25	5	0	100%
28	5	0	100%
30	5	0	100%
31	5	0	100%
33	5	0	100%
35	5	0	100%
39	5	0	100%
40	5	0	100%
44	5	0	100%
53	5	0	100%
<b>Average Precision</b>			<b>98%</b>

**Table (4.23): Precision of CBBIR System (BT =53), Similarity Measure: Standardized L2**

Patient No.(Query MRI)	Brain Tumor	Non-Brain Tumor	Precision
1	4	1	80%
2	5	0	100%
3	5	0	100%
4	4	1	80%
5	5	0	100%
13	5	0	100%
16	5	0	100%
17	5	0	100%
19	5	0	100%
22	5	0	100%
25	5	0	100%
28	5	0	100%
30	4	1	80%
31	3	2	60%
33	5	0	100%
35	5	0	100%
39	4	1	80%
40	5	0	100%
44	5	0	100%
53	4	1	80%
<b>Average Precision</b>			<b>93%</b>
Patient No.(Query MRI)	Brain Tumor	Non-Brain Tumor	Precision
1	6	4	60%
2	10	0	100%
3	9	1	90%
4	7	3	70%
5	10	0	100%
13	9	1	90%
16	9	1	90%
17	8	2	80%
19	10	0	100%
22	10	0	100%
25	10	0	100%
28	10	0	100%
30	8	2	80%
31	8	2	80%
33	10	0	100%
35	10	0	100%
39	8	2	80%
40	9	1	90%
44	9	1	90%
53	9	1	90%
<b>Average Precision</b>			<b>89.5%</b>
Patient No.(Query MRI)	Brain Tumor	Non-Brain Tumor	Precision
1	7	8	46.67%
2	15	0	100%
3	13	2	86.67%
4	9	6	60%
5	11	4	73.33%
13	10	5	66.67%
16	11	4	73.33%
17	10	5	66.67%
19	13	2	86.67%
22	13	2	86.67%
25	14	1	93.33%
28	13	2	86.67%
30	12	3	80%
31	11	4	73.33%
33	14	1	93.33%
35	14	1	93.33%
39	13	2	86.67%
40	11	4	73.33%
44	12	3	80%
53	11	4	73.33%
<b>Average Precision</b>			<b>79%</b>

**Table (4.24): Precision of CBBIR System (BT =53), Similarity Measure: Chebychev**

Patient No.(Query MRI)	Brain Tumor	Non-Brain Tumor	Precision
1	5	0	100%
2	5	0	100%
3	5	0	100%
4	4	1	80%
5	5	0	100%
13	5	0	100%
16	5	0	100%
17	5	0	100%
19	5	0	100%
22	5	0	100%
25	5	0	100%
28	5	0	100%
30	5	0	100%
31	5	0	100%
33	5	0	100%
35	5	0	100%
39	5	0	100%
40	5	0	100%
44	5	0	100%
53	5	0	100%
<b>Average Precision</b>			<b>99%</b>
Patient No.(Query MRI)	Brain Tumor	Non-Brain tumor	Precision
1	5	0	100%
2	5	0	100%
3	5	0	100%
4	4	1	80%
5	5	0	100%
13	5	0	100%
16	5	0	100%
17	5	0	100%
19	5	0	100%
22	5	0	100%
25	5	0	100%
28	5	0	100%
30	5	0	100%
31	5	0	100%
33	5	0	100%
35	5	0	100%
39	5	0	100%
40	5	0	100%
44	5	0	100%
53	5	0	100%
<b>Average Precision</b>			<b>99%</b>
Patient No.(Query MRI)	Brain Tumor	Non-Brain Tumor	Precision
1	5	0	100%
2	5	0	100%
3	5	0	100%
4	4	1	80%
5	5	0	100%
13	5	0	100%
16	5	0	100%
17	5	0	100%
19	5	0	100%
22	5	0	100%
25	5	0	100%
28	5	0	100%
30	5	0	100%
31	5	0	100%
33	5	0	100%
35	5	0	100%
39	5	0	100%
40	5	0	100%
44	5	0	100%
53	5	0	100%
<b>Average Precision</b>			<b>99%</b>

**Table (4.25): Precision of CBBIR System (BT =53), Similarity Measure: Cityblock**

Patient No.(Query MRI)	Brain Tumor	Non-Brain Tumor	Precision
1	4	1	80%
2	5	0	100%
3	5	0	100%
4	5	0	100%
5	5	0	100%
13	5	0	100%
16	5	0	100%
17	5	0	100%
19	5	0	100%
22	5	0	100%
25	5	0	100%
28	5	0	100%
30	5	0	100%
31	5	0	100%
33	5	0	100%
35	5	0	100%
39	5	0	100%
40	5	0	100%
44	5	0	100%
53	5	0	100%
<b>Average Precision</b>			<b>99%</b>
Patient No.(Query MRI)	Brain Tumor	Non-Brain Tumor	Precision
1	6	4	60%
2	10	0	100%
3	10	0	100%
4	7	3	70%
5	10	0	100%
13	10	0	100%
16	10	0	100%
17	10	0	100%
19	10	0	100%
22	10	0	100%
25	10	0	100%
28	10	0	100%
30	10	0	100%
31	10	0	100%
33	10	0	100%
35	10	0	100%
39	10	0	100%
40	10	0	100%
44	10	0	100%
53	10	0	100%
<b>Average Precision</b>			<b>96.5%</b>
Patient No.(Query MRI)	Brain Tumor	Non-Brain Tumor	Precision
1	8	7	53.33%
2	15	0	100%
3	15	0	100%
4	10	5	66.67%
5	15	0	100%
13	15	0	100%
16	14	1	93.33%
17	15	0	100%
19	15	0	100%
22	15	0	100%
25	15	0	100%
28	14	1	93.33%
30	15	0	100%
31	13	2	86.67%
33	14	1	93.33%
35	14	1	93.33%
39	15	0	100%
40	15	0	100%
44	15	0	100%
53	15	0	100%
<b>Average Precision</b>			<b>94%</b>

**Table (4.26): Precision of CBBIR System (BT =53), Similarity Measure: Correlation**

Patient No.(Query MRI)	Brain Tumor	Non-Brain Tumor	Precision
1	5	0	100%
2	5	0	100%
3	5	0	100%
4	5	0	100%
5	5	0	100%
13	5	0	100%
16	5	0	100%
17	5	0	100%
19	5	0	100%
22	5	0	100%
25	5	0	100%
28	5	0	100%
30	5	0	100%
31	5	0	100%
33	5	0	100%
35	5	0	100%
39	5	0	100%
40	5	0	100%
44	5	0	100%
53	5	0	100%
<b>Average Precision</b>			<b>100%</b>
Patient No.(Query MRI)	Brain Tumor	Non-Brain Tumor	Precision
1	10	0	100%
2	10	0	100%
3	10	0	100%
4	10	0	100%
5	10	0	100%
13	10	0	100%
16	10	0	100%
17	10	0	100%
19	10	0	100%
22	10	0	100%
25	10	0	100%
28	10	0	100%
30	10	0	100%
31	10	0	100%
33	10	0	100%
35	10	0	100%
39	10	0	100%
40	10	0	100%
44	10	0	100%
53	10	0	100%
<b>Average Precision</b>			<b>100%</b>
Patient No.(Query MRI)	Brain Tumor	Non-Brain Tumor	Precision
1	14	1	93.33%
2	15	0	100%
3	15	0	100%
4	15	0	100%
5	15	0	100%
13	15	0	100%
16	15	0	100%
17	15	0	100%
19	15	0	100%
22	15	0	100%
25	15	0	100%
28	15	0	100%
30	15	0	100%
31	15	0	100%
33	15	0	100%
35	15	0	100%
39	15	0	100%
40	15	0	100%
44	15	0	100%
53	15	0	100%
<b>Average Precision</b>			<b>99.67%</b>

Table (4.27): Precision of CBBIR System (BT =53), Similarity Measure: Cosine

Patient No.(Query MRI)	Brain Tumor	Non-Brain Tumor	Precision
1	5	0	100%
2	5	0	100%
3	5	0	100%
4	5	0	100%
5	5	0	100%
13	5	0	100%
16	5	0	100%
17	5	0	100%
19	5	0	100%
22	5	0	100%
25	5	0	100%
28	5	0	100%
30	5	0	100%
31	5	0	100%
33	5	0	100%
35	5	0	100%
39	5	0	100%
40	5	0	100%
44	5	0	100%
53	5	0	100%
<b>Average Precision</b>			<b>100%</b>
Patient No.(Query MRI)	Brain Tumor	Non-Brain Tumor	Precision
1	10	0	100%
2	10	0	100%
3	10	0	100%
4	10	0	100%
5	10	0	100%
13	10	0	100%
16	10	0	100%
17	10	0	100%
19	10	0	100%
22	10	0	100%
25	10	0	100%
28	10	0	100%
30	10	0	100%
31	10	0	100%
33	10	0	100%
35	10	0	100%
39	10	0	100%
40	10	0	100%
44	10	0	100%
53	10	0	100%
<b>Average Precision</b>			<b>100%</b>
Patient No.(Query MRI)	Brain Tumor	Non-Brain Tumor	Precision
1	14	1	93.33%
2	15	0	100%
3	15	0	100%
4	15	0	100%
5	15	0	100%
13	15	0	100%
16	15	0	100%
17	15	0	100%
19	15	0	100%
22	15	0	100%
25	15	0	100%
28	15	0	100%
30	15	0	100%
31	15	0	100%
33	15	0	100%
35	15	0	100%
39	15	0	100%
40	15	0	100%
44	15	0	100%
53	15	0	100%
<b>Average Precision</b>			<b>99.67%</b>

Table (4.28): Precision of CBBIR System (BT =53), Similarity Measure: Spearman

Patient No.(Query MRI)	Brain Tumor	Non-Brain Tumor	Precision
1	2	3	40%
2	5	0	100%
3	3	2	60%
4	3	2	60%
5	5	0	100%
13	5	0	100%
16	5	0	100%
17	5	0	100%
19	3	2	60%
22	5	0	100%
25	4	1	80%
28	4	1	80%
30	4	1	80%
31	2	3	40%
33	5	0	100%
35	4	1	80%
39	4	1	80%
40	4	1	80%
44	3	2	60%
53	5	0	100%
<b>Average Precision</b>			<b>80%</b>
Patient No.(Query MRI)	Brain Tumor	Non-Brain Tumor	Precision
1	4	6	40%
2	8	2	80%
3	7	3	70%
4	4	6	40%
5	10	0	100%
13	8	2	80%
16	9	1	90%
17	8	2	80%
19	6	4	60%
22	7	3	70%
25	7	3	70%
28	7	3	70%
30	5	5	50%
31	3	7	30%
33	8	2	80%
35	5	5	50%
39	7	3	70%
40	8	2	80%
44	4	6	40%
53	8	2	80%
<b>Average Precision</b>			<b>66.5%</b>
Patient No.(Query MRI)	Brain Tumor	Non-Brain Tumor	Precision
1	7	8	46.67%
2	9	6	60%
3	9	6	60%
4	6	9	40%
5	12	3	80%
13	12	3	80%
16	12	3	80%
17	11	4	73.33%
19	9	6	60%
22	7	8	46.67%
25	8	7	53.33%
28	8	7	53.33%
30	6	9	40%
31	3	12	20%
33	10	5	66.67%
35	6	9	40%
39	7	8	46.67%
40	11	4	73.33%
44	6	9	40%
53	9	6	60%
<b>Average Precision</b>			<b>56%</b>

Table (4.29): Precision of CBBIR System (BT =53), Similarity Measure: Minkowski

Patient No.(Query MRI)	Brain Tumor	Non-Brain Tumor	Precision
1	3	2	60%
2	5	0	100%
3	5	0	100%
4	5	0	100%
5	5	0	100%
13	5	0	100%
16	5	0	100%
17	5	0	100%
19	5	0	100%
22	5	0	100%
25	5	0	100%
28	5	0	100%
30	5	0	100%
31	5	0	100%
33	5	0	100%
35	5	0	100%
39	5	0	100%
40	5	0	100%
44	5	0	100%
53	5	0	100%
<b>Average Precision</b>			<b>98%</b>
Patient No.(Query MRI)	Brain Tumor	Non-Brain Tumor	Precision
1	6	4	60%
2	10	0	100%
3	10	0	100%
4	6	4	60%
5	10	0	100%
13	10	0	100%
16	10	0	100%
17	10	0	100%
19	10	0	100%
22	10	0	100%
25	10	0	100%
28	10	0	100%
30	10	0	100%
31	10	0	100%
33	10	0	100%
35	10	0	100%
39	10	0	100%
40	10	0	100%
44	10	0	100%
53	10	0	100%
<b>Average Precision</b>			<b>96%</b>
Patient No.(Query MRI)	Brain Tumor	Non-Brain Tumor	Precision
1	7	8	46.67%
2	15	0	100%
3	15	0	100%
4	10	5	66.67%
5	15	0	100%
13	15	0	100%
16	13	2	86.67%
17	15	0	100%
19	14	1	93.33%
22	15	0	100%
25	15	0	100%
28	14	1	93.33%
30	15	0	100%
31	14	1	93.33%
33	13	2	86.67%
35	13	2	86.67%
39	15	0	100%
40	15	0	100%
44	15	0	100%
53	14	1	93.33%
<b>Average Precision</b>			<b>92.33%</b>

Table (4.30): Precision of CBBIR System (BT =53), Similarity Measure: Normalized L2

Patient No.(Query MRI)	Brain Tumor	Non-Brain Tumor	Precision
1	3	2	40%
2	5	0	100%
3	5	0	100%
4	5	0	100%
5	5	0	100%
13	5	0	100%
16	5	0	100%
17	5	0	100%
19	5	0	100%
22	5	0	100%
25	5	0	100%
28	5	0	100%
30	5	0	100%
31	5	0	100%
33	5	0	100%
35	5	0	100%
39	5	0	100%
40	5	0	100%
44	5	0	100%
53	5	0	100%
<b>Average Precision</b>			<b>98%</b>
Patient No.(Query MRI)	Brain Tumor	Non-Brain Tumor	Precision
1	6	4	60%
2	10	0	100%
3	10	0	100%
4	6	4	60%
5	10	0	100%
13	10	0	100%
16	10	0	100%
17	10	0	100%
19	10	0	100%
22	10	0	100%
25	10	0	100%
28	10	0	100%
30	10	0	100%
31	10	0	100%
33	10	0	100%
35	10	0	100%
39	10	0	100%
40	10	0	100%
44	10	0	100%
53	10	0	100%
<b>Average Precision</b>			<b>96%</b>
Patient No.(Query MRI)	Brain Tumor	Non-Brain Tumor	Precision
1	6	4	60%
2	10	0	100%
3	10	0	100%
4	6	4	60%
5	10	0	100%
13	10	0	100%
16	10	0	100%
17	10	0	100%
19	10	0	100%
22	10	0	100%
25	10	0	100%
28	10	0	100%
30	10	0	100%
31	10	0	100%
33	10	0	100%
35	10	0	100%
39	10	0	100%
40	10	0	100%
44	10	0	100%
53	10	0	100%
<b>Average Precision</b>			<b>96%</b>

Figure (4.25) shows graphical representation of the retrieval performance of the different similarity metrics when we change the number of retrieved image per query image.

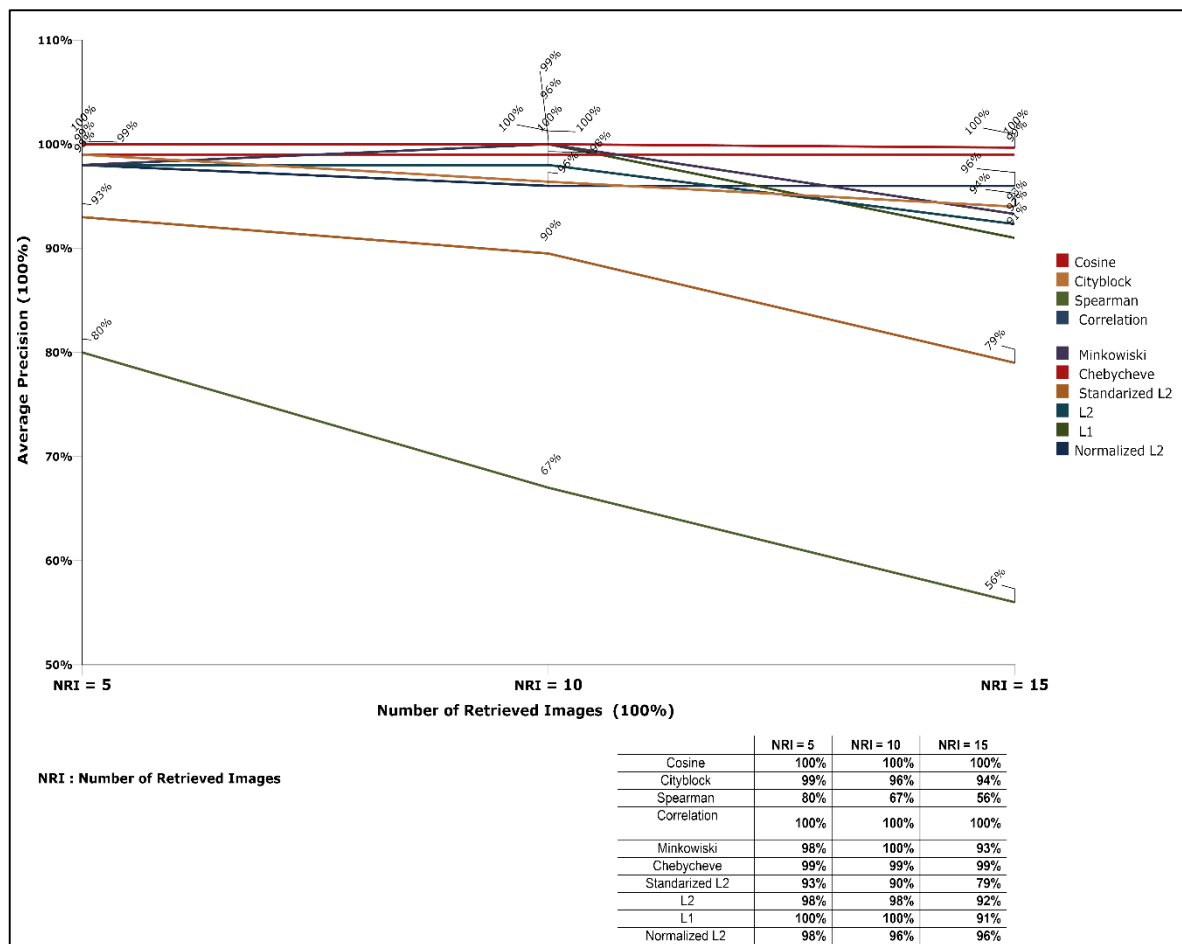


**Figure (4.25): Performance Comparison of Similarity Measures for Different Number of Retrieved Images**

As elaborated in Figure (4.25), most of similarity measures achieve high performance in terms of precision if the number of retrieved images is (5), which is a natural response of the proposed system. When the number of retrieved images decrease the probability to represent the correct patient case becomes higher in terms of KNN mechanism, and the performance shows a tiny degradation in performance as we increase the number of retrieve images.

### 4.6 Comparison of CBBIR System Performance to other Retrieval Systems Based on BRATS Dataset

Based on BRATS dataset, the retrieval performance of our proposed CBBIR system will be compared with the following existing state-of-the-art retrieval techniques that used same BRATS dataset.

Figure (4.26) elaborates a quantitative comparison with four state-of-the-art brain tumor segmentation, classification and retrieval techniques and followed by an exposition of each system.

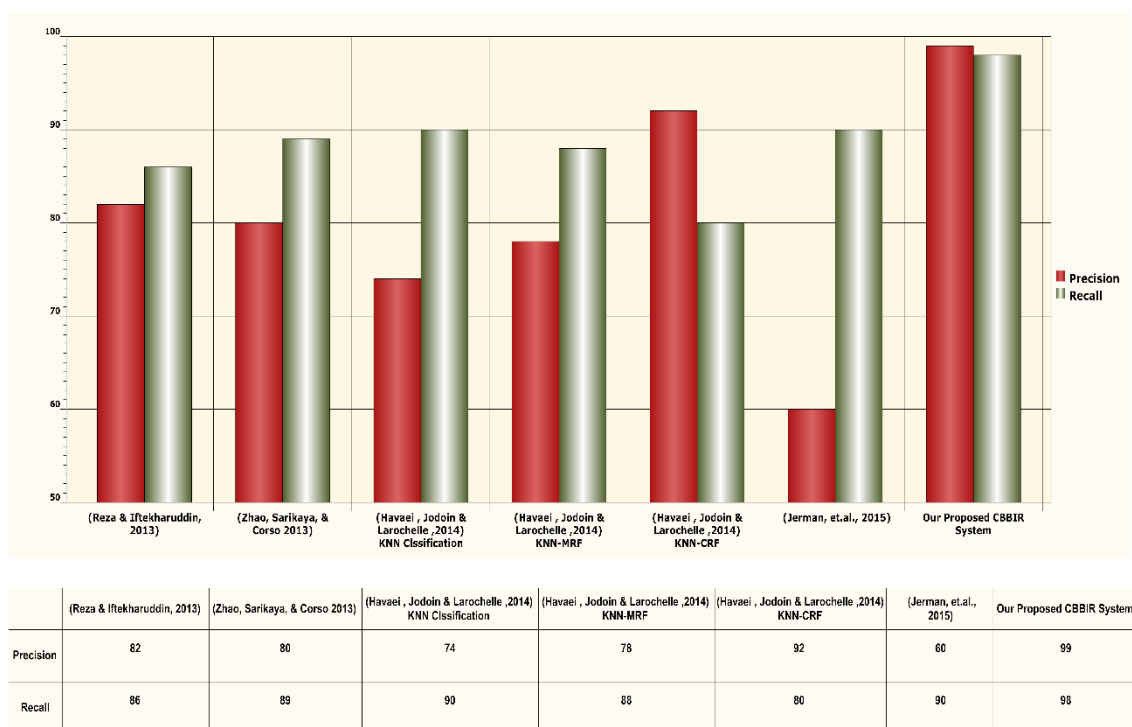


**Figure (4.26): Performance Comparison in terms of Precision and Recall for Different Retrieval Systems based on BRATS Dataset**

(Reza & Iftekharuddin, 2013) have used a classical random forests technique for classification where they used  $T_1$ ,  $T_2$ , and FLAIR brain MR images based on intensity and texture features.

(Zhao, Sarikaya, & Corso 2013) have used a technique based on the histogram matching where a 3D joint histogram was built based on  $T_{1c}$ ,  $T_2$  and FLAIR. During the testing phase, the likelihood for every voxel is evaluated by mapping the brain MR image under consideration to every training brain MR image and performing the histogram matching. Then the value of likelihood is later used in a conditional Random Field (CRF) in order to perform segmentation.

(Havaei, Jodoin & Larochelle ,2014) have used three classification techniques in one paper: KNN, KNN with Markov Random Field as label dependency model and as a technique to enforce the special regularity of the brain tumor pixels and KNN with Conditional Random Field (CRF) as label dependency model. Based on three MRI modalities:  $\{T_1, T_2, \text{ and FLAIR}\}$ .

(Jerman, et al., 2015) used a combination between supervised and unsupervised approaches for white matter lesion segmentation where the supervised method is used to extract the candidate lesion voxels. Then, the supervised method is learned a set of low-level MR intensity features in order to perform the accurate classification of lesion candidates.

## 4.7 Comparison of CBBIR System Performance to other Retrieval Systems Based on Different Brain MR Datasets

In this section, the retrieval performance of our proposed CBBIR system will be compared with the following existing retrieval techniques as shown in Figure (4.27) and Figure (4.28):

- **R1** : Retrieval using multiple features (Emmanuel, et al.,2007)
- **R2** : Retrieval based on classification (Dube, El-Saden, Cloughesy, & Sinha, 2006)
- **R3** : Retrieval based on machine learning and clustering techniques (Rahman, Bhattacharya & Desai, 2007)
- **R4** : Retrieval based on K-Means clustering , ensemble of classifiers (SVM,ANN,KNN) and ensemble of simalrity measures (Arakeri & Reddy,2013).

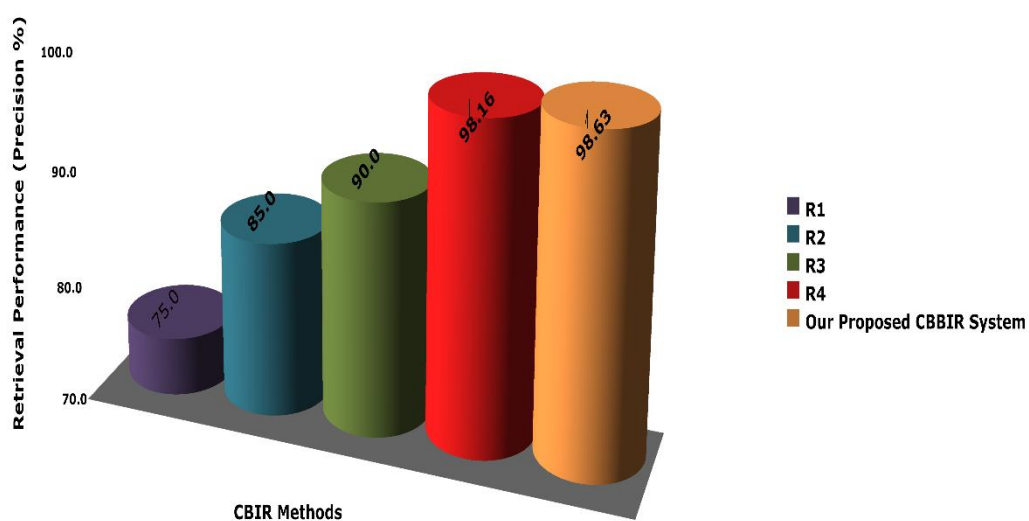


**Figure (4.27): Performance Comparison of CBMIR Systems in terms of Precision**

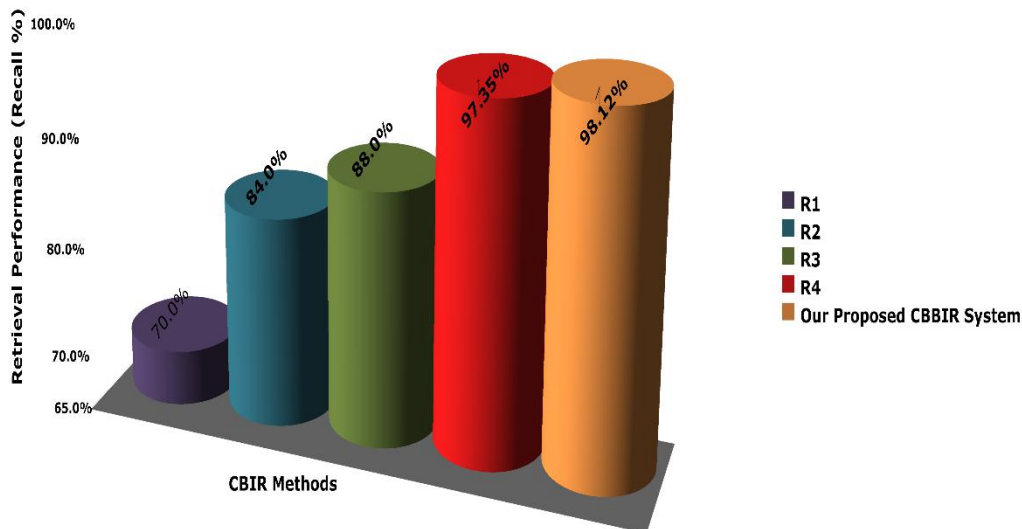


**Figure (4.28): Performance Comparison of CBMIR Systems in terms of Recall**

(Emmanuel et al., 2007) built their CBMIR system based on multiple features in order to characterize the brain tumor in complete manner. However, this leads to high dimensionality of features dataset which consider one of a curse for many content based medical image retrieval systems.

Therefore, (Dube et.al. , 2006) retrieved the brain tumor MR images based on classification where they reported a classification accuracy of (87%) since the system cannot match the MR images of subclasses.

In an attempt to enhance the similarity learning, (Rahman et al., 2007) integrated the clustering with classification, however, they used the same features set for both classification and retrieval after classification. Thus, the retrieval precision was not enhanced as that gained in case of (Dube et.al. 2006).

A noticeable performance (in terms of precision and recall) that can be shown in Figures (4.27) and (4.28) has been achieved by (Arakeri & Reddy,2013) where it reached up to (98.16% ) for precision and (97.35%) for recall where they used a retrieving strategy that fill the semantic gap by learning the similarity with different sets of feaures in hierarchiacl way in order to represent the brain tumor .

Our proposed system achieved a comparable performance in terms of both precision and recall without the need for separated sets of features. We have used novel feature extraction techniques such as : Wavelet transform and Log-Gabor filter , Colour correleogram that have the high capability to extract the colour, shape and texture feature in high effecincy. Therefore , our proposed CBBIR system outperforms all of these CBMIR systems in both : Precision and Recall .

## Chapter Five

### Conclusions, Recommendations and Future work

In this thesis, we have presented and implemented a novel, efficient, and automatic framework to brain tumor diagnosis using hybrid combination of low-level features (colour, shape and texture) in a multistage manner which gives a higher retrieval precision and recall than other existing content based medical image retrieval systems.

Our proposed CBBIR system has the capability to resolve the MR image misalignment problems through Log-Gabor filters and Correlogram feature descriptors where the system is made accurate by the proposed automatic brain tumor zones segmentation and through extracting more effective features for representing the brain tumor.

Also, the system is made more efficient by incorporating powerful and accurate indexing techniques, namely, KNN with an ensemble of similarity measures instead of one similarity metric where these similarity measures are compared to select the measure that retrieves the most similar brain MR images.

The performance evaluation demonstrated that the hybrid combination of features yields better retrieval recall and precision than using features in independent manner and in spite of multistage retrieval, our proposed CBBIR system is observed to be efficient in terms of time complexity also.

The proposed system achieved high average precision reached up to (98.63%) and average recall reached up to (98.16%). Therefore, the proposed CBBIR system can be a

good candidate to be implemented in hospitals for assisting the radiologists, neurologists, and neurosurgeons in diagnosing brain tumours with good precision and speed.

As a future work , we would like to extend this framework through using different classification techniques such as Artificial Neural Networks (ANN), Self Organized Map (SOM) or Support Vector Machine (SVM).

Since we have succeeded to segment the brain tumor automatically via MATLAB where even the zones of the brain tumor and its distribution was specified in high accuracy, we can use our proposed CBBIR system as an efficient interactive brain tumor segmentation with high and competitive performance that can be compared to that achieved by (Havaei, Jodoin, & Larochelle, 2014), (Tustion, Wintermark, Durst & Avants, 2013), (Zhao, Sarikaya & Corso, 2013), (Festa, et.al., 2013), (Meier, et.al.,2013), (Doyle, Vasseur & Forbes, 2013) and (Guo, Schwartz & Zhao ,2013).

## References

Abdulbaqi, H. A., Sulong, G., & Hashem, S. H. (2014). A sketch based image retrieval: a review of literature. *Journal of theoretical and applied information technology*, 63(1).158-167.

Adegoke, B.O, Olarinoye, A.A, Omotayo, M.E, & Olawuni, A., (2013). Medical image feature extraction: A survey. *International Journal of Electronics Communication and Computer Technology (IJECCCT)*, 464-467.

Arajujo, D. A., Crucianu, M., & Gouet-Brunet, V, (2013). Sketch-Finder: efficient and effective sketch-based retrieval for large image collections. *In Graphics, Patterns and Images (SIBGRAPI), SIBGRAPI-Conference on*, 234-241.

Arakeri, M. P., & Reddy, G. R. M. (2012). Medical image retrieval system for diagnosis of brain tumor based on classification and content similarity. *In India Conference (INDICON), Annual IEEE*, 416-421.

Arakeri, M. P., & Reddy, G. R. M. (2013). An intelligent content-based image retrieval system for clinical decision support in brain tumor diagnosis. *International Journal of Multimedia Information Retrieval*, 2(3), 175-188.

Arróspide, J., & Salgado, L. (2013). Log-Gabor filters for image-based vehicle verification. *Image Processing, IEEE Transactions on*, 22(6), 2286-2295.

Bach, J. R., Fuller, C., Gupta, A., Hampapur, A., Horowitz, B., Humphrey, R., & Shu, C. F. (1996). Virage image search engine: an open framework for image management. *In Electronic Imaging: Science & Technology International Society for Optics and Photonics*, 76-87.

Bauer, S., Wiest, R., Nolte, L. P., & Reyes, M. (2013). A survey of MRI-based medical image analysis for brain tumor studies. *Physics in medicine and biology*, 58(13), R97.1-44

Berkhin, P. (2006). A survey of clustering data mining techniques. In grouping multidimensional data. *Springer Berlin Heidelberg*. 25-71.

BRATS DATABASE (2015 AND 2013) available on-line: **Ischemic Stroke Lesion Segmentation (ISLES)** (<http://www.isles-challenge.org/>).

Burges, C. J. (2010). Geometric methods for feature extraction and dimensional reduction-a guided tour. In Data mining and knowledge discovery handbook, *Springer US*, 53-82.

Chary, R., Lakshmi, D. R., and Sunitha, K. V. N. (2012). Feature extraction methods for colour image similarity. *arXiv preprint arXiv: 1204.2336*.

Chitari, A. and BAG, V. V. (2014) Detection of brain tumor using classification algorithm. *International Journal of Inventions in Computer Science and Engineering*, 31-34.

Cover, T. and Hart, P. (1967), Nearest Neighbor Pattern Classification. *IEEE Transactions on Information Theory*, 13(1), 21-27.

Datta, R., Joshi, D., Li, J., & Wang, J. Z. (2008). Image retrieval: Ideas, influences, and trends of the new age. *ACM Computing Surveys (CSUR)*, 40(2), 5, 1-60.

Daugman, J. G. (1985). Uncertainty relation for resolution in space, spatial frequency, and orientation optimized by two-dimensional visual cortical filters. *JOSA A*, 2(7), 1160-1169.

DeAngelis, L. M. (2001). Brain tumors. *The New England journal of medicine*, 344(2):114-23.

Desai, P., Pujari, J., & Goudar, R. H. (2012). Image Retrieval using Wavelet based Shape Features. *Journal of Information Systems and Communication*, 3(1), 162-166.

Do, M. N., & Vetterli, M. (2005). The contourlet transform: an efficient directional multiresolution image representation. *Image Processing, IEEE Transactions on*, 14(12), 2091-2106.

Dópido, I., Villa, A., Plaza, A., & Gamba, P. (2012). A quantitative and comparative assessment of unmixing-based feature extraction techniques for hyperspectral image classification. *Selected Topics in Applied Earth Observations and Remote Sensing, IEEE Journal of*, 5(2), 421-435.

Dube, S., El-Saden, S., Cloughesy, T. F., & Sinha, U. (2006, August). Content based image retrieval for MR image studies of brain tumors. In *Engineering in Medicine and Biology Society, 2006. EMBS'06. 28th Annual International Conference of the IEEE. IEEE*. 3337-3340.

Eitz, M., Hildebrand, K., Boubekeur, T., & Alexa, M. (2011). Sketch-based image retrieval: Benchmark and bag-of-features descriptors. *Visualization and Computer Graphics, IEEE Transactions on*, 17(11), 1624-1636.

Emmanuel, M.; Babu, D.R.R.; Potdar, G.P.; Sonkamble, B.A.; Game, P., (2007). "Content-based medical Image Retrieval," *in Information and Communication Technology in Electrical Sciences (ICTES 2007)*, 2007. ICTES. IET-UK International Conference on, 20-22 Dec. 2007, vol., no., *IEEE*. 712-717,

Esther, J., & Sathik, M. M. (2014, March). Retrieval of Brain Image Using Soft Computing Technique. In *Intelligent Computing Applications (ICICA), 2014 International Conference on. IEEE*. 285-290.

Field, D. J. (1987). Relations between the statistics of natural images and the response properties of cortical cells. *JOSA A*, 4(12), 2379-2394.

Fischer, S., Šroubek, F., Perrinet, L., Redondo, R., & Cristóbal, G. (2007). Self-invertible 2D log-Gabor wavelets. *International Journal of Computer Vision*, 75(2), 231-246.

Flickner, M., Sawhney, H., Niblack, W., Ashley, J., Huang, Q., Dom, B., & Yanker, P. (1995). Query by image and video content: *The QBIC system*. *Computer. IEEE*, 28(9), 23-32.

G. Beylkin, R. Coifman, and V. Rokhlin (1991), Fast wavelet transforms and numerical algorithms, *Comm. Pure Appl. Math*, 44, 141-183

Gevers, T. (2001). Colour-based retrieval. In *Principles of visual information retrieval*. *Springer London*. 11-49.

Gevers, T., & Stokman, H. (2003). Classifying colour edges in video into shadow-geometry, highlight, or material transitions. *Multimedia, IEEE Transactions on*, 5(2), 237-243.

Gonzalez, R. C., Woods, R. E., & Eddins, S. L. (2004). Digital image processing using MATLAB. *Pearson Education India*. 11-50.

Gross, M. H., & Koch, R. (1995). Visualization of multidimensional shape and texture features in laser range data using complex-valued Gabor wavelets. *Visualization and Computer Graphics, IEEE Transactions on*, 1(1), 44-59.

Guan, H., & Wada, S. (2002, August). Flexible colour texture retrieval method using multi-resolution mosaic for image classification. In *Signal Processing, 2002 6th International Conference on* (Vol. 1). *IEEE*. 612-615.

Ha, J. Y., Kim, G. Y., & Choi, H. I. (2008, September). The content-based image retrieval method using multiple features. In *Networked Computing and Advanced Information Management, 2008. NCM'08. Fourth International Conference on* (Vol. 1). *IEEE*. 652-657.

Haeghen, Y. V., Naeyaert, J. M. A. D., Lemahieu, I., & Philips, W. (2000). An imaging system with calibrated colour image acquisition for use in dermatology. *Medical Imaging, IEEE Transactions on*, 19(7), 722-730.

Han, J., & Ma, K. K. (2007). Rotation-invariant and scale-invariant Gabor features for texture image retrieval. *Image and vision computing*, 25(9), 1474-1481.

Havaei, M., Jodoin, P. M., & Larochelle, H. (2014, August). Efficient interactive brain tumor segmentation as within-brain kNN classification. In *Pattern Recognition (ICPR), 2014 22nd International Conference on IEEE*. 556-561.

Huang, J., Kumar, S. R., Mitra, M., Zhu, W. J., & Zabih, R. (1997, June). Image indexing using colour correlograms. In *Computer Vision and Pattern Recognition, 1997. Proceedings. , 1997 IEEE Computer Society Conference on. IEEE*. 762-768.

Huang, M., Yang, W., Yao, W., Jiang J., Gao Y., Chen, Y., Feng Q., Chen, W., & Lu, Z., (2014). Content-Based Image Retrieval Using Spatial Layout Information in Brain Tumor T1-Weighted Contrast-Enhanced MR Images. **PLoS ONE 9(7): e102754. doi:10.1371/journal.pone.0102754.777-780.**

Hussein, S. E. (2009). Picture archiving and communication system analysis and deployment. *In Computer Modelling and Simulation, UKSIM'09. 11th International Conference on, IEEE*. 520-525.

Ibraheem, N. A., Hasan, M. M., Khan, R. Z., & Mishra, P. K. (2012). Understanding colour models: a review. *ARPJN Journal of Science and Technology*, 2(3), 265-75.

J. Festa, S. Pereira, J. Mariz, N. Sousa, and C. Silva, (2013) “Automatic brain tumor segmentation of multi-sequence MR images using random decision forests,” *Proc. Workshop on Brain Tumor Segmentation MICCAI.*, 23–26.

Jau-Ling, S., & Ling-Hwei, C. (2002). Colour image retrieval based on primitives of colour moments. In *Recent Advances in Visual Information Systems. Springer Berlin Heidelberg*. 88-94.

Jivani, A. (2013), The Novel k Nearest Neighbor Algorithm. *IEEE International Conference on Computer Communication and Informatics (ICCCI)*, Coimbatore, *IEEE*, 1-4.

Kang, Y., Lei, H., Lin, S., & Li, Y. (2014, November). Sketch-Based Shape Retrieval Using Orientation Histogram with Gabor Filters. In *Digital Home (ICDH), 2014 5th International Conference on. IEEE*. 277-281.

Karthikeyan .T & Vembandasamy .K (2014). A Study on CBIR for Brain Tumor Magnetic Resonance Imaging. *International Journal of innovative research in electrical electronics, Instrumentation and control engineering*, 535-538.

Keysers, D., Ney, H., Wein, B. B., & Lehmann, T. M. (2003). Statistical framework for model-based image retrieval in medical applications. *Journal of Electronic Imaging*, 12(1), 59-68.

Kingsbury, N. (2001). Complex wavelets for shift invariant analysis and filtering of signals. *Journal of Applied and computational harmonic analysis*, 10(3), 234-253.

Kumar, A., Kim, J., Cai, W., Fulham, M., & Feng, D. (2013). Content-based medical image retrieval: A survey of applications to multidimensional and multimodality data. *Journal of digital imaging*, 26(6), 1025-1039.

L. Zhao, D.Sarikaya, and J. Corso, (2013) “Automatic brain tumor segmentation with mef on supervoxels,” Proc. Workshop on Brain Tumor Segmentation *MICCAI*. 51–54.

Lacoste, C., Lim, J. H., Chevallet, J. P., & Le, D. T. H. (2007). Medical-image retrieval based on knowledge-assisted text and image indexing. Circuits and Systems for Video Technology, *IEEE Transactions on*, 17(7), 889-900.

Lee, Y. H., Rhee, S. B., & Kim, B. (2012). Content-based Image Retrieval Using Wavelet Spatial-Colour and Gabor Normalized Texture in Multi-resolution Database. *In Innovative Mobile and Internet Services in Ubiquitous Computing (IMIS), International Conference on, IEEE*. 371-377.

Lew, M. S., Sebe, N., Djeraba, C., & Jain, R. (2006). Content-based multimedia information retrieval: State of the art and challenges. *ACM Transactions on Multimedia Computing, Communications, and Applications (TOMM)*, 2(1), 1-19.

Li, C. H., & Yuen, P. C. (2002). Tongue image matching using colour content. *Pattern Recognition, Elsevier* 35(2), 407-419.

Lin, Y. L., Huang, C. Y., Wang, H. J., & Hsu, W. (2013). 3D Sub-query Expansion for Improving Sketch-Based Multi-view Image Retrieval. *In Computer Vision (ICCV), 2013 IEEE International Conference on*, 3495-3502.

Madheswaran, M., & Dhas, A. S. (2014, July). An adroit naïve Bayesian based sequence mining approach for prediction of MRI brain tumor image. In Computing, Communication and Networking Technologies (ICCCNT), 2014 International Conference on. *IEEE*. 1-7

Madugunki, M., Bormane, D. S., Bhadoria, S., & Dethé, C. G. (2011). Comparison of different CBIR techniques. *In Electronics Computer Technology (ICECT), IEEE International Conference on* 4, 372-375.

Manjunath, B. S., & Ma, W. Y. (1996). Texture features for browsing and retrieval of image data. *Pattern Analysis and Machine Intelligence, IEEE Transactions on*, 18(8), 837-842.

Marchiori, A., Brodley, C., Dy, J., Pavlopoulou, C., Kak, A., Broderick, L., & Aisen, A. M. (2001). CBIR for medical images-an evaluation trial. *In Content-Based Access of Image and Video Libraries, Workshop on*, 89-93.

Mathew, S. P., Balas, V. E., & Zachariah, K. P. (2015). A Content-based Image Retrieval System Based On Convex Hull Geometry. *Acta Polytechnica Hungarica*, 12(1), 103-116.

Moghaddam, H. A., Khajoie, T. T., & Rouhi, A. H. (2003, September). A new algorithm for image indexing and retrieval using wavelet correlogram. In *Image Processing, 2003. ICIP 2003. Proceedings. 2003 International Conference on* (Vol. 3). *IEEE*. III-497.

Müller, H., & SO, H. (2010). Text-based (image) retrieval.

Müller, H., Michoux, N., Bandon, D., & Geissbuhler, A. (2004). A review of content-based image retrieval systems in medical applications—clinical benefits and future directions. *International journal of medical informatics*, 73(1), 1-23.

N. Tustison, M. Wintermark, C. Durst, and B. Avants, (2013) “Ants and arboles,” Proc. Workshop on Brain Tumor Segmentation *MICCAI.*, 47–50.

Nangai, L. (2015), Automatic brain tumor medical image classification using hyperbolic Hopfield neural network, *Journal of Chemical and Pharmaceutical Research*, 7(2), 190-199.

Nava, R., Escalante-Ramírez, B., & Cristóbal, G. (2011, September). A comparison study of Gabor and log-Gabor wavelets for texture segmentation. In *Image and Signal Processing and Analysis (ISPA), 2011 7th International Symposium on*. *IEEE*. 189-194.

Nestares, O., Navarro, R., Portilla, J., & Taberero, A. (1998). Efficient spatial-domain implementation of a multiscale image representation based on gabor functions. *Journal of Electronic Imaging*, 7(1), 166-173.

Nicu Sebe, Michael S. Lew.(2001) Colour-based retrieval, Pattern Recognition Letters, Volume 22, Issue 2, February 2001, ,ISSN 0167-8655, Pages 223-230, available on line : [http://dx.doi.org/10.1016/S0167-8655\(00\)00092-1](http://dx.doi.org/10.1016/S0167-8655(00)00092-1)

Nixon, M. S., & Aguado, A. S. (2012). Feature extraction & image processing for computer vision. *Academic Press*.

Ouyang, A., & Tan, Y. P. (2002, December). A novel multi-scale spatial-colour descriptor for content-based image retrieval. In *Control, Automation, Robotics and Vision, 2002. ICARCV 2002. 7th International Conference on* (Vol. 3). *IEEE*. 1204-1209.

Park, H. and Jun, C. (2009), A Simple and Fast Algorithm for K-Medoids Clustering. *Expert Systems with Applications*, 36(2), 3336-3341.

Phillips, J. M (2013). Data mining lecture notes. (CS 6955) Lecture (7) *University of Utah* ., 1-4.

Portilla, J., Navarro, R., Nestares, O., & Taberero, A. (1996). Texture synthesis-by-analysis method based on a multiscale early-vision model. *Optical Engineering*, 35(8), 2403-2417.

Prasad, T. V., Babu, R. P., & Ahson, S. I. (2006). GEDAS-Gene Expression Data Analysis Suite. *Bioinformatics*, 1(3), 83-85.

Qazi, M. Y., & Farid, M. S. (2013). Content-Based Image Retrieval Using Localized Multi-Texton Histogram. *In Frontiers of Information Technology (FIT), International Conference on IEEE*, 107-112.

R. Meier, S. Bauer, J. Slotboom, R. Wiest, and M. Reyes, (2013) "A hybrid model for multimodal brain tumor segmentation," Proc. Workshop on Brain Tumor Segmentation *MICCAI.*, 31–36.

Rahman, M. M., Bhattacharya, P., & Desai, B. C. (2007). A framework for medical image retrieval using machine learning and statistical similarity matching techniques with relevance feedback. *Information Technology in Biomedicine, IEEE Transactions on*, 11(1), 58-69.

Rui, Y., Huang, T. S., & Chang, S. F. (1999). Image retrieval: Current techniques, promising directions, and open issues. *Journal of visual communication and image representation*, 10(1), 39-62.

S. Doyle, F. Vasseur, and F. Forbes, (2013) "Fully automatic brain tumor segmentation from multiple mr sequences using hidden markov fields and variational em," Proc. Workshop on Brain Tumor Segmentation *MICCAI.*, 18–22.

S. Reza and K. Iftekharuddin,(2013) “Multi-class abnormal brain tissue segmentation using texture features,” Proc. Workshop on Brain Tumor Segmentation *MICCAI.*, 38–42.

Seidl, T., & Kriegel, H. P. (1998, June). Optimal multi-step k-nearest neighbor search. *In ACM SIGMOD Record* (Vol. 27, No. 2). ACM. 154-165.

Shaik, K. B., Ganesan, P., Kalist, V., Sathish, B. S., & Jenitha, J. M. M. (2015). Comparative Study of Skin Colour Detection and Segmentation in HSV and YCbCr Colour Space. *Procedia Computer Science*, 57, 41-48.

Shen, C. Y., Zhou, L., Teng, Z. W., & Wang, J. X. (2015, June). A New Approach for Recognition and Position of Traffic Lights. In International Conference on Computer Information Systems and Industrial Applications. Atlantis Press.

Shih, P., & Liu, C. (2005). Comparative assessment of content-based face image retrieval in different colour spaces. *International Journal of Pattern Recognition and Artificial Intelligence*, 19(07), 873-893.

Simoncelli, E. P., Freeman, W. T., Adelson, E. H., & Heeger, D. J. (1992). Shiftable multiscale transforms. Information Theory, *IEEE Transactions on*, 38(2), 587-607.

Singh, S. (2014). Classification of human brain tumors from MRI using K-NN algorithm. *Proceedings of 16th IRF International Conference*,1-14.

Smith, J. R. (1997). Integrated spatial and feature image systems: Retrieval, analysis and compression (*Doctoral dissertation, Columbia University*).

Smith, J. R., & Chang, S. F. (1997, February). VisualSEEK: a fully automated content-based image query system. In Proceedings of the fourth ACM international conference on Multimedia, *ACM*, 87-98.

Starck, J. L., Candès, E. J., & Donoho, D. L. (2002). The curvelet transform for image denoising. *Image Processing, IEEE Transactions on*, 11(6), 670-684.

Steinbach, M., Karypis, G., & Kumar, V. (2000, August). A comparison of document clustering techniques. In *KDD workshop on text mining* (Vol. 400, No. 1), 525-526.

Stricker, M. A., & Orengo, M. (1995, March). Similarity of colour images. *In IS&T/SPIE's Symposium on Electronic Imaging: Science & Technology*. International Society for Optics and Photonics. 381-392.

Tang, J., Peli, E., & Acton, S. (2003). Image enhancement using a contrast measure in the compressed domain. *Signal Processing Letters, IEEE*, 10(10), 289-292.

Teknomo, K. (2006). Similarity measurement. Available: <http://people.revoledu.com/kardi/tutorial/Similarity/>.

Tim Jerman\*, Alfia Galimzianova, Franjo Pernu's, Bo'stjan Likar, and 'Ziga 'Spiclin (2015), "Combining Unsupervised and Supervised Methods for Lesion Segmentation". Proc. Workshop on Brain Tumor Segmentation *MICCAI*. 28-35.

Viriyavisuthisakul, S., Sanguansat, P., Charnkeitkong, P., & Haruechaiyasak, C. (2015, June). A comparison of similarity measures for online social media Thai text classification. In Electrical Engineering/Electronics, Computer, Telecommunications and Information Technology (ECTI-CON), 2015 12th International Conference on. *IEEE*. 1-6

Wang, Y., & Yuan, B. (2001). A novel approach for human face detection from colour images under complex background. *Pattern Recognition*, 34(10), 1983-1992.

Wei, C. H., Li, C. T., & Wilson, R. (2005). A content-based approach to medical image database retrieval. *Database Modeling for Industrial Data Management: Emerging Technologies and Applications*, 258-290.

Weldon, T. P., Higgins, W. E., & Dunn, D. F. (1996). Gabor filter design for multiple texture segmentation. *Optical Engineering*, 35(10), 2852-2863.

Wen, P. Y., Macdonald, D. R., Reardon, D. A., Cloughesy, T. F., Sorensen, A. G., Galanis, E., Degroot, J., Wick, W., Gilbert, M. R., Lassman, A. B., Tsien, C., Mikkelsen, T., Wong, E. T., Chamberlain, M. C., Stupp, R., Lamborn, K.

R., Vogelbaum, M. A., van den Bent, M. J., and Chang, S. M. (2010). Updated response assessment criteria for high-grade gliomas: response assessment in neuro-oncology working group. *Journal of clinical oncology: official journal of the American Society of Clinical Oncology*, 28(11):1963-1972.

X. Guo, L. Schwartz, and B. Zhao, (2013) "Semi-automatic segmentation of multimodal brain tumor using active contours," Proc. Workshop on Brain Tumor Segmentation *MICCAI*, 27-30.

Yang, J., & Zhu, S. J. (2012). Narrowing semantic gap in content-based image retrieval. *In Computer Distributed Control and Intelligent Environmental Monitoring (CDCIEM), International Conference on, IEEE*, 433-438.

Yang, W., Feng, Q., Yu, M., Lu, Z., Gao, Y., Xu, Y., & Chen, W. (2012). Content-based retrieval of brain tumor in contrast-enhanced MRI images using tumor margin information and learned distance metric. *Medical physics*, 39(11), 6929-6942.

Yao, J., Li, M., Li, Z., Zhang, L., & Ma, W. Y. (2005). Natural Image Retrieval with Sketches. *In ICME, IEEE*, 1198-1201. On-Line), available: [http://www.ijecct.org/v3n5/464-467CRP\\_10.pdf](http://www.ijecct.org/v3n5/464-467CRP_10.pdf).

Yu, H., Li, M., Zhang, H. J., & Feng, J. (2002, June). Colour texture moments for content-based image retrieval. In *Image Processing. 2002. Proceedings. 2002 International Conference on (Vol. 3)*. *IEEE*. 929-932.

MRICron CAD (available online at:

<http://www.mccauslandcenter.sc.edu/mricro/>).

((On-line),available:<http://www.hpengage.com/solutions/web/rich-media-management>).